GENERIC SITE AMPLIFICATION FACTORS FOR NORTHWESTERN TURKIYE AND THEIR USE IN GROUND MOTION SIMULATIONS

A THESIS SUBMITTED TO
THE GRADUATE SCHOOL OF NATURAL AND APPLIED SCIENCES
OF
MIDDLE EAST TECHNICAL UNIVERSITY

BY

GAMZE MURATOĞLU

IN PARTIAL FULFILLMENT OF THE REQUIREMENTS
FOR
THE DEGREE OF MASTER OF SCIENCE
IN
CIVIL ENGINEERING

JULY 2022

Approval of the thesis:

GENERIC SITE AMPLIFICATION FACTORS FOR NORTHWESTERN TURKIYE AND THEIR USE IN GROUND MOTION SIMULATIONS

submitted by **GAMZE MURATOĞLU** in partial fulfillment of the requirements for the degree of **Master of Science** i**n Civil Engineering, Middle East Technical University** by,

Prof. Dr. Halil Kalıpçılar
Dean, Graduate School of **Natural and Applied Sciences** _____

Prof. Dr. Erdem Canbay
Head of the Department, **Civil Engineering** _____

Prof. Dr. Ayşegül Askan Gündoğan
Supervisor, **Civil Engineering, METU** _____

Examining Committee Members:

Prof. Dr. Murat Altuğ Erberik
Civil Engineering, METU _____

Prof. Dr. Ayşegül Askan Gündoğan
Civil Engineering, METU _____

Prof. Dr. Berna Unutmaz
Civil Engineering, Hacettepe University _____

Assoc. Prof. Dr. Mustafa Kerem Koçkar
Civil Engineering, Hacettepe University _____

Assoc. Prof. Dr. Onur Pekcan
Civil Engineering, METU _____

Date: 29.07.2022

I hereby declare that all information in this document has been obtained and presented in accordance with academic rules and ethical conduct. I also declare that, as required by these rules and conduct, I have fully cited and referenced all material and results that are not original to this work.

Name Last name : Gamze Muratoğlu

Signature :

ABSTRACT

GENERIC SITE AMPLIFICATION FACTORS FOR NORTHWESTERN TURKIYE AND THEIR USE IN GROUND MOTION SIMULATIONS

Muratoğlu, Gamze
Master of Science, Civil Engineering
Supervisor: Prof. Dr. Ayşegül Askan Gündoğan

July 2022, 121 pages

Earthquake ground motions are influenced by source, path and local site properties. Among these three factors, local site conditions have a great effect on ground shaking and thus the structural damages observed during large earthquakes. Soil layers on top of hard rock can amplify the ground motions, which makes it essential to quantify the site amplifications.

In this thesis, generic site amplification factors in Northwestern Türkiye are obtained according to the NEHRP (National Earthquake Hazards Reduction Program) site classes for selected stations by following a 1-D site response analyses with an equivalent linear analysis method. A total of 76 shear wave velocity profiles are compiled with varying resolutions and depths. Strong and weak motion datasets are used as input bedrock ground motions throughout the analyses. Next, Gaussian functions are fitted to the generic site amplification data based on NEHRP site classes A, B, C and D. Comparisons of the developed amplification functions are made with available amplification factors in the literature for different regions. The amplification functions obtained from the 1-D site response analyses with strong and weak input motions show significant differences. Next, the proposed amplification factors are used as input to the stochastic ground motion simulations of the 1999 Düzce Earthquake. The simulated data at selected stations are compared to the

corresponding real ground motions. Finally, the goodness-of-fit values are computed to demonstrate the variations between the simulated and recorded motions. This study constitutes the first attempt to develop and test generic site amplification functions for Türkiye, focusing on the Northwestern regions.

Keywords: Site amplification, strong and weak ground motion, 1-D site response analysis, ground motion simulation, Northwestern Türkiye

ÖZ

KUZEYBATI TÜRKİYE İÇİN GENEL ZEMİN BÜYÜTME FAKTÖRLERİ VE YER HAREKETİ SİMÜLASYONLARINDA KULLANIMLARI

Muratoğlu, Gamze
Yüksek Lisans, İnşaat Mühendisliği
Tez Yöneticisi: Prof. Dr. Ayşegül Askan Gündoğan

Temmuz 2022, 121 sayfa

Deprem yer hareketleri kaynak, yayılım ve yerel zemin özelliklerinden etkilenir. Bu üç faktörden yerel zemin koşulları, yer sarsıntısı ve dolayısıyla büyük depremler sırasında gözlenen yapısal hasarlar üzerinde büyük etkiye sahiptir. Sert kayanın üzerindeki zemin tabakaları yer hareketini büyütmektedir, bu da zemin büyütme faktörlerinin hesaplanmasını zorunlu kılmaktadır.

Bu tezde, KuzeyKuzeybatı Türkiye'deki genel zemin büyütme faktörleri, eşdeğer lineer analiz yöntemi ile 1-boyutlu zemin tepki analizleri uygulanarak, seçilen istasyonlar için NEHRP (Ulusal Deprem Tehlikelerini Azaltma Programı) zemin sınıflarına göre elde edilmiştir. Farklı çözünürlük ve derinliklerde toplam 76 kayma dalgası hızı profili derlenmiştir. Analizler boyunca anakaya yer hareketi girdisi olarak kuvvetli ve zayıf hareket veri setleri kullanılmıştır. Daha sonra, Gaussian fonksiyonları, NEHRP zemin sınıfları A, B, C ve D'ye dayalı olarak genel zemin büyütme verilerine uyarlanmıştır. Geliştirilen zemin büyütme fonksiyonlarının karşılaştırmaları farklı bölgeler için literatürde mevcut olan büyütme faktörleri ile yapılmıştır. Girdi olarak kuvvetli ve zayıf yer hareketleriyle yapılan bir boyutlu zemin tepki analizlerinden elde edilen büyütme fonksiyonları önemli farklılıklar göstermektedir. Daha sonra, önerilen büyütme faktörleri 1999 Düzce Depremi'nin stokastik yer hareketi simülasyonlarına girdi olarak kullanılmıştır. Seçilen istasyonlarda simüle edilen veriler, karşılık gelen gerçek yer hareketleriyle

karşılaştırılmıştır. Son olarak, simüle edilen ve kaydedilen hareketler arasındaki varyasyonları göstermek için uyum iyiliği değerleri hesaplanmıştır. Bu çalışma, Kuzeybatı bölgelerine odaklanarak Türkiye için genel zemin büyütme fonksiyonları geliştirmeye ve test etmeye yönelik ilk girişimi oluşturmaktadır.

Anahtar Kelimeler: Zemin büyütmesi, kuvvetli ve zayıf yer hareketi, bir boyutlu zemin tepki analizi, yer hareketi simülasyonu, Kuzeybatı Türkiye

To all my loved ones

ACKNOWLEDGMENTS

First, I would like to express my deepest appreciation to my thesis advisor Prof. Dr. Ayşegül Askan Gündoğan, for her endless support throughout my master's degree. She has not only been a thesis advisor to me during my studies but also always guided, mentored, motivated, and supported me. I am grateful to her for always making time for me, even when she was swamped. Without her energy, smiling face, ideas, and support, I could never have finished this thesis. I can't thank her enough for always being there for me.

I would like to thank Alan Yong for his support during my studies. He made a significant contribution to my thesis with his critical comments and noticing even the smallest details that no one else could see. His contributions to my dissertation process were not only in terms of knowledge but also, he always guided me to be more confident in myself. I am fortunate to have known him, learned from his perspective, and got his ideas.

I would like to thank my committee members Prof. Dr. Murat Altuğ Erberik, Prof. Dr. Berna Unutmaz and Assoc. Prof. Dr. Mustafa Kerem Koçkar for their valuable comments and supports during my thesis defense. I am indebted Assoc. Prof. Dr. Onur Pekcan, for his life-oriented advice, academic advice, perspective and encouraging speeches throughout my undergraduate and graduate education.

I would like to thank Volkan Özsaraç for guiding me at the beginning of my thesis and for providing me the strong-motion dataset. Also, I would like to express my gratitude to Shaghayegh Karimzadeh Naghshineh for providing the input files of the strong ground motion simulations and for her support.

I would like to thank Abdullah Altındal for his assistance with the GMT plots, for reviewing my thesis and making critical comments. I want to give thanks to Berk Karakuş for reviewing my thesis and ever-present support and understanding throughout my dissertation process. I wish to express my gratitude to my dear

officemate Bilgin Koçak for his supports, he was always there for me whenever I need.

I owe a debt of gratitude to my father Osman Muratoğlu, my mother Nalan Muratoğlu and my brother Görkem Muratoğlu for always being there for me and for their unconditional love. They never lacked their support, and they were always proud of my achievements.

I am grateful to my best friend Ecem Çelik for her friendship and being always by my side. She always cheered me up when I needed as the only person who understands me better than I do. I appreciate that I had a chance to know Alperen Yayla during my graduate education. He contributed a lot to both my thesis and me. He never stopped asking if I needed anything until the last day. I wish to express my gratitude to him for the moments I shared with him, for his endless support and motivation.

I would like to express my appreciation to Caner Temiz who has always been with me for years. His belief in me has always made me a more confident me. I am more grateful to you than you'll ever know. We have faced many difficulties on this path we followed together, and we have made them all easier. Without his endless presence, patience, and love, I could not have successfully come out of this path that we entered together. Working with him and having his ideas got me to this point. Words cannot express how much he means to me.

Finally, I would like to thank the Scientific and Technological Research Council of Turkey (TUBITAK) since the institute financially supports this study under the coverage of the TUBITAK-BIDEB National Excellence Scholarship Programme for MSc Students (2210-A).

TABLE OF CONTENTS

LIST OF TABLES

TABLES

LIST OF FIGURES

FIGURES

LIST OF ABBREVIATIONS

ABBREVIATIONS

κ_0:	High-Frequency Spectral Decay Parameter
1-D:	One-Dimensional
AF:	Amplification Factor
AFAD:	Disaster And Emergency Management Presidency of Turkey
D_{min}:	Small-Damping Ratio
EQL:	Equivalent Linear
FAS:	Fourier Amplitude Spectra
GM:	Ground Motion
MDOF:	Multi-Degree-Of-Freedom
M_w:	Moment Magnitude
NL:	Nonlinear
PI:	Plasticity Index
SRA:	Site Response Analysis
V_s:	Shear Wave Velocity
V_{s30}:	Time-Averaged Shear Wave Velocity to a Depth of 30 Meters

CHAPTER 1

INTRODUCTION

1.1 General

Earthquakes are among the most destructive natural hazards that cause significant structural and economical losses and, more to the point, threat to lives and health of thousands of people. Nearly 20,000 earthquakes are recorded per year around the world by The National Earthquake Information Center (USGS, NEIC, 2022), which is approximately 55 per day. About 15 major earthquakes with moment magnitudes around 7 are anticipated each year according to the NEIC.

Ground motions generated during earthquakes are influenced by source and path effects as well as the local site properties. Thus, it is not possible to evaluate the ground shaking or structural damage caused by an earthquake without considering the effect of local soil conditions. Ground motions can be particularly amplified by the softer soil layers on top of hard rock, which has the potential to cause serious structural damage. Therefore, it is essential to estimate the site amplification factors.

Soil amplification occurs as a result of the increase in the amplitude of the waves as they propagate from one soil layer to another. Site amplification depends on the shear wave velocity, density of the soil, damping, and impedance differences between soil layers. The amplitude of the waves at the bedrock level differs from the amplitude of ground motion at the earth's surface. This difference is expressed as a function of frequency in terms of the soil amplification factors.

Site amplification is expressed in terms of a selected ground motion intensity measure and calculated as the ratio of that measure at a ground surface to the one for the motion at bedrock (Sandıkkaya & Dinsever, 2018). It is possible to calculate amplification factors with either Fourier amplitude spectrum (FAS) or response

spectra (RS). Boore & Joyner (1997) followed the Fourier amplitude spectrum approach for amplifications. Tran et al. (2021) define the amplification spectrum as the acceleration spectrum at the ground surface divided by the one at the bedrock. Similarly, Boudghene Stambouli et al. (2017) describe the amplification as the response spectra for ground surface divided by the one for outcropping reference rock and emphasize that the response spectrum is mainly used for the engineering approach.

Site amplification factors can be determined with both empirical and theoretical methods. Among the empirical methods, Horizontal-to-Vertical Spectral Ratio (HVSR) method proposed by Nakamura (1989) is widely used when there is no available velocity profile. It is defined as the Fourier amplitude of the horizontal component at the surface divided by that of the vertical component of the motion. This method is based on the assumption that the vertical component of the waves stay unchanged while propagating to the surface (Xu & Wang, 2021).

The quarter wavelength method and 1D site response analysis are among the theoretical methods for site amplification derivations. The quarter wavelength approximation method proposed by Joyner & Boore (1981) uses seismic impedance parameter (density times velocity) for the site amplification. Throughout this thesis, the latter approach which is 1-D site response analyses is followed to obtain generic site amplifications. The amplification factor in frequency domain is obtained by dividing the response spectrum of ground surface by the response spectrum of input motions as a result of the 1D site response analyses by DEEPSOIL (Hashash et al., 2020).

In addition to being an important phenomenon in geotechnical and structural perspectives, the frequency-dependent amplification factors are also one of the main ingredients in stochastic ground motion simulations. Simulated ground motions have become popular recently to be used in seismic design, ground motion prediction equations (GMPEs) and in nonlinear time history analyses. Amplification factors are

among the most critical site parameters used in the simulations which underlines the importance of generic site amplification factors in any region of interest.

1.2 Literature Survey

Various methods, ranging from theoretical to empirical, are available for the estimation of site amplifications in the literature. Joyner & Fumal (1985) and Boore & Joyner (1997) used the theoretical quarter-wavelength approximation which was originally proposed by Joyner & Boore (1981). Borcherdt (1970) defined the empirical standard spectral ratio (SSR) technique for the amplifications. Lermo & Chavez-Garcia (1993) and H. C. Huang & Teng (1999) applied the most common empirical approach, Horizontal-to-Vertical Spectral Ratio (HVSR) technique, also known as Nakamura's method, which was developed originally by Nakamura (1989).

Most well-known studies in the literature followed the empirical techniques (Borcherdt, 1994, 2002; Choi & Stewart, 2005; Crouse & McGuire, 1996; Dobry et al., 1999; Field, 2000; Harmsen, 1997; Joyner & Boore, 2000; Rodriguez-Marek et al., 1999; Steidl, 2000; Stewart et al., 2003).

One-dimensional site response analysis (SRA) is one of the frequently used techniques in geotechnical engineering for the theoretical estimations of site amplifications. Among the common commercial programs are SHAKE and DEEPSOIL, which compute theoretical transfer functions in time and frequency domains, respectively (Hashash et al., 2020; Schnabel et al., 1972). As a recent application in Türkiye, Sisman et al. (2018) used SRA among others to compute the theoretical transfer functions at selected stations with strong and weak motion inputs.

Site classification is critical for defining generic or generalized site amplifications. In literature, there are different site classification systems. Rodriguez-Marek et al. (1999) defines the site conditions with a geotechnical classification system as site class B, C and D by utilizing soil stiffness and depth to rock, which is different than

NEHRP site classification. The time-averaged shear wave velocity (V_{s30}) is the most common site proxy used for classification in building codes (Anderson et al., 1996; Boore et al., 1993; Building Seismic Safety Council (BSSC), 2003; Dobry et al., 1997; Finn, 1996). Stewart et al. (2003) classifies the sites according to surface geology, NEHRP category, and geotechnical data. Borcherdt (2002), Choi & Stewart (2005), Crouse & McGuire (1996), and Stewart et al. (2003) uses NEHRP site classification system based on V_{s30} parameter.

Most of the time, to define generalized or generic amplification factors, it is adequate to do the simulations for a representative or generic rock site. Boore & Joyner (1997) defined a generic rock site in eastern and western North America. A generic rock site is described as one with a velocity at shallow depths, which equals the average of velocities from the rock sites. Boore & Joyner (1997) dealt with two types of generic rock sites: rock and very hard rock. The shear wave velocities were determined from borehole data for these generic rock sites, and used to estimate amplification factors in the frequency domain with the quarter-wavelength approximation. The same study also presented site amplifications as a function of frequency for three site classes: NEHRP site class C and D, and the average soil class.

Klimis et al. (1999) provided frequency-dependent amplification factors, calculated by quarter-wavelength approximation, based on NEHRP site classes for selected sites in Greece. The authors used V_{s30} values in site classifications. The velocities were obtained from the borehole data at particular sites in Greece to yield Hellenic amplification functions for NEHRP site classes C and D with mean shear wave velocities of 485 and 275 m/s, respectively.

Sokolov et al. (2004) obtained empirical amplification functions for site classes B, C, and D in Taiwan using Fourier amplitude spectra. Later, Huang et al. (2005) computed the frequency-dependent amplification factors for $f > 1$ Hz (high-frequency regime) at 87 selected strong-motion stations in central Taiwan with the quarter-wavelength approximation proposed by Boore & Joyner (1997). Borehole data at selected sites in central Taiwan were used to compute V_{s30}. The authors

classified the sites as 33 sites as Class-C, 48 as Class-D and 6 as Class-E based on Lee et al. (2001) classification system.

As an improvement to Huang et al. (2005), Huang et al. (2007) computed the frequency-dependent amplification factors in central Taiwan in a lower frequency band. The authors considered the amplifications for $f = 0.01 - 1$ Hz from earthquake and microtremor data as proposed by Chen et al. (2001) and Satoh et al. (2001), respectively.

Huang et al. (2009) later estimated the frequency-dependent site amplification factors with a quarter wavelength approximation at 18 strong motion stations in and near the Taipei Basin. The authors classified 1 site as class B, 6 as class C, 10 as class D, and 1 as class E based on Lee et al. (2001) classification system. Huang et al. (2009) also compared the results with Boore & Joyner (1997) and Klimis et al. (1999).

Farrugia et al. (2018) used HVSRs obtained from earthquake and microtremor records in order to provide empirical amplification models at selected stations in Alberta, Canada.

Sedaghati et al. (2018) estimated frequency-dependent site amplification factors at 11 selected stations in the Mississippi embayment (ME) in the U.S. using the HVSR technique.

Sandıkkaya & Dinsever (2018) developed the empirical nonlinear soil amplification factor for crustal earthquakes using a set of global NGA-West2 records. Period-dependent amplifications were presented based on the V_{s30} value in that study.

Baram et al. (2019) defined the Israeli reference rock conditions and provided generic rock profiles. That study included 43 velocity profiles, which were used to obtain frequency-dependent Fourier amplifications for Israeli sites.

Finally, a topic of growing interest in the seismology and earthquake engineering literature is ground motion simulations. As one of the main input parameters in these simulations, site amplification factors are commonly employed. When no local site

information at a site of interest is available, it is typically convenient to use a representative generic site. Previously, Boore & Joyner (1997) and Klimis et al. (1999) developed frequency-dependent site amplification factors which were in use as input for stochastic simulations for representative sites in western North America and Greece, respectively.

As of now, there is no generic site amplification functions in Türkiye. In this study, as a first attempt to fill this gap in the literature, generic site amplifications are developed for representative sites in Northwestern Türkiye.

1.3 Objectives and Scope

Therefore, the main objective of this thesis is to obtain generic site amplification factors in Northwestern Türkiye, one of the most seismically active regions in the country, according to the NEHRP (National Earthquake Hazards Reduction Program) site classes for selected stations. Another objective is to validate the resulting generic site amplifications by using them as input for stochastic ground motion simulations at selected stations.

In order to achieve the main objective, the scope of the study includes 1-D site response analyses with an equivalent linear analysis method. The DEEPSOIL program is employed using available S-wave velocity profiles in Northwestern Türkiye. Resulting generic amplifications are expressed as a function of the NEHRP site classification based on the V_{s30} value of the sites.

1.4 Organization of the Thesis

This thesis follows a 1-D site response analysis method to obtain generic site amplifications for Northwestern Türkiye. In total, 76 shear wave velocity profiles are considered with varying vertical resolutions and depths. Strong and weak motion datasets as input bedrock ground motions are used throughout the analyses. The

equivalent linear analysis method is used with several assumptions for the soil models in DEEPSOIL program. The ratio between response spectra of the ground motion at the surface layer and input motion at the bedrock layer gives the site amplification spectrum in the frequency domain. Next, Gaussian functions are fitted to the generic site amplification data based on each NEHRP site class. Comparisons of the results with available amplification factors are made. Next, the proposed amplification factors are used as an input for stochastic ground motion simulations at selected stations, and the simulated data are compared to real ground motion data. The goodness-of-fit (GOF) values are tabulated to better represent the variations between simulated and real data. Figure 1.1 summarizes the methods, inputs and analyses implemented within this thesis.

Chapter 2 introduces the methodology of this thesis. 1-D site response analyses with the equivalent linear model and stress-strain behavior of cyclically loaded soils are presented. Theory and the assumptions for this method are provided.

Chapter 3 includes the database used for the implementation of the methodology. The essential inputs such as S-wave velocity profiles and ground motion database are presented. General information on S-wave velocity profiles and ground motions is given followed by the particular data used in this thesis.

Chapter 4 presents the results of site response analyses. Generic site amplification factors are presented separately based on the available NEHRP site classes. These amplification factors are then fitted with the Gaussian approach. A comparison of amplification factors obtained in this thesis with available generic amplification factors is made in this chapter.

Chapter 5 presents ground motion simulations with the proposed generic site amplification factors used as input site parameter. Goodness-of-fit values are investigated.

Finally, Chapter 6 summarizes and concludes the thesis. Future recommendations are also provided.

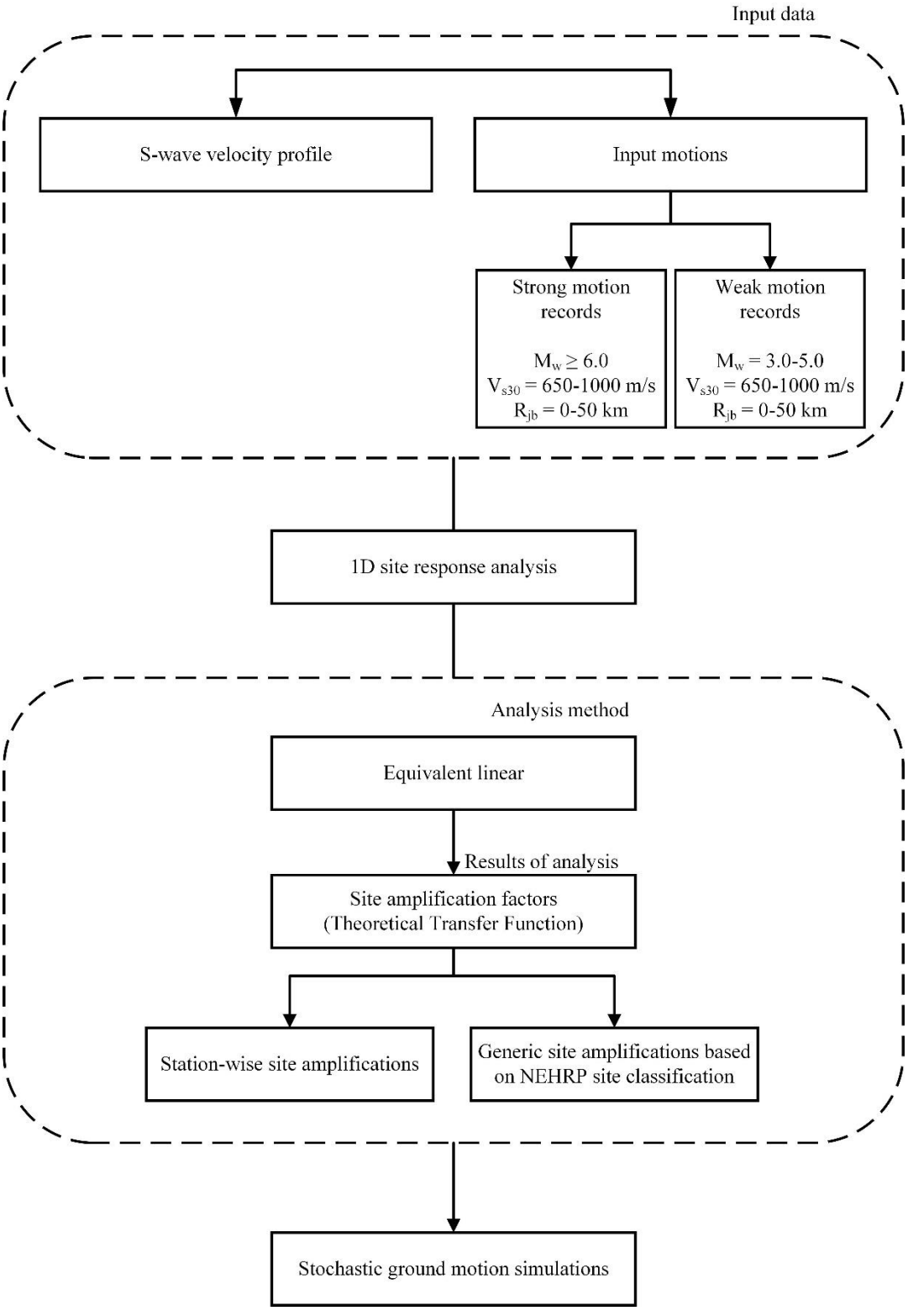

Figure 1.1. Flow chart for the methods, inputs and analyses presented in this thesis

CHAPTER 2

ONE DIMENSIONAL (1-D) SITE RESPONSE ANALYSES

Several methods are employed in the computation of site amplification. This thesis follows 1-D site response analysis, which is one of the most commonly used methods. Site response analyses provide not only amplifications but also the design response spectrum and earthquake-induced forces that cause unstable earth-retaining structures. DEEPSOIL (Hashash et al., 2020), a computer program that can perform 1-D equivalent-linear analyses in the frequency domain, is used to perform the analyses in this thesis. In this chapter, both the DEEPSOIL algorithm and the theory will be reviewed.

2.1 Theory of 1-D Site Response Analyses

The motions recorded on engineering bedrock are used as input to ground response analyses in order to yield acceleration time histories at the surface. Site response analyses are based on the assumptions that the soil and bedrock extend to infinity in the horizontal direction and that only horizontal boundaries exist (Kramer, 1996). Also, the response of the soil layer is due to the SH waves, which propagate in the vertical direction. As the body waves travel in all directions, they are refracted and reflected. After the inclined rays hit horizontal layers, they go in the vertical direction due to reflection. When the rays arrive at the surface, numerous refractions bend them in an almost vertical direction (Kramer, 1996). The concepts mentioned earlier, and assumptions through site response analyses are illustrated in Figure 2.1.

If a motion is recorded on top of a rock layer without a soil deposit above, it is called outcrop motion. Within motion, on the other hand, is a motion either recorded at any soil depth from the surface or computed by SRA (Amin, 2018).

Figure 2.2 summarizes the 1-D site response analysis flow which consists of 4 steps in DEEPSOIL which are described next.

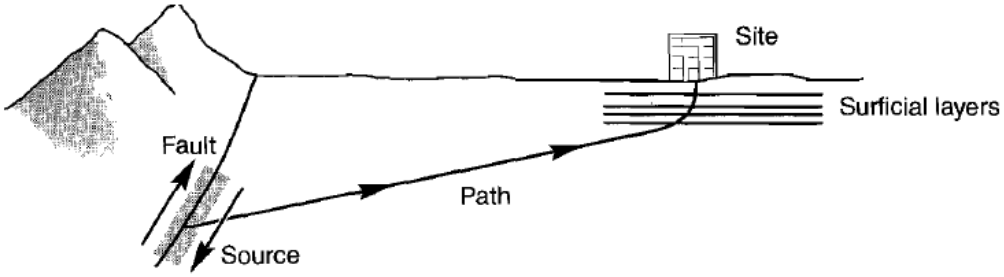

Figure 2.1. The concepts and the assumptions in 1-D site response analyses (adopted from Kramer (1996))

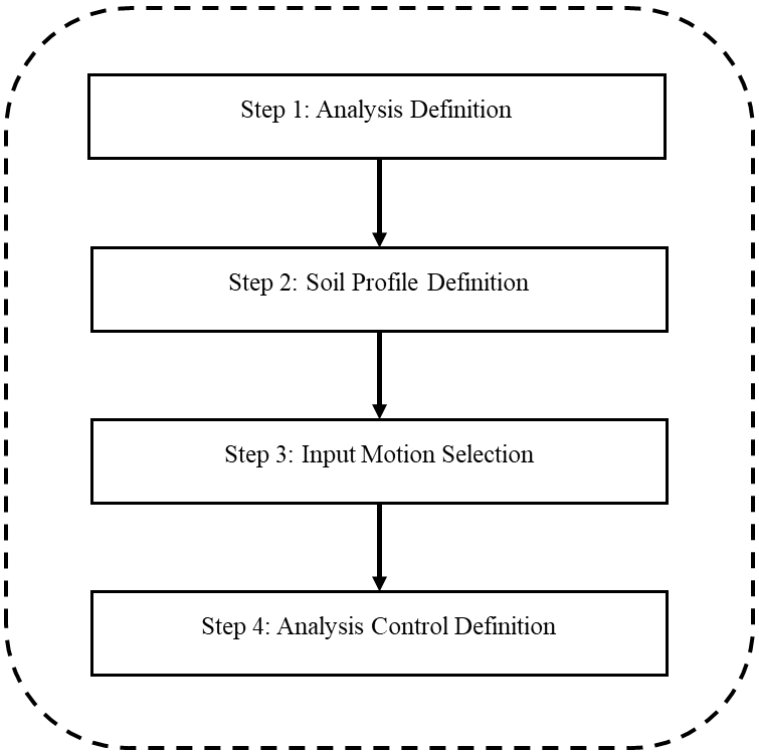

Figure 2.2. Analysis flow in DEEPSOIL

i) Step 1

Linear, equivalent linear (EQL), and nonlinear (NL) analysis methods are available in Step 1. Different solution types are available per the selected analysis method. For linear analysis, both frequency and time-domain solutions are possible. On the other hand, the only solution type offered is the time domain for nonlinear analysis and the frequency domain for the equivalent-linear analysis method. The soil curve is defined among many alternatives depending on the analysis method and solution type. Concepts explained after this point is based on the frequency domain analyses.

ii) Step 2

After selection of the analysis type, the soil profile needs to be defined. The thickness, shear wave velocity, and unit weight of each layer are required as basic soil properties; small-damping ratio (D_{min}) (%) is required as a soil model property. Additional parameters are necessary based on the selected soil curve, as discussed in section 2.3.2. The reference curve, which provides strain (%), G/G_{max} (shear modulus ratio), and damping ratio, is specified for each soil layer.

Bedrock characteristics needs to be defined additionally in the soil profile definition part, namely that two preferences of half-space definition, either elastic or rigid half-space, exist. Elastic half-space and rigid half-space are preferred for outcrop and within motion, respectively. A rigid one requires no parameters, while an elastic one needs a V_s value, unit weight, and damping ratio. A bedrock level with a V_s value larger than those of the soil layers should be identified.

An option is given in the frequency domain analysis to select either forward analysis or deconvolution. Deconvolution of the recorded surface motion is a possible option in the absence of input rock motions and the difficulties of precisely defining the stratigraphy (layer information) under the analyzed sites to a bedrock depth (Markham et al., 2015). The deconvolution process is explained in a way that an outcrop motion at the ground surface or anywhere in a soil column is given as an input to equivalent linear analysis. The output is the acceleration time history at a

location under the ground surface. The computed rock motion (within motion) can be then used for forward analysis.

iii) Step 3:

Input motions are selected from the library in DEEPSOIL. An option is given to select either one motion or multiple records at the same time. Software calculates spectral plots, acceleration, Housner and Arias intensity time histories, and Fourier amplitude spectra for each motion.

iv) Step 4:

For the selected type of analysis, options and output settings can be specified. This step defines the number of iterations during the analyses, effective shear strain and complex shear modulus type for equivalent linear analysis. Maximum number of iterations can be defined.

All of the physical properties and models mentioned in these steps are explained in detail next.

2.2 Stress-Strain Behavior of Cyclically Loaded Soils

Under seismic loads, the mechanical behavior of soils can be highly complicated. Three alternative soil models are offered to describe the most significant characteristics of cyclic soil behavior: equivalent linear, cyclic nonlinear, and advanced constitutive models (Kramer, 1996). Although the equivalent linear model is the most common and the simplest, it cannot accurately reflect soil behavior when subjected to cyclic loadings. On the other hand, advanced models provide many details about soil behavior, but they are very complex, and it is challenging to select the model parameters. In this study, equivalent linear model is chosen due to the lack of several soil parameters and the relative simplicity of the model.

2.2.1 Equivalent Linear Model

A hysteresis loop, which an equivalent linear model can represent, might be observed when soil is under symmetric cyclic loading (Figure 2.3). The stiffness of the soil is deduced from the slope of the loop, which gives the tangent shear modulus (G_{tan}). Since G_{tan} is not constant on the curve, the secant shear modulus (G_{sec}) is used to approximate the average inclination of the loop by the ratio of shear stress (τ_c) to shear strain (γ_c) (2.1). Damping ratio (ξ) defines the broadness of the loop, calculated by the ratio of the dissipated energy to the input energy. These two equivalent linear material parameters, G_{sec} and ξ, are utilized to characterize the soil behavior precisely. It is noted that the equivalent linear model only approximates the actual nonlinear behavior of soil (Kramer, 1996).

$$G_{sec} = \frac{\tau_c}{\gamma_c} \tag{2.1}$$

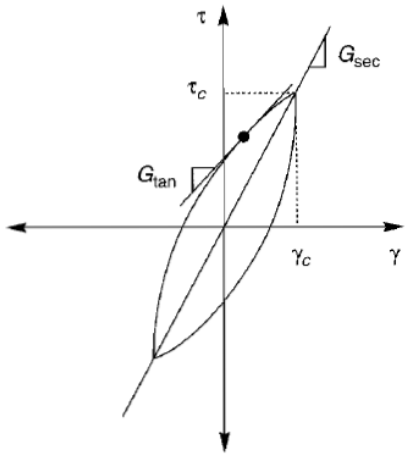

Figure 2.3. Hysteresis loop with secant shear modulus (G_{sec}) and tangent shear modulus (G_{tan}) (Adopted from Kramer (1996))

2.2.1.1 Shear Modulus and Damping Ratio

The secant modulus attains the maximum value at the origin which is called G_{max}. This modulus depends on the shear strain value, i.e., G_{sec} decreases with an increase in shear strain value since the slope becomes steeper (Figure 2.4). The variation of the modulus ratio G/G_{max} with shear strain is called the modulus reduction curve and it significantly affects the soil stiffness. The shape of the modulus reduction curve is affected considerably by the plasticity index of soils: It shifts right as the plasticity index increases, which results in greater cyclic shear strain (Figure 2.5a) (Dobry & Vucetic, 1987; Kokusho et al., 1982; Sun et al., 1988; Zen et al., 1978). The quantity of clay in the soil mainly determines the plasticity index (PI). A high PI value indicates abundant clay in the soil, which causes the soil to be more plastic. Since coarse-grained soils have no clay content, they are classified as non-plastic soils.

PI also affects the damping behavior of the soil: Soils with higher plasticity have lower damping ratios at the same cyclic shear strain when compared to non-plastic soils (Figure 2.5b) (Dobry & Vucetic, 1987; Kokusho et al., 1982; Sun et al., 1988). The plasticity index strongly influences how a soil layer amplifies or attenuates seismic motions. A higher PI value results in slower degradation by cyclic loading, where soil amplification is high and the damping ratio is small (Vucetic & Dobry, 1991).

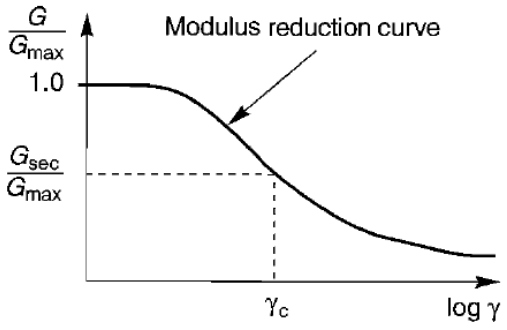

Figure 2.4. Modulus reduction curve (Adopted from Kramer (1996))

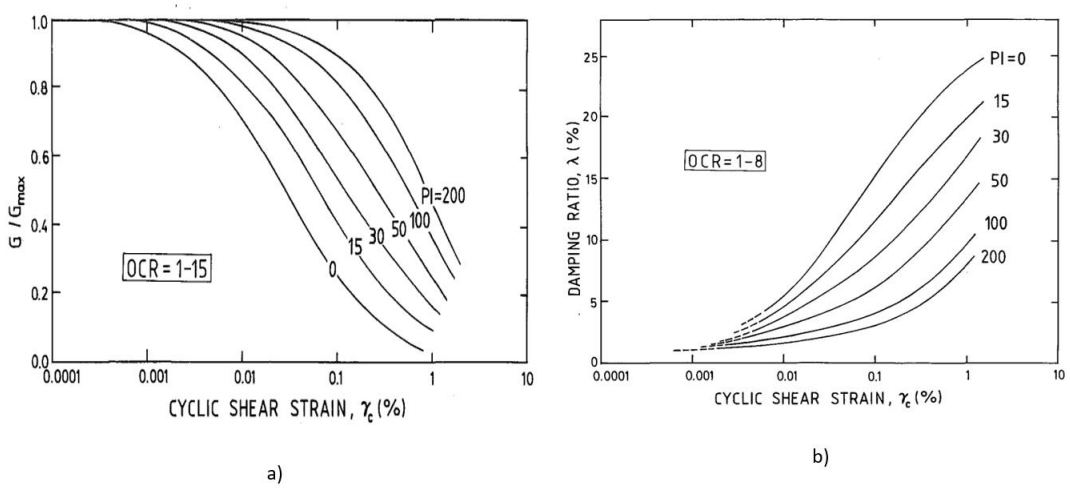

Figure 2.5. Relationship between the modulus reduction and damping ratio curves and different plasticity index values of fine-grained soils (Adopted from Vucetic & Dobry (1991))

2.3 Equivalent Linear Analyses Method

This thesis follows the equivalent linear approach to perform 1-D site response analysis. Before explaining the theory, it is helpful to make a brief comparison of the equivalent linear and the nonlinear methods. Site response studies based on EQL approach use solutions for SH wave propagation, whereas site response analyses based on NL approach deal with the dynamic response of multi-degree-of-freedom model of the soils under input base excitations by direct integrations (Kim et al., 2016). The equivalent-linear model can avoid parameterization of complicated nonlinear soil models while maintaining the theoretical simplicity of linear analysis as opposed to the nonlinear analysis. Although the EQL method is still a coarse approximation for the actual nonlinear behavior, it is preferred due to its simplicity and fewer input variables than the NL method.

2.3.1 Theory of Equivalent Linear Analyses

Actual soil behavior is nonlinear and complex, which requires the linear methods to be modified for acceptable ground response estimates. Equivalent-linear soil parameters can be used to approximate the actual nonlinear hysteretic stress-strain behavior of cyclically loaded soils (Kramer, 1996).

Since G and ξ must be constant through the soil profile in the linear method, strain values must be determined for each layer. The effective shear strain is commonly calculated as 65% of the peak strain in shear strain time histories (Kramer, 1996). Because the computed strain level is dependent on the EQL properties, an iterative method is necessary. This iterative procedure is demonstrated in Figure 2.6.

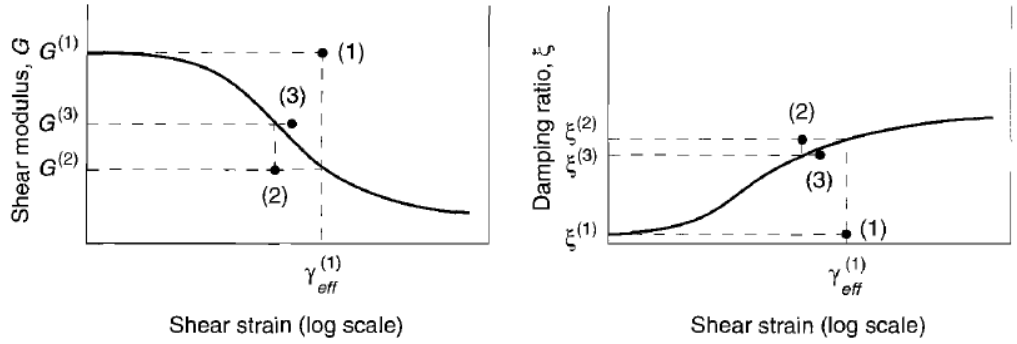

Figure 2.6. Iterative procedure for shear modulus and damping ratio (Adopted from Kramer (1996))

Next, the steps are summarized:

1. For each layer, initial estimations of G and ξ are established.
2. Shear strain time histories for each layer are obtained by 1-D site response analysis, which uses the initially estimated G and ξ values.
3. The effective shear strain (γ_{eff}) is commonly calculated as 65% of the peak shear strain (γ_{max}) in shear-strain time history for each layer using following equation:

$$\gamma_{eff\ j}^{i} = R_{\gamma} * \gamma_{\max j}^{i} \tag{2.2}$$

where i and j indicates iteration number and layer number, respectively. R_{γ}, which is the ratio between effective shear strain and peak shear strain, is a function of earthquake magnitude (Idriss & Sun, 1972) and is calculated by

$$R_{\gamma} = \frac{M-1}{10} \tag{2.3}$$

4. Using R_{γ} and γ_{max} correlation, effective shear strain is computed. From this effective strain, a new shear modulus (G^{i+1}) and damping ratio (ξ^{i+1}) values are selected for the next step.
5. These steps are repeated until the computed G and ξ values are nearly equal to the values determined in the previous step (with an allowable variation of 5 to 10%).

2.3.2 Assumptions in the Equivalent Linear Analyses in This Study

This study uses an equivalent linear analysis method in the frequency domain. Soil curves are defined using discrete points, which require G/G_{max} (shear modulus ratio) and damping ratio (%) in terms of shear strain (%) (Hashash et al., 2020). Selected input motions are recorded on engineering bedrock; therefore, the analyses performed in this thesis require no deconvolution. Since the selected motions are rock outcrop motions, bedrock is represented by an elastic half-space.

The values of layer thickness, V_s, unit weight, reference curve, and D_{min} for each soil layer are required in DEEPSOIL software. The S-wave velocity profiles and input ground motions used in this thesis to derive generic amplification factors are explained in Chapter 3. If there is no information regarding the type of soil layer of

which the velocity profile is taken from the AFAD web page, it is assumed to be sand.

i) Unit Weight:

The unit weight of each soil layer is calculated as follows (Mayne, 2001):

$$\gamma = 8.32log(V_s) - 1.61 * log(z) \quad (2.4)$$

where γ is the unit weight for any soil layer in kN/m^3, V_s is in m/s, and z is the depth of the corresponding soil layer in meters.

ii) Reference Curve:

DEEPSOIL has the option to select a reference curve for equivalent linear analysis. The selected reference curve provides models for modulus reduction and variation of damping ratio with shear strain.

- The mean of Seed & Idriss (1970) curve is used as a reference for sand layers.
- The mean of Vucetic & Dobry (1991) curve is used as a reference for clay layers.

iii) Small-damping ratio, D_{min}:

Small-damping ratio, D_{min} is used to obtain initial shear strain time histories for each layer. D_{min} value is assumed to correspond to the smallest shear strain (%) value in the damping ratio curve. In the reference damping curves of Seed & Idriss (1970) (Figure 2.7) and Vucetic & Dobry (1991), damping values corresponding to 0.0001% shear strain are 0.48 and 1.0, respectively. Therefore, the following values are assumed:

- D_{min} is taken as 0.48 for sand layers.
- D_{min} is taken as 1.0 for clay layers.

iv) Plasticity Index:

The reference curve of Vucetic & Dobry (1991) requires the plasticity index of the soil layer, which affects the shape of the modulus reduction curve significantly. The following assumptions are made for PI:

- For silty clay layers, the plasticity index is assumed to be 20.
- For sandy clay layers, the plasticity index is assumed to be 10.
- Limestone layers are considered non-plastic, i.e., PI=0.
- Marl layers are supposed to behave like clay layers.

v) Half-space Definition:

In this thesis, elastic half-space is preferred for outcrop bedrock motions. The elastic half-space option requires the following parameters: V_s value, unit weight, and damping ratio. In this thesis, these values for the elastic bedrock are taken as 2000 m/s, 22 kN/m^{3,} and 2%, respectively.

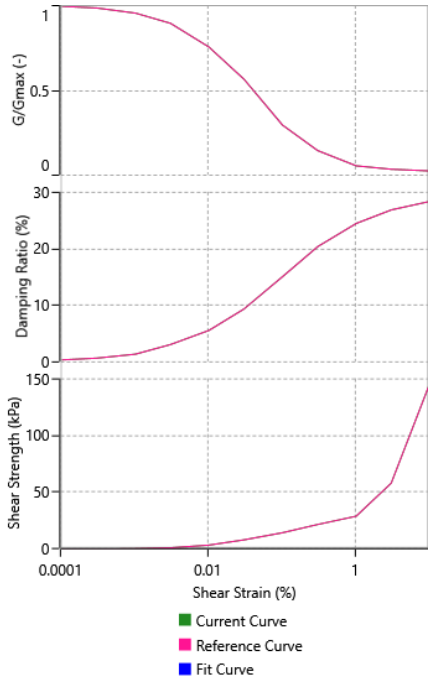

Figure 2.7. (Mean) reference curve of Seed & Idriss (1970)

vi) Analysis Control Definition:

For the selected type of analysis, options and output settings can be specified. Number of iterations during the analyses and effective shear strain are defined in this step for equivalent linear analysis. The value of effective shear strain is taken 0.65 (65%) as recommended based on Equation (2.3).

CHAPTER 3

DATABASE FOR THE IMPLEMENTATION OF 1-D SITE RESPONSE ANALYSES

3.1 General

The main input parameters for site response analyses are the S-wave velocity profiles and input bedrock ground motions at any selected sites. In this chapter, both the velocity profiles and the input ground motion datasets will be presented in detail.

3.2 S-Wave Velocity Profiles

Waves propagate through the earth via three-dimensional velocity structures. However, for simplicity, in both earth sciences and earthquake engineering, earth materials can be modeled as infinite horizontal layers which can be represented by a 1D shear wave velocity profile. The 1D S-wave velocity models are essential inputs in site characterization since they determine how the incoming waves will behave from the bedrock level to the ground surface. The accurate estimation of the surface ground motions is crucial for both seismic design and analyses of the structures. Used in the world as the major site proxy, the time-averaged shear wave velocity to a depth of 30 meters (V_{s30}) is a key index for the earthquake engineering to account for seismic site conditions (Yong et al., 2016). Thus, it is important to accurately estimate velocity models at site of interests. Various methods to perform numerical analyses of datasets acquired through field tests are used to obtain velocity models (Yong et al., 2022) which is necessary for site response analyses. The theory of site characterization is out of scope of this thesis, but a recent review on the state-of-the-art methods for site characterization can be found in Yong et al. (2022).

In the next section, the velocity models at selected stations in Northwestern Türkiye are presented.

3.2.1 Selected Stations

Herein, information on S-wave velocity profiles at the sites of interest is presented. These sites are located at strong-motion stations operated by the Disaster and Emergency Management Presidency (AFAD) in Northwestern Türkiye. Available 1D S-wave velocity models at the selected strong-motion stations are taken from the AFAD web page (https://tadas.afad.gov.tr/). These models include the layer thicknesses and corresponding shear wave velocities. In the geotechnical survey reports provided by AFAD, soil profiles, including the soil types for each layer, are available for only a few strong-motion stations. Therefore, several assumptions are made about the other stations' soil properties, as previously explained in detail in Chapter 2.

Seismicity of the regions is considered while selecting the cities to be included in this study. North Anatolian Fault Zone (NAFZ) is the most active fault zone in Türkiye with its well-known activity. The western segments of the NAFZ have generated 46 and 10 large earthquakes in the historical and instrumental era, respectively (Duman et al., 2018). A westward migration of earthquakes has been observed on NAFZ within the last century. As a result of ten large earthquakes, a total of 1000 km of NAFZ have been ruptured (Duman et al., 2018). These events on NAFZ are listed in Table 3.1 in chronological order. Due to the existence of seismic gaps along with the high population density and industrial facilities, the Northwestern parts of Türkiye are of constant interest, which also motivated this study.

Table 3.1. Major Earthquakes on NAFZ in the Instrumental Period

Event Name	**Magnitude (Reported by AFAD)**	**Date**
Mürefte Earthquake	M_s=7.4	Aug. 9, 1912
Erzincan Earthquake	M_s=7.9	Dec. 27, 1939
Erbaa-Niksar Earthquake	M_s=7.1	Dec. 20, 1942
Tosya Earthquake	M_s=7.4	Nov. 26, 1943
Bolu-Gerede Earthquake	M_s=7.3	Feb. 1, 1944
Abant Earthquake	M_s=7.1	May 26, 1957
Mudurnu Earthquake	M_s =7.2	July 22, 1967
Erzincan Earthquake	M_w =6.3	March 13, 1992
Izmit Earthquake	M_w =7.4	Aug. 17, 1999
Düzce Earthquake	M_w =7.2	Nov. 12, 1999

Figure 3.1 demonstrates the areas of interest with the major tectonic structures in Northwestern Türkiye. Cities that have experienced severe earthquakes so far in this region are selected because they are located either on or near the active faults. Information on the selected cities and the number of stations per city are given in Table 3.2. In total, 76 sites (strong-motion stations) located in 7 different cities in Northwestern Türkiye are used in this study.

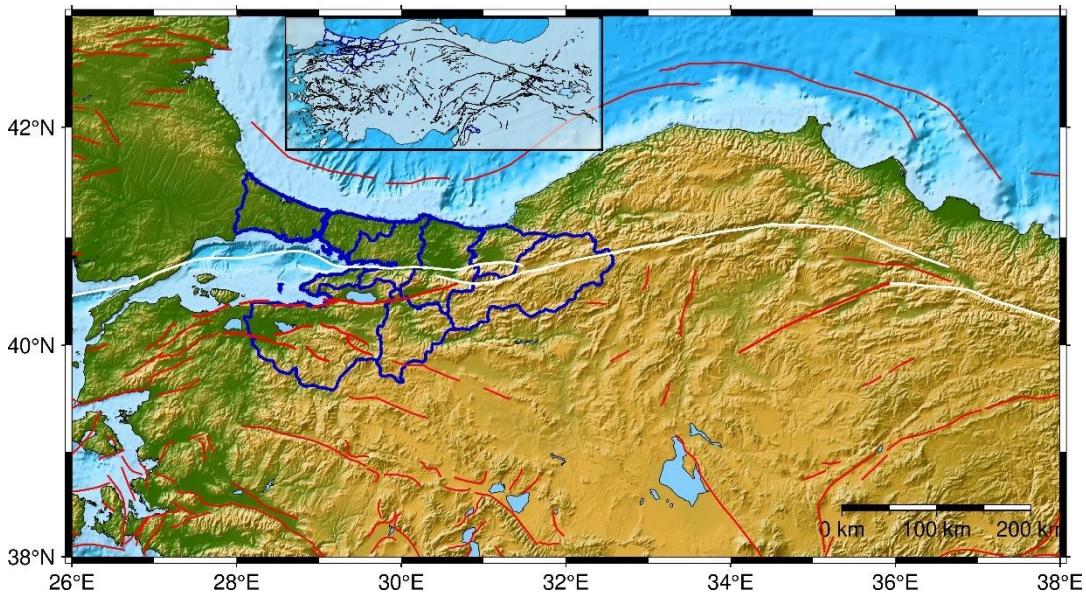

Figure 3.1. Selected Regions and Active Faults in Northwestern Türkiye (White lines indicate earthquake surface ruptures and NAFZ, red lines indicate Holocene and Quaternary active faults, blue lines indicate the cities included in this study) (Fault lines are taken from Danciu et al. (2021))

Table 3.2. Number of Selected Stations

City	Number of Selected Stations
Düzce	3
Bolu	10
Sakarya	5
İstanbul	13
Kocaeli	21
Bursa	19
Yalova	5

As the main site proxy for site classifications, time-averaged shear wave velocity, V_{S30} parameter, to a depth of 30 m is used globally in accordance with the National Earthquake Hazards Reduction Program (NEHRP) Recommended Seismic Provisions for New Buildings and Other Structures (BSSC, 2003). The selected sites

in this thesis are classified according to the NEHRP classification system (Table 3.3). According to NEHRP, Vs_{30} at a specific site is calculated as follows:

$$V_{s30} = \frac{\sum_{i=1}^{n} d_i}{\sum_{i=1}^{n} \frac{d_i}{V_{si}}} \tag{3.1}$$

where i indicates each layer, d_i is the thickness of any layer between 0 and 30 m, V_{si} is the shear wave velocity of the layer (m/s).

Table 3.3. NEHRP site classification (BSSC, 2003)

NEHRP Site Class	**Soil Description**	**Average shear wave velocity, V_{s30} (m/s)**
A	Hard Rock	>1500
B	Rock	760-1500
C	Very dense soil, and soft rock	360-760
D	Stiff soil	180-360
E	Soft soil	<180

Information regarding the locations, coordinates, Vs_{30} values, and corresponding NEHRP site classes are provided in Table 3.4 - Table 3.10. Vs_{30} values have revealed that A, B, C, and D NEHRP site classes exist in the study region, where 3 out of 76 sites are class A, 6 are class B, 28 are class C, 38 are class D. As can be inferred from the map (Figure 3.2), NEHRP site classes A and B are less in number than C and D, which can be explained by the following reasons: Most of these cities have agricultural lands and are close to the water resources leading to softer soil conditions. Indeed, Düzce, Kocaeli, and Sakarya are located on alluvial basins. Distribution of the selected stations in Northwestern Türkiye are not geometrically

uniform since only the stations with available shear wave velocity profiles are collected in this study.

Table 3.4. Information on the selected sites in Düzce

Station Code	City	District	Longitude	Latitude	Vs_{30} (m/s)	NEHRP
8101	Düzce	Düzce Merkez	31.14811	40.84392	282	D
8109	Düzce	Gölyaka	31.01439	40.78100	183	D
8110	Düzce	Akçakoca	31.14278	41.09000	407	C

Table 3.5. Information on the selected sites in Bolu

Station Code	City	District	Longitude	Latitude	Vs_{30} (m/s)	NEHRP
1401	Bolu	Bolu Merkez	31.60732	40.74567	294	D
1402	Bolu	Gerede	32.20593	40.79248	445	C
1403	Bolu	Göynük	30.78975	40.39842	472	C
1404	Bolu	Göynük	30.78307	40.39659	348	D
1405	Bolu	Mengen	32.07602	40.93811	365	C
1406	Bolu	Mudurnu	31.20994	40.46843	355	D
1407	Bolu	Mudurnu	31.00276	40.58175	273	D
1409	Bolu	Dörtdivan	32.06378	40.71744	362	C
1410	Bolu	Yeniçağa	32.03699	40.77113	338	D
1411	Bolu	Bolu Merkez	31.61749	40.68464	229	D

Table 3.6. Information on the selected sites in Sakarya

Station Code	City	District	Longitude	Latitude	Vs_{30} (m/s)	NEHRP
5401	Sakarya	Adapazarı	30.38005	40.73707	412	C
5403	Sakarya	Sapanca	30.26995	40.69078	215	D
5404	Sakarya	Geyve	30.29315	40.51912	381	C
5405	Sakarya	Hendek	30.7352	40.79609	401	C

Table 3.7. Information on the selected sites in Istanbul

Station Code	City	District	Longitude	Latitude	Vs_{30} (m/s)	NEHRP
3411	İstanbul	Fatih	28.97605	41.01187	323	D
3412	İstanbul	Büyükçekmece	28.57821	41.02058	247	D
3416	İstanbul	Bakırköy	28.83635	40.97466	420	C
3413	İstanbul	Eyüp	28.94818	41.09433	452	C
3417	İstanbul	Sultanbeyli	29.25627	40.95471	1747	A
3403	İstanbul	Küçükçekmece	28.7587	41.02646	283	D
3402	İstanbul	Üsküdar	29.06223	41.06344	415	C
3401	İstanbul	Beşiktaş	29.00951	41.0582	595	C
3404	İstanbul	Silivri	28.2557	41.07316	639	C
3405	İstanbul	Kartal	29.15668	40.91111	1862	A
3406	İstanbul	Ümraniye	29.15884	41.02262	436	C
3410	İstanbul	Şile	29.60816	41.17189	587	C
3418	İstanbul	Tuzla	29.27546	40.81459	1182	B

Table 3.8. Information on the selected sites in Kocaeli

Station Code	City	District	Longitude	Latitude	Vs_{30} (m/s)	NEHRP
4101	Kocaeli	İzmit	29.91721	40.7665	826	B
4102	Kocaeli	İzmit	30.02649	40.78463	1000	B
4104	Kocaeli	Başiskele	29.96998	40.68038	770	B
4105	Kocaeli	Başiskele	29.96935	40.67441	289	D
4106	Kocaeli	Gebze	29.45003	40.78627	701	C
4114	Kocaeli	Çayırova	29.40776	40.86897	344	D
4115	Kocaeli	Körfez	29.78015	40.74328	253	D
4116	Kocaeli	Başiskele	29.86583	40.71956	181	D
4117	Kocaeli	Kartepe	30.02665	40.66989	282	D
4118	Kocaeli	Kartepe	30.07805	40.72163	190	D
4119	Kocaeli	Dilovası	29.52061	40.77286	884	B
4120	Kocaeli	İzmit	30.02737	40.76761	214	D
4121	Kocaeli	Başiskele	29.96985	40.72277	286	D
4123	Kocaeli	Gölcük	29.84794	40.71515	279	D
4124	Kocaeli	Körfez	29.60625	40.78308	906	B
4126	Kocaeli	İzmit	29.91485	40.76252	188	D
4127	Kocaeli	İzmit	29.90473	40.76087	215	D
4128	Kocaeli	Kartepe	30.02435	40.7249	258	D
4129	Kocaeli	Kartepe	30.11217	40.71745	203	D
4130	Kocaeli	Darıca	29.38787	40.75446	484	C
4131	Kocaeli	İzmit	29.92186	40.82054	445	C

Table 3.9. Information on the selected sites in Bursa

Station Code	City	District	Longitude	Latitude	Vs_{30} (m/s)	NEHRP
1633	Bursa	Karacabey	28.36262	40.21397	375	C
1621	Bursa	Nilüfer	28.97558	40.22686	396	C
1631	Bursa	Orhangazi	29.2993	40.49411	410	C
1612	Bursa	İznik	29.71688	40.44163	197	D
1609	Bursa	Gemlik	29.16658	40.42539	229	D
1602	Bursa	Osmangazi	29.05087	40.19405	272	D
1606	Bursa	Gemlik	29.12207	40.36298	301	D
1615	Bursa	Orhangazi	29.2907	40.42236	348	D
1608	Bursa	Gemlik	29.17928	40.41049	366	C
1607	Bursa	Gemlik	29.09803	40.39437	370	C
1603	Bursa	Yıldırım	29.1296	40.1824	459	C
1605	Bursa	Osmangazi	29.09589	40.27343	488	C
1616	Bursa	Orhangazi	29.25875	40.44975	570	C
1617	Bursa	Orhangazi	29.2993	40.49411	1602	A
1610	Bursa	İnegöl	29.50882	40.06708	252	D
1611	Bursa	İznik	29.71682	40.42923	251	D
1613	Bursa	Keles	29.23367	39.91509	412	C
1614	Bursa	Mustafakemal	28.39392	40.03471	265	D
1618	Bursa	Mudanya	28.92815	40.35095	314	D

Table 3.10. Information on the selected sites in Yalova

Station Code	City	District	Longitude	Latitude	Vs_{30} (m/s)	NEHRP
7707	Yalova	Çınarcık	29.0788	40.6381	312	D
7711	Yalova	Çiftlikköy	29.32709	40.65942	199	D
7706	Yalova	Armutlu	28.82662	40.51305	277	D
7712	Yalova	Altınova	29.50883	40.69286	280	D
7709	Yalova	Yalova Merkez	29.30603	40.56416	382	C

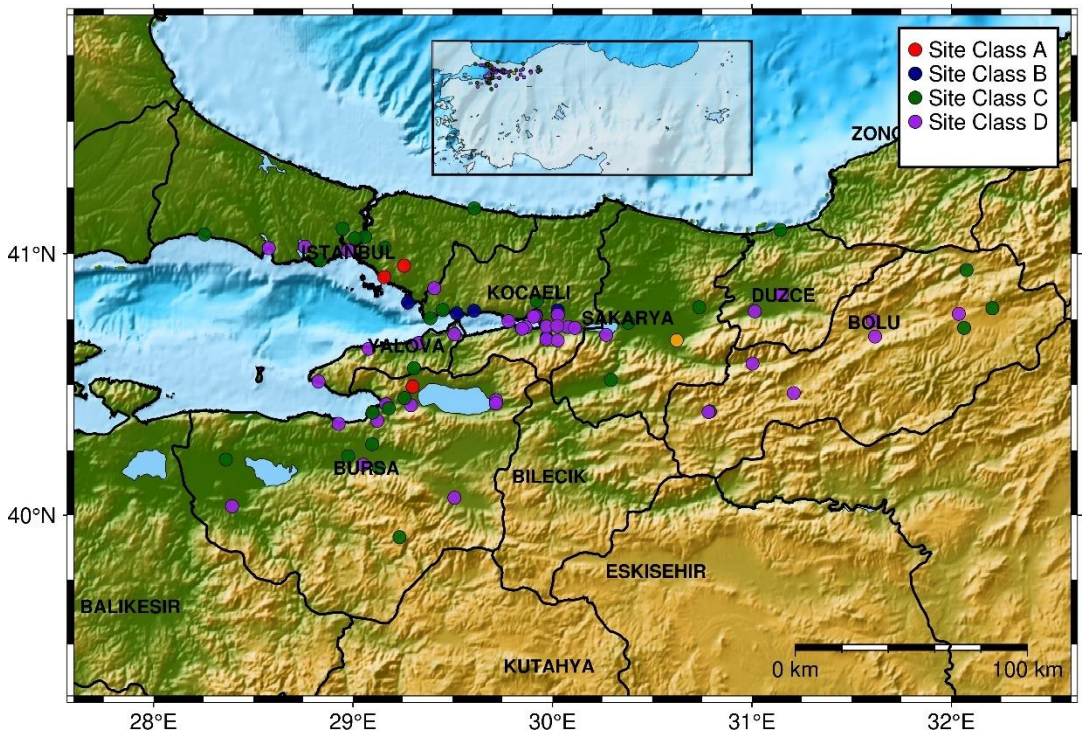

Figure 3.2. Location map of the selected stations and distribution of their NEHRP site classes in Northwestern Türkiye (red point indicates site class A, blue indicates B, green indicates C, purple indicates D)

Counts for V_{s30} values of the selected sites along with the boundaries of NEHRP site classes are provided in Figure 3.3. Per each NEHRP site class, shear wave velocity profiles at the selected stations are demonstrated in Figure 3.4 - Figure 3.7.

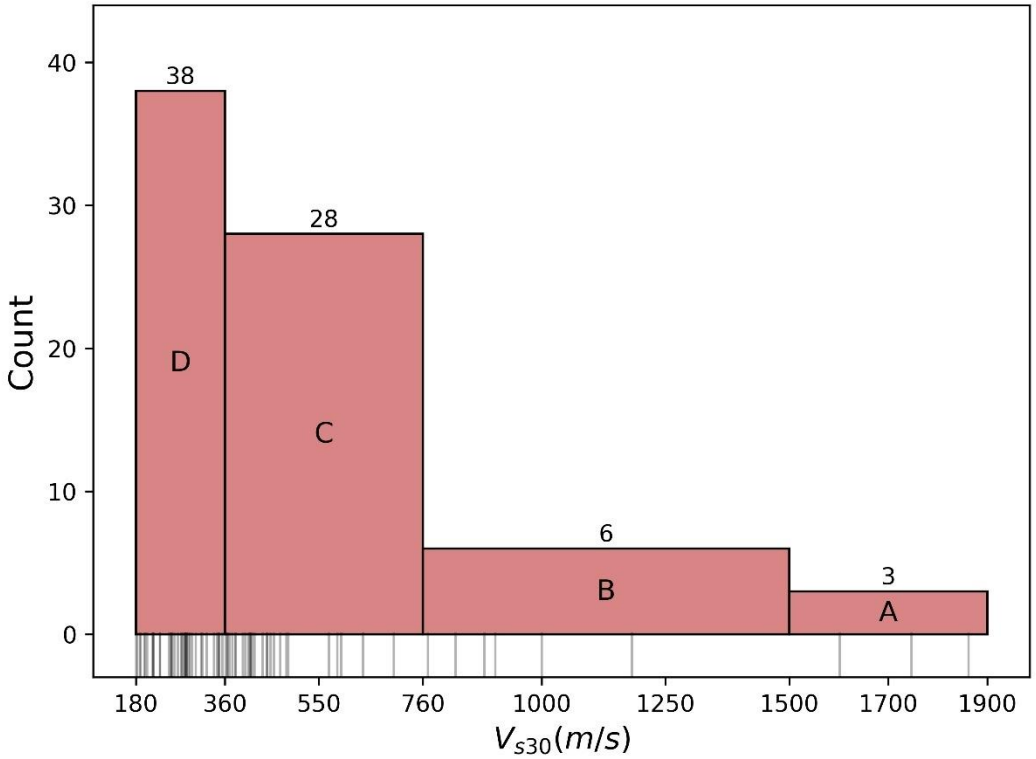

Figure 3.3. Counts for various V_{s30} bins and boundaries for NEHRP site classes

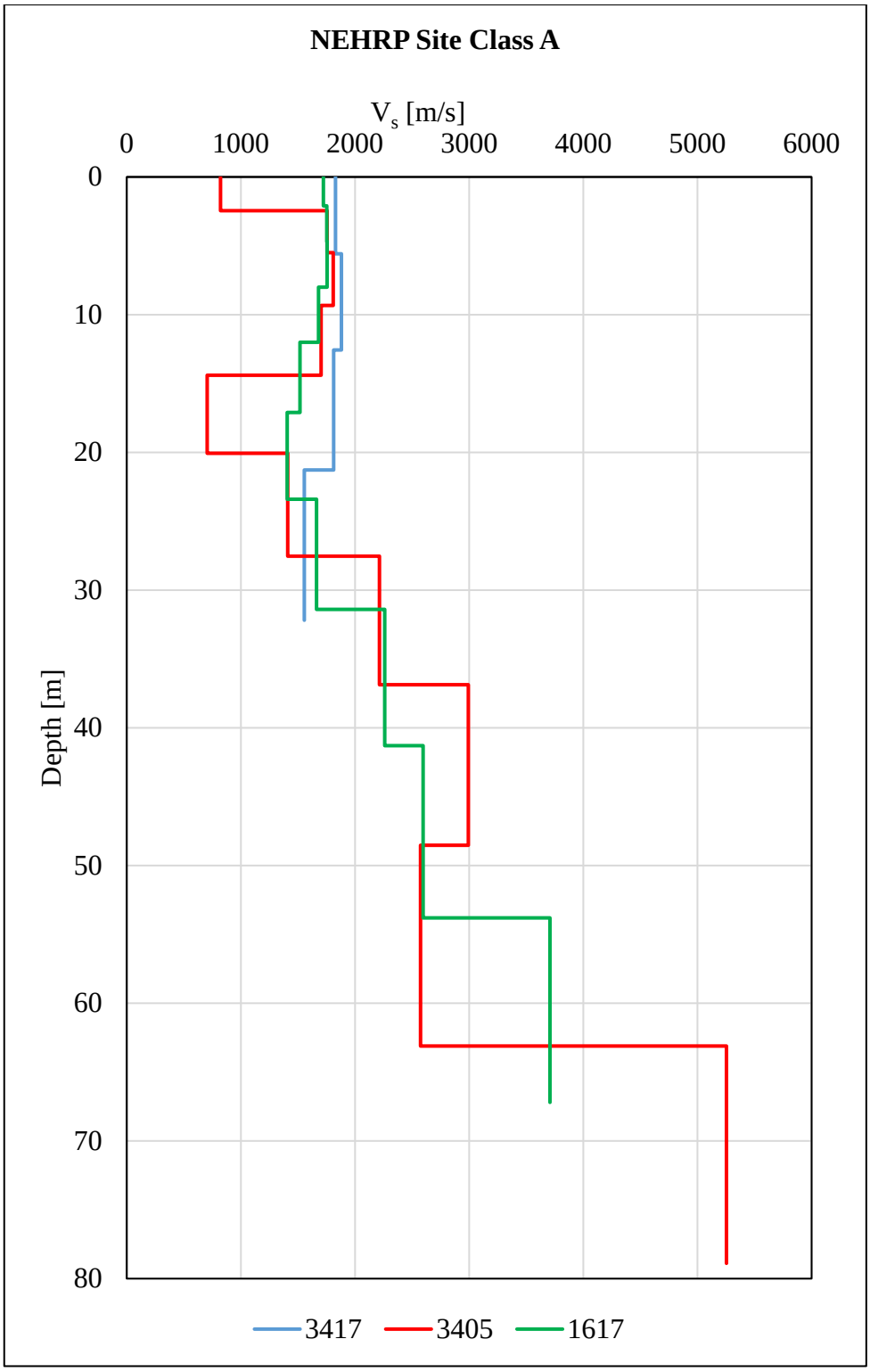

Figure 3.4. Shear wave velocity profiles at each selected stations with site class A according to NEHRP site classification

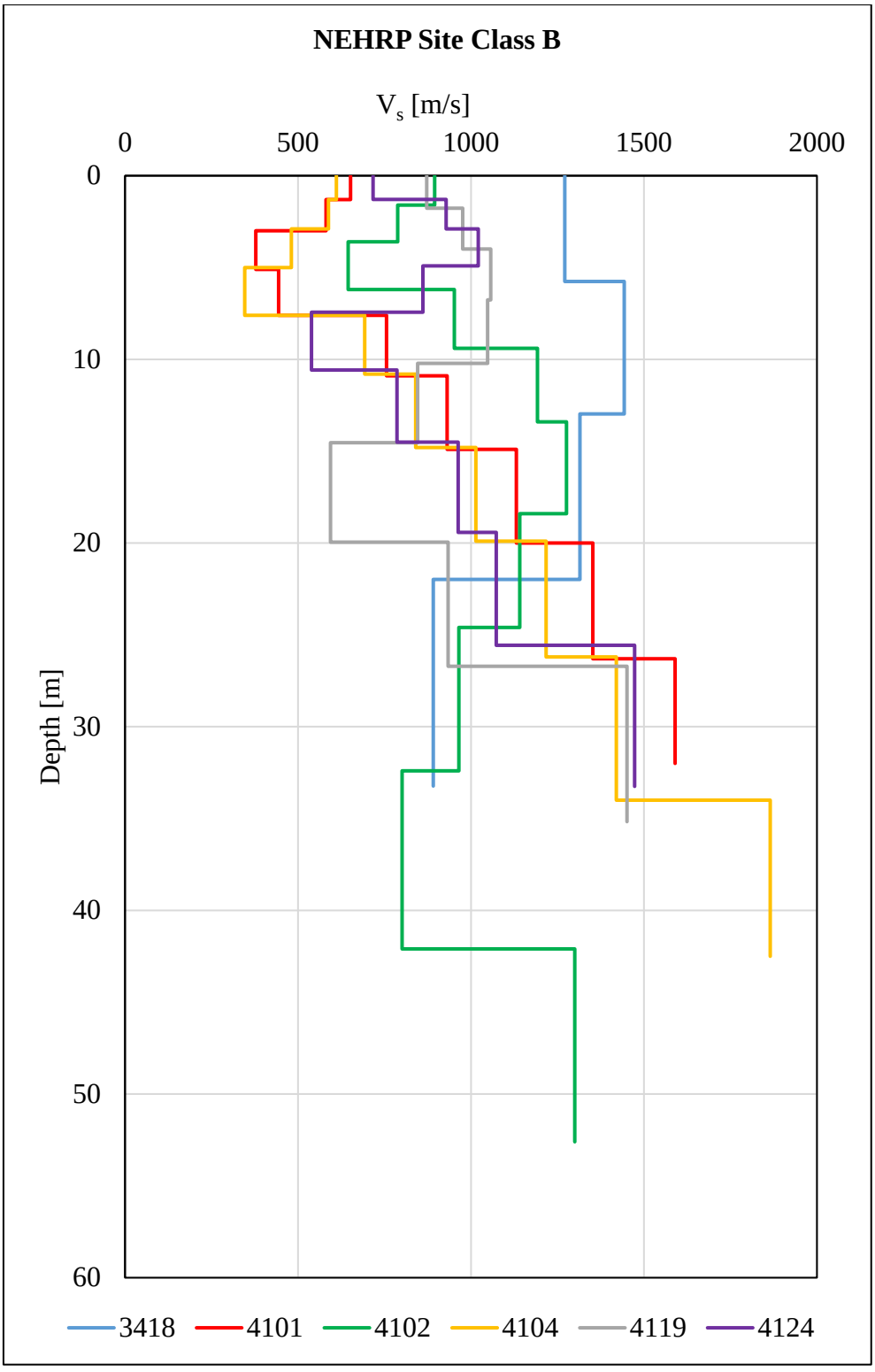

Figure 3.5. Shear wave velocity profiles at each selected station with site class B according to NEHRP site classification

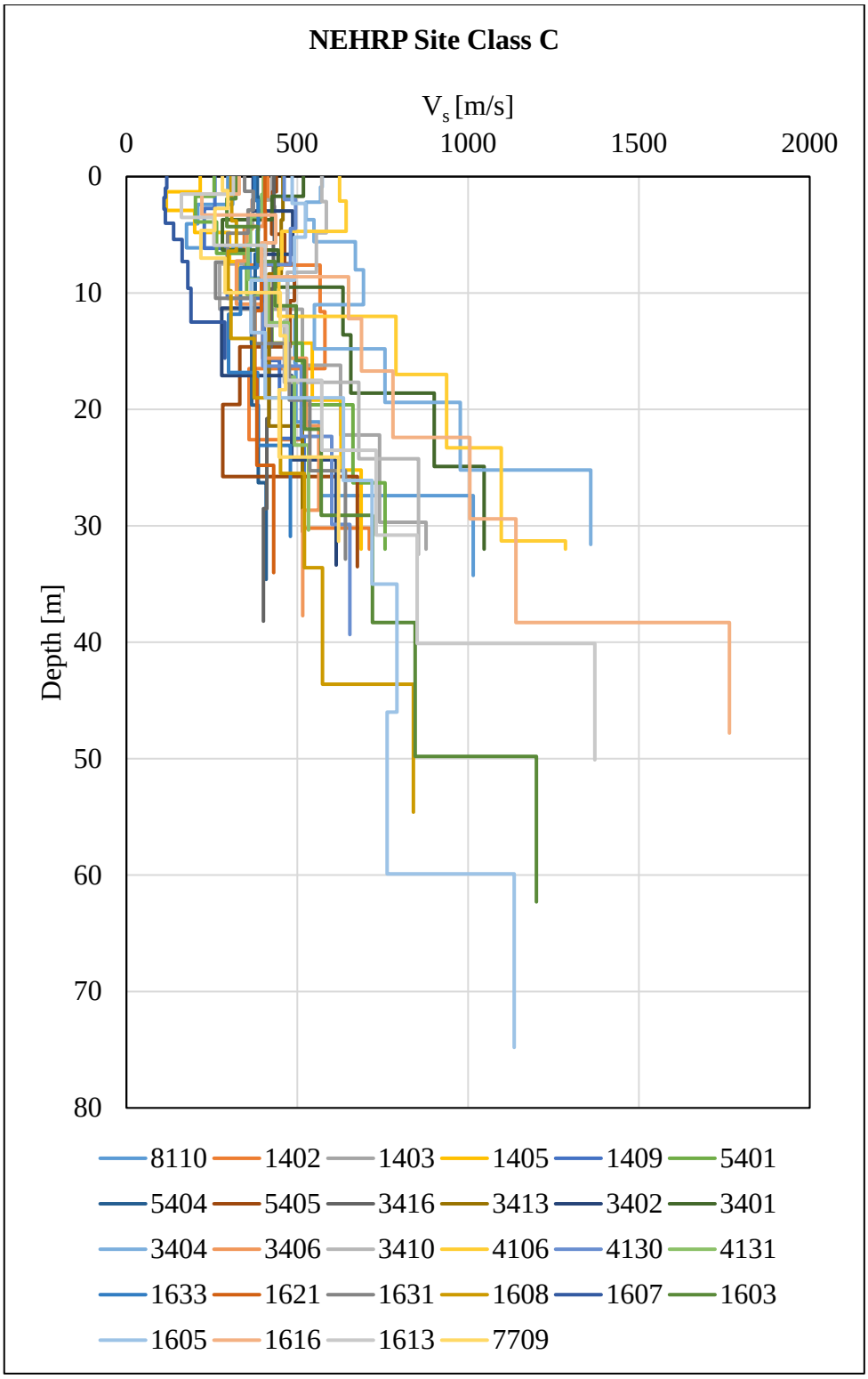

Figure 3.6. Shear wave velocity profiles at each selected station with site class C according to NEHRP site classification

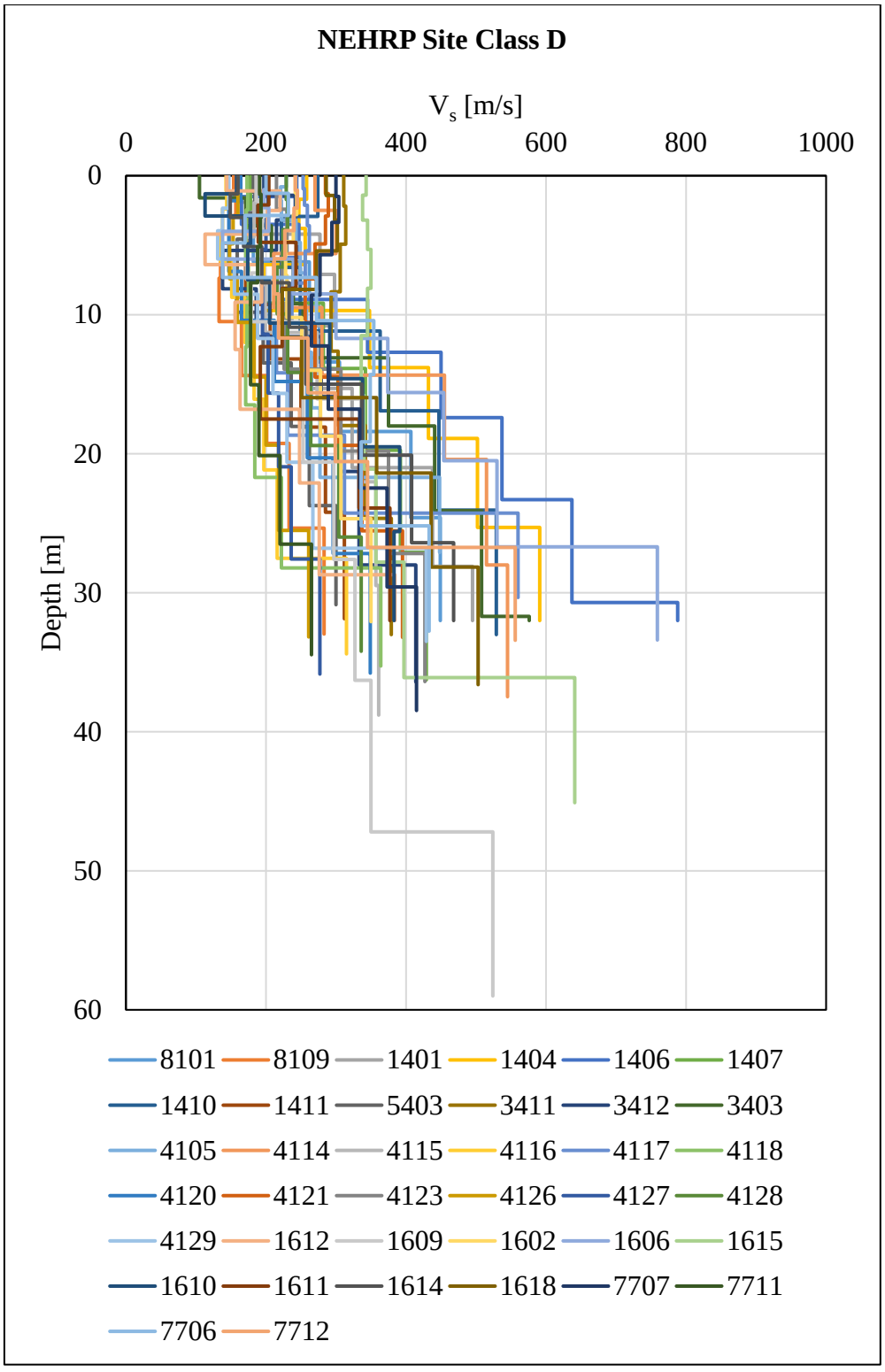

Figure 3.7. Shear wave velocity profiles at each selected station with site class D according to NEHRP site classification

The S-wave velocity profile estimations at the presented stations are performed with multichannel analysis of surface waves (MASW) method by Sandikkaya et al. (2010). MASW method is performed using 48 receivers with 4.5-Hz geophones at 2 m spacings under a 50 kg weight drop. Further details which are omitted herein can be found in Sandikkaya et al. (2010) and the corresponding technical report by Middle East Technical University Earthquake Engineering Research Center (2006). Shear wave velocity (V_s) profiles used in this study and shown in Figure 3.4 -Figure 3.7 are tabulated in Tables A.1-A.17 (Appendix A).

3.3 Input Rock Ground Motion Database

3.3.1 General

Past global earthquake records obtained at rock sites are selected from the NGA-West2 database and used as input rock motions in site response analyses. Weak motions show elastic soil behavior while strong motions represent the inelastic and indeed more realistic behavior during large events including soil nonlinearity. Thus, in this study, both strong and weak motions are used in order to see the effect of the events with different magnitudes on the amplification factors.

The strong-motion dataset includes 40 different strong motion records with V_{s30} values between 650 and 1000 m/s, of events with magnitudes greater than 6.0, and Joyner-Boore (R_{jb}) distances up to 50 km. R_{jb} distance indicates the closest distance to the horizontal projection of the rupture.

The weak motion dataset includes 40 different weak motion records with V_{s30} values between 650 and 1000 m/s, magnitudes between 3.0 and 5.0, and R_{jb} distances up to 50 km. Selection criteria for strong and weak motions are summarized in Table 3.11. The records, i.e., acceleration time histories, satisfying these criteria are randomly selected from the PEER NGA-West2 ground motion database.

Table 3.11. Selection criteria for input ground motion records

Criteria	Strong Motion Records	Weak Motion Records
Number of Records	40	40
V_{s30} (m/s)	650 - 1000	650 - 1000
Magnitude (M_w)	≥ 6.0	3.0 – 5.0
R_{jb} distance (km)	0 – 50	0 – 50

3.3.2 Strong Motion Dataset

Among the selected strong motion records, 5 out of 40 are from Northwestern Türkiye, and the remaining are from different regions in the world with similar seismotectonics (e.g., Taiwan, Japan, Northridge, Iwate, Loma Prieta earthquakes). The peak ground acceleration (PGA) of the selected strong motion records varies between 0.06 and 0.73 g, with a mean of 0.29 g. The mean V_{s30} values of the recording stations is 823 m/s. Further information on the selected strong motion records including the earthquake name and magnitude, the sequence number, R_{jb}, PGA of the record and V_{S30} of the recording station are provided (Table 3.12).

Table 3.12. Information on the selected strong motion records

Record Sequence Number	Earthquake Name	Earthquake Magnitude (M_w)	Joyner-Boore Dist. (km)	V_{s30} (m/s) at the recording station	PGA (g)
1520	Chi-Chi, Taiwan	7.6	4.7	665	0.52
3925	Tottori, Japan	6.6	15.2	940	0.15
5810	Iwate	6.9	21.1	655	0.16

Table 3.12. (cont'd.)

Record Sequence Number	Earthquake Name	Earthquake Magnitude (M_w)	Joyner-Boore Dist. (km)	V_{s30} (m/s) at the recording station	PGA (g)
5810	Iwate	6.9	21.1	655	0.16
1520	Chi-Chi, Taiwan	7.6	4.7	665	0.52
5809	Iwate	6.9	17.3	655	0.25
3926	Tottori, Japan	6.6	24.8	694	0.24
3954	Tottori, Japan	6.6	15.6	967	0.2
1011	Northridge-01	6.7	15.1	1223	0.14
1161	Kocaeli, Türkiye	7.5	7.6	792	0.19
4842	Chuetsu-oki	6.8	18.6	655	0.46
1023	Northridge-01	6.7	24.9	671	0.19
5815	Iwate	6.9	22.4	655	0.2
1165	Kocaeli, Türkiye	7.5	3.6	811	0.19
1165	Kocaeli, Türkiye	7.5	3.6	811	0.19
4213	Niigata, Japan	6.6	25.3	655	0.39
2632	Chi-Chi, Taiwan-03	6.2	3.7	665	0.12
5618	Iwate	6.9	16.3	826	0.27
763	Loma Prieta	6.9	9.2	730	0.34
5806	Iwate	6.9	22.4	655	0.2
1023	Northridge-01	6.7	24.9	671	0.19
1350	Chi-Chi, Taiwan	7.6	33.3	665	0.21
2661	Chi-Chi, Taiwan-03	6.2	21.1	653	0.13
879	Landers	7.3	2.2	1369	0.73
810	Loma Prieta	6.9	12	714	0.46
8164	Duzce, Türkiye	7.1	2.7	690	0.29
879	Landers	7.3	2.2	1369	0.73
3548	Loma Prieta	6.9	3.2	1070	0.44

Table 3.12. (cont'd.)

Record Sequence Number	**Earthquake Name**	**Earthquake Magnitude (M_w)**	**Joyner-Boore Dist. (km)**	**V_{s30} (m/s) at the recording station**	**PGA (g)**
1234	Chi-Chi, Taiwan	7.6	27.6	665	0.17
1161	Kocaeli, Türkiye	7.5	7.6	792	0.19
1050	Northridge-01	6.7	4.9	2016	0.42
3509	Chi-Chi, Taiwan-06	6.3	32.1	653	0.06
1284	Chi-Chi, Taiwan	7.6	44	677	0.08
1787	Hector Mine	7.1	10.4	726	0.31
1551	Chi-Chi, Taiwan	7.6	9.8	653	0.21
765	Loma Prieta	6.9	8.8	1428	0.43
5806	Iwate	6.9	22.4	655	0.2
1633	Manjil, Iran	7.4	12.6	724	0.52
809	Loma Prieta	6.9	12.2	714	0.37
3954	Tottori, Japan	6.6	15.6	967	0.2

3.3.3 Weak Motion Dataset

In this study, 40 weak motions are selected from different global regions. PGA of the selected weak motion records varies between 0.001 and 0.214 g, with a mean of 0.029 g. The mean V_{s30} value of the recording strong motion stations is 721 m/s. Further information on the selected strong motion records including the earthquake name and magnitude, the sequence number, R_{jb}, PGA of the record and Vs_{30} of the recording station are provided (Table 3.13).

Table 3.13. Information on the selected weak motion records

Record Sequence Number	**Earthquake Name**	**Station Name**	**Earthquake Magnitude (M_w)**	**Joyner-Boore Dist. (km)**	**V_{s30} (m/s) at the recording station**	**PGA (g)**
278	Mammoth Lakes-09	USC McGee Creek	4.9	6.7	654	0.159
1943	Anza-02	Idyllwild - Keenwild Fire Sta.	4.9	2.2	730	0.214
2021	Gilroy	Gilroy Array #6	4.9	11.7	663	0.095
8171	Anza-02	Agave Hill	4.3	20.4	699	0.007
8225	Anza-02	Keenwild Fire Station, Mountain Center, Usa	4.7	15.9	715	0.008
8261	Anza-02	Red Mountain, Riverside Co., Ca, Usa	4.7	48.3	760	0.001
9308	14155260	San Bernardino - Devil Canyon Penstock	4.7	21	669	0.010
9393	14155260	Red Mountain, Riverside Co., Ca, Usa	4.6	33.3	729	0.029
9484	10410337	Donna Jones Jenkins	4.5	33.8	760	0.001
10607	10370141	Lake Arrowhead - Hwy 173 & Oak	4.5	43.7	699	0.002
10703	14312160	Donna Jones Jenkins	4.5	18.8	699	0.057

Table 3.13. (cont'd)

Record Sequence Number	Earthquake Name	Station Name	Earthquake Magnitude (M_w)	Joyner -Boore Dist. (km)	V_{s30} (m/s) at the recording station	PGA (g)
11059	21522424	Gilroy - Gavilan Coll.	4.5	19.4	686	0.018
11067	21522424	Pacheco Peak, CA, USA	4.5	20.2	695	0.018
11101	21530368	Carmenet Vineyards, Sonoma, CA, USA	4.3	23	796	0.011
11123	21530368	Beebe Ranch	4.3	37.5	763	0.002
11126	21530368	Forestville	4.3	29.7	786	0.003
11128	21530368	Mt. St. Helena South	4.3	44.3	691	0.003
11133	21530368	Sonoma Mountain	4.3	29.2	710	0.002
11162	21149422	Lick Observatory, Mt. Hamiliton, CA, USA	4.3	14.9	730	0.023
11434	10275733	Pleasants Peak	4.3	7.4	663	0.106
11686	40234037	Lick Observatory, Mt. Hamiliton, CA, USA	4.3	20.4	687	0.006
11703	40234037	San Jose - Santa Teresa Hills	4.5	49.8	688	0.031

Table 3.13. (cont'd)

Record Sequence Number	**Earthquake Name**	**Station Name**	**Earthquake Magnitude (M_w)**	**Joyner-Boore Dist. (km)**	**V_{s30} (m/s) at the recording station**	**PGA (g)**
11786	9173365	Arcadia; Chantry Flat Forest Station Foothill Blvd	4.5	10.7	760	0.034
11811	9173365	Griffith Park Observatory	4.5	29.9	652	0.007
11998	14077668	Wheeler Gorge Ranger Station	4.5	11.1	760	0.018
12150	30225889	Forestville	4.5	40.6	760	0.011
12178	21455182	Atlas Peak	4.5	28.4	742	0.006
12229	40199209	China Camp	4.5	32.9	760	0.003
12256	40199209	Mill Valley MUNI Golf Course	4.5	31.3	760	0.003
12448	21266207	Russellman Park	4.5	24	760	0.007
12539	51207740	San Andreas Cal.	4.5	1	665	0.119

Table 3.13. (cont'd)

Record Sequence Number	**Earthquake Name**	**Station Name**	**Earthquake Magnitude (M_w)**	**Joyner-Boore Dist. (km)**	**V_{s30} (m/s) at the recording station**	**PGA (g)**
12975	30226086	Geyserville; Warm Springs Dam; Right Abutment	4.5	48.1	760	0.018
12977	30226086	Geyserville; Warm Springs Dam; Right Abutment, Downstream	4.5	6.4	760	0.027
13737	9735129	Pleasants Peak	4.4	4.9	710	0.018
13798	10295849	Lake Arrowhead - Hwy 173 & Oak	4.4	40.1	669	0.003
14398	10319993	Hector	4.4	22.2	750	0.002
14963	51177644	Taylor Mountain	4.4	42.2	847	0.001
18025	14517500	Manuel Prospect Mine	4.8	15.8	699	0.020
18174	14519940	Cerro Gordo	4.7	45.7	652	0.014
18378	14158696	Mentone, Greenspot Rd.	4.7	11.7	699	0.024

CHAPTER 4

RESULTS OF 1-D SITE RESPONSE ANALYSES

4.1 Generic Site Amplification Factors

One-dimensional site response analysis yields the motion at the ground surface layer (top layer) given the input bedrock motion. Site amplification factors are calculated as follows:

$$AF(T) = SA_{GS}(T)/SA_I(T) \tag{4.1}$$

where T is the period of response spectra, SA_{GS} and SA_I are the 5% damped spectral acceleration in units of g at the ground surface and of the input motion at bedrock level, respectively. In other words, the amplification factors in the period domain are simply obtained by dividing the response spectrum of the motion computed at the top layer by the response spectrum of input motions. One example output from DEEPSOIL program can be found in Appendix B.

The mean amplification factors for each NEHRP site class in this thesis are obtained by taking the average amplification at the stations of the same site class in Northwestern Türkiye. Eight different mean curves are obtained for four different NEHRP site classes (A, B, C, and D) from site response analyses performed with strong and weak input motions. The number of stations used in this study concerning their NEHRP site classification is shown in Table 4.1. It is worth mentioning that the amplification factors from this thesis corresponds to mean shear wave velocities of 1737, 928, 452, and 264 m/sec for classes A, B, C, and D, respectively. Figure 4.1 - Figure 4.4 display the average amplifications with standard deviations for each site class.

Table 4.1. Number of stations used in this thesis based on NEHRP site classification

NEHRP Site Class	Number of Stations
A	3
B	6
C	28
D	38

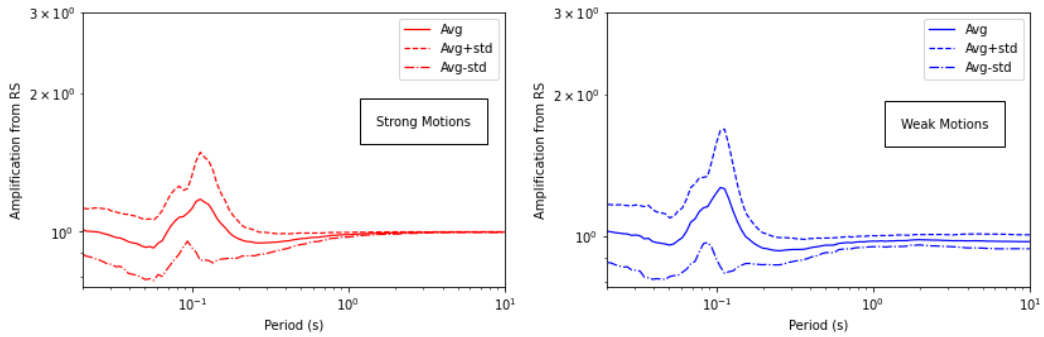

(a) (b)

Figure 4.1. Mean amplification factors in Northwestern Türkiye for NEHRP Site Class A with (a) strong motion (b) weak motion inputs

The characteristics of mean amplification factors for NEHRP site class A are shown in Figure 4.1. For NEHRP site class A, the amplification curve from strong motion records leads to a predominant period of 0.11 s., with a corresponding mean peak amplification factor of 1.18, while these values are found as 0.10 s. and 1.27, respectively, with weak motion records. The strong motion input for site class A yields an 8% lower mean amplification value than the weak motion input. However, the predominant period values do not show any significant difference for weak and strong ground motion inputs.

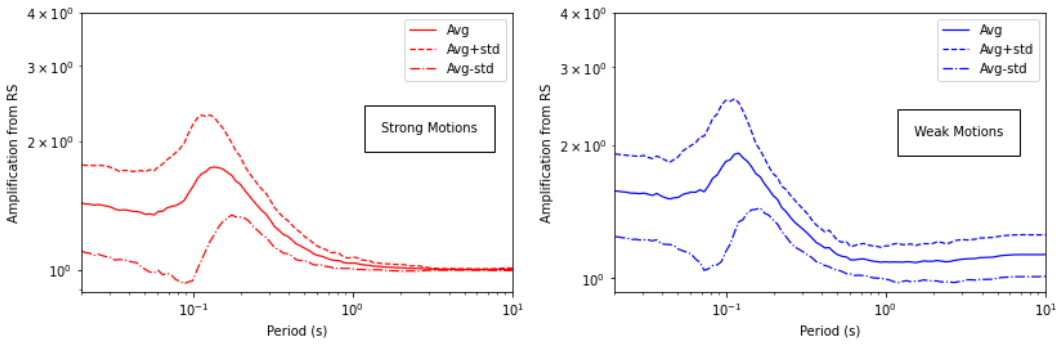

(a) (b)

Figure 4.2. Mean amplification factors in Northwestern Türkiye for NEHRP Site Class B with (a) strong motion (b) weak motion inputs

For NEHRP site class B, the transfer function from strong motion records gives a fundamental period of 0.14 s. with a corresponding peak amplification factor of 1.74, while these values are 0.12 s. and 1.92, respectively, with weak motion records (Figure 4.2). The strong motion input for site class B yields a 10% lower mean amplification factor when compared to weak motion input. Yet, similar to site class A, the predominant period values for site class B do not show any significant difference for weak and strong ground motion inputs. The standard deviations for site B are larger than those of site A. This is anticipated due to the more variable and complex behavior of soil layers (including both amplification and damping) as the soil gets softer at any site of interest.

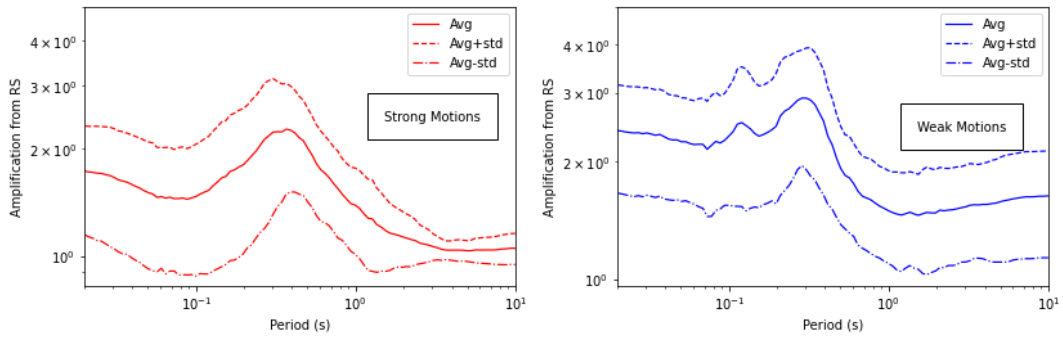

(a) (b)

Figure 4.3. Mean amplification factors in Northwestern Türkiye for NEHRP Site Class C with (a) strong motion (b) weak motion inputs

For NEHRP site class C, the transfer function with strong motion input gives a fundamental period of 0.37 s. with a corresponding peak amplification factor of 2.26, while these values are 0.29 s. and 2.91, respectively, with weak motion records (Figure 4.3). The analyses with strong motion input for site class C have 29% lower peak amplification factors when compared to that with weak motion input. The fundamental period with strong motion input is 28% larger when compared to the one with weak motion input. It is observed that, as the soil class gets softer differences between strong and weak motion inputs become more significant and clearer.

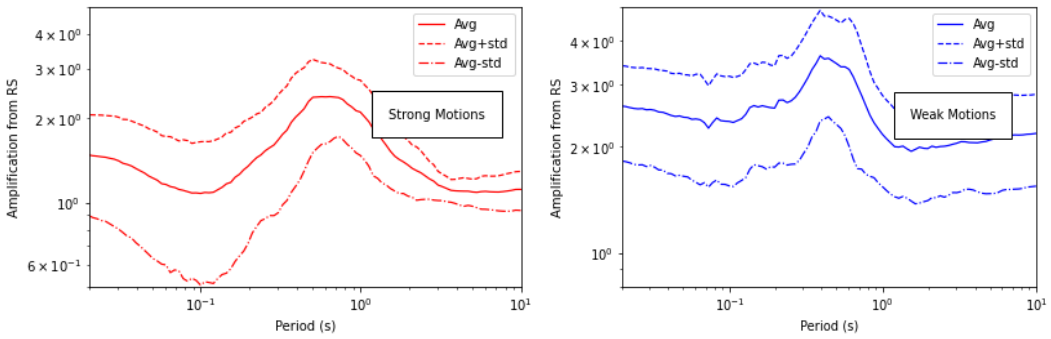

(a) (b)

Figure 4.4. Mean amplification factors in Northwestern Türkiye for NEHRP Site Class D with (a) strong motion (b) weak motion inputs

For NEHRP site class D, the amplification curve from strong motion records yields a fundamental period of 0.64 s. with a corresponding peak amplification factor of 2.38, while these values are 0.39 s. and 3.62, respectively, with weak motion records (Figure 4.4). The site response analyses with strong motion input for site class D have 52% lower peak amplification factors when compared to that with weak motion input. The fundamental period for site class D with strong motion input is 64% larger when compared to the one with weak motion input.

Amplification curves obtained with strong and weak motion inputs for different site classes are similar in shape but different in amplitudes. In contrast to hard rock sites, where amplifications are often less than 1.27, stiff soil sites can have amplifications up to 3.6 at longer periods.

As a general trend, the fundamental peaks shift to longer periods when analyzed with strong motion records. Similarly, amplifications have higher values when analyzed with weak motion records compared to strong motion records at soil sites. Both of these observations which are more obvious at softer soil sites could be attributed to nonlinearity. When the mean transfer functions are examined according to the NEHRP classes, very clear and anticipated physical differences are observed: Stiffer

sites will amplify high frequencies, while softer sites will amplify low frequencies (e.g.: Kramer, 1996).

4.2 Gaussian Fits for the Site Amplification Spectra

The resulting mean generic amplification factors are next fitted by a Gaussian function. The Gaussian function is found to be the one that best represents the period-dependent generic amplification functions.

The goal is to define the best fit model for the amplification factors as a function of period. These fitted Gaussian functions can be used to deduce values of amplification factors when there is no available local or site-specific data. A Gaussian function is in the following form:

$$f(x) = \alpha * e^{-(x-b)^2/2c^2} \tag{4.2}$$

where α,b and c are the arbitrary constants. The number of terms used in Gaussian functions depends completely on the target model. As the number of terms increases, the model fit can get closer to the actual data. The goodness-of-fit measure for the regression model is indicated with R-square (R^2) term which takes values between 0 and 1 (0% – 100%). Usually, as the R^2 value gets larger, the regression model fits the data better.

All of the theoretical transfer functions obtained in this study as a function of NEHRP site class A, B, C and D with both strong motion and weak motion records are fitted (Figure 4.5 - Figure 4.8). The constants for the Gaussian fits are provided along with the corresponding figures placed directly below the fit.

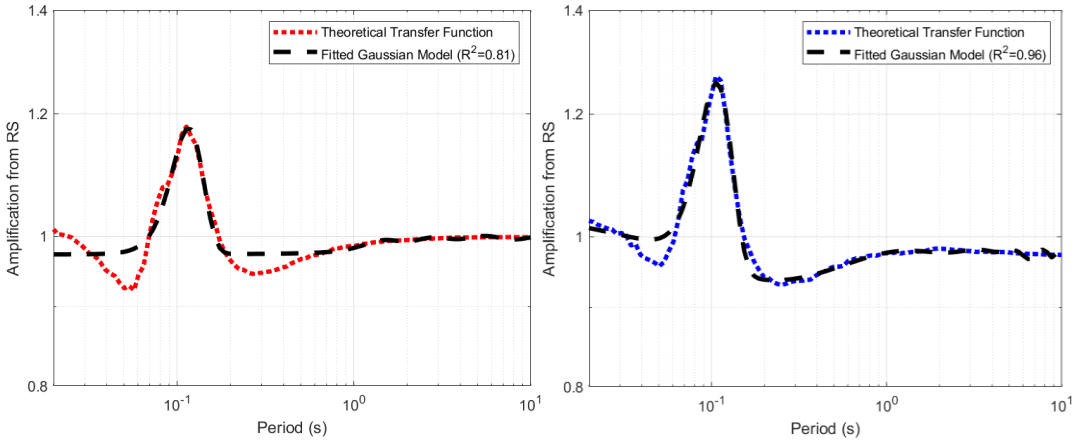

(a) (b)

$$AF_{strong-A}(f) =$$
$$a1 * \exp\left(-\left((f-b1)/c1\right)^2\right) +$$
$$a2 * \exp\left(-\left((f-b2)/c2\right)^2\right) +$$
$$a3 * \exp\left(-\left((f-b3)/c3\right)^2\right) +$$
$$a4 * \exp\left(-\left((f-b4)/c4\right)^2\right) +$$
$$a5 * \exp\left(-\left((f-b5)/c5\right)^2\right)$$

a1 = 0.2016
b1 = 0.1161
c1 = 0.03294
a2 = 1.162
b2 = 134.3
c2 = 318.7
a3 = 0.01384
b3 = 5.082
c3 = 2.048
a4 = 0.0144
b4 = 2.63
c4 = 0.9677
a5 = 0.01345
b5 = 1.421
c5 = 0.4641

R-square: 0.8079

$$AF_{weak-A}(f) =$$
$$a1 * exp(-(f-b1)/c1)^2) +$$
$$a2 * \exp\left(-\left((f-b2)/c2\right)^2\right) +$$
$$a3 * \exp\left(-\left((f-b3)/c3\right)^2\right) +$$
$$a4 * \exp\left(-\left((f-b4)/c4\right)^2\right) +$$
$$a5 * \exp\left(-\left((f-b5)/c5\right)^2\right) +$$
$$a6 * \exp\left(-\left((f-b6)/c6\right)^2\right) +$$
$$a7 * \exp\left(-\left((f-b7)/c7\right)^2\right) +$$
$$a8 * \exp\left(-\left((f-b8)/c8\right)^2\right)$$

a1 = 0.3033	b1 = 0.1071
c1 = 0.03207	a2 = 1.755e+12
b2 = -5.419	c2 = 0.9871
a3 = 0.7344	b3 = 3.7
c3 = 2.235	a4 = 0.8101
b4 = 7.907	c4 = 1.916
a5 = 0.7712	b5 = 10.42
c5 = 1.673	a6 = 0.4221
b6 = 5.726	c6 = 1.618
a7 = 0	b7 = 10.26
c7 = 0.005749	a8 = 0.8623
b8 = 0.3357	c8 = 2.54

R-square: 0.9688

Figure 4.5. Gaussian fit for the mean theoretical transfer function in Northwestern Türkiye based on NEHRP site class A with (a) strong motion (b) weak motion records

Gaussian function for the theoretical transfer function in Northwestern Türkiye based on NEHRP site class A with strong motion is indicated with $AF_{strong-A}(f)$ as a function of frequency in Figure 4.5. The R^2 value is found to be 0.81 with five terms for this function. $AF_{weak-A}(f)$ represents the function derived for NEHRP site class A with weak motion records. The R^2 value is found to be 0.97 with eight terms for this function.

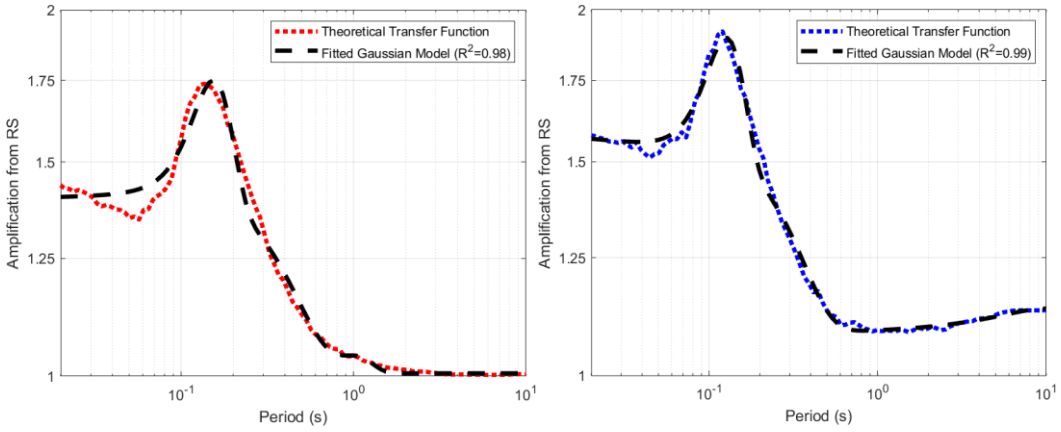

(a) (b)

$AF_{strong-B}(f) =$

$$a1 * \exp\left(-\left((f - b1)/c1\right)^2\right) + a2 * \exp\left(-\left((f - b2)/c2\right)^2\right) + a3 * \exp\left(-\left((f - b3)/c3\right)^2\right) + a4 * \exp\left(-\left((f - b4)/c4\right)^2\right)$$

a1 =	0.3656
b1 =	0.1558
c1 =	0.05727
a2 =	0.4006
b2 =	0.05913
c2 =	0.4186
a3 =	1.006
b3 =	55.4
c3 =	2386
a4 =	0.03245
b4 =	1.037
c4 =	0.3345

R-square: 0.9827

$AF_{weak-B}(f) =$

$$a1 * \exp\left(-\left((f - b1)/c1\right)^2\right) + a2 * \exp\left(-\left((f - b2)/c2\right)^2\right) + a3 * \exp\left(-\left((f - b3)/c3\right)^2\right) + a4 * \exp\left(-\left((f - b4)/c4\right)^2\right) + a5 * \exp\left(-\left((f - b5)/c5\right)^2\right)$$

a1 =	0.4045
b1 =	0.1278
c1 =	0.04659
a2 =	2.773
b2 =	-1.253
c2 =	28.5
a3 =	0.3751
b3 =	0.1119
c3 =	0.2648
a4 =	-1.701
b4 =	-2.09
c4 =	21.44
a5 =	1.318e+12
b5 =	-4.472
c5 =	0.8227

R-square: 0.9937

Figure 4.6. Gaussian fit for the mean theoretical transfer function in Northwestern Türkiye based on NEHRP site class B with (a) strong motion (b) weak motion records

Gaussian fit for the theoretical transfer function based on NEHRP site class B with strong motion is indicated with $AF_{strong-B}(f)$. The R^2 value is found 0.98 with four terms for this function. Similarly, $AF_{weak-B}(f)$ symbolize the function based on NEHRP site class B with weak motion records. The R^2 value is found to be 0.99 with five terms for this function.

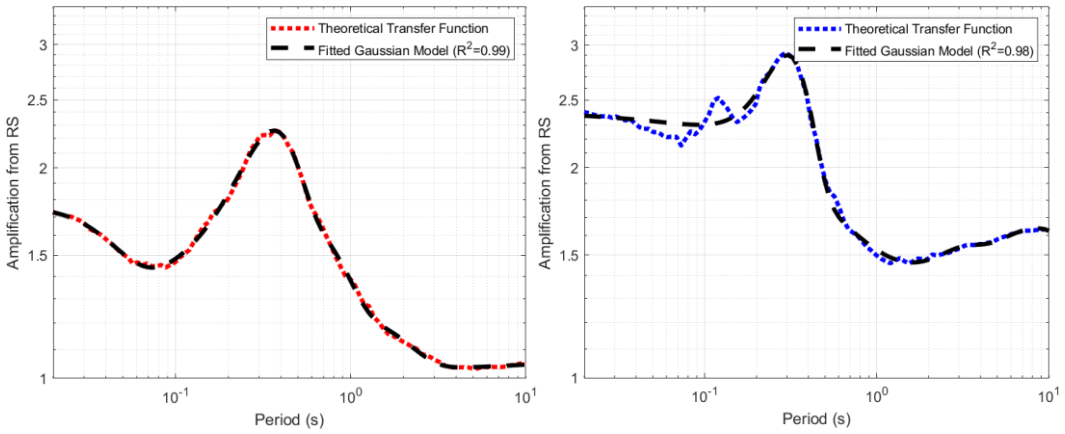

(a) (b)

$AF_{strong-C}(f) =$

$$a1 * \exp\left(-\left((f - b1)/c1\right)^2\right) +$$
$$a2 * \exp\left(-\left((f - b2)/c2\right)^2\right) +$$
$$a3 * \exp\left(-\left((f - b3)/c3\right)^2\right) +$$
$$a4 * \exp\left(-\left((f - b4)/c4\right)^2\right) +$$
$$a5 * \exp\left(-\left((f - b5)/c5\right)^2\right)$$

a1 =	0.7433
b1 =	0.345
c1 =	0.2024
a2 =	0.4532
b2 =	0.009168
c2 =	0.03854
a3 =	0.4136
b3 =	0.5586
c3 =	0.472
a4 =	0.1761
b4 =	0.9666
c4 =	1.397
a5 =	1.08
b5 =	48.91
c5 =	220

R-square: 0.9989

$AF_{weak-C}(f) =$

$$a1 * \exp\left(-\left((f - b1)/c1\right)^2\right) +$$
$$a2 * \exp\left(-\left((f - b2)/c2\right)^2\right) +$$
$$a3 * \exp\left(-\left((f - b3)/c3\right)^2\right) +$$
$$a4 * \exp(-((f - b4)/c4)\text{^}2)$$

a1 =	0.9654
b1 =	0.3133
c1 =	0.1366
a2 =	1.638
b2 =	8.48
c2 =	16.63
a3 =	1.648e+12
b3 =	-30.69
c3 =	5.8
a4 =	0.06598
b4 =	2.833
c4 =	1.277

R-square: 0.9873

Figure 4.7. Gaussian fit for the mean theoretical transfer function in Northwestern Türkiye based on NEHRP site class C with (a) strong motion (b) weak motion records

The Gaussian fit for the theoretical transfer function based on NEHRP site class C with strong motion is indicated with $AF_{strong-C}(f)$. R^2 value is found 0.99 with five terms for this function. $AF_{weak-C}(T)$ symbolize the function based on NEHRP site class C with weak motion records. The R^2 value is found to be 0.98 with four terms for this function.

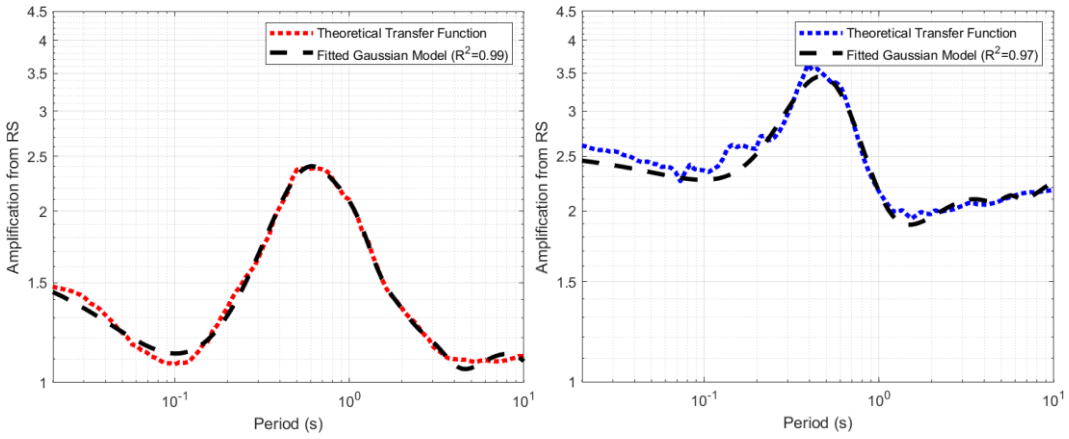

(a) (b)

$$AF_{strong-D}(f) =$$
$$a1 * exp\left(-\left((x-b1)/c1\right)^2\right) +$$
$$a2 * exp\left(-\left((x-b2)/c2\right)^2\right) +$$
$$a3 * exp\left(-\left((x-b3)/c3\right)^2\right) +$$
$$a4 * exp\left(-\left((x-b4)/c4\right)^2\right) +$$
$$a5 * exp\left(-\left((x-b5)/c5\right)^2\right) +$$
$$a6 * exp\left(-\left((x-b6)/c6\right)^2\right) +$$
$$a7 * exp\left(-\left((x-b7)/c7\right)^2\right)$$

a1 =	0.9681	b1 =	0.8419
c1 =	0.4811	a2 =	0.3621
b2 =	1.42	c2 =	0.7438
a3 =	0.8514	b3 =	0.4782
c3 =	0.2994	a4 =	0
b4 =	1.319	c4=	0.002782
a5 =	1.395e+07	b5 =	-1.655
c5 =	0.4061	a6 =	0.2999
b6 =	2.331	c6 =	1.415
a7 =	1.123	b7 =	7.99
c7 =	11.72		

R-square: 0.994

$$AF_{weak-D}(f)$$
$$a1 * exp(-(f-b1)/c1)^2) +$$
$$a2 * \exp\left(-\left((f-b2)/c2\right)^2\right) +$$
$$a3 * \exp\left(-\left((f-b3)/c3\right)^2\right) +$$
$$a4 * \exp\left(-\left((f-b4)/c4\right)^2\right) +$$
$$a5 * \exp\left(-\left((f-b5)/c5\right)^2\right) +$$
$$a6 * \exp\left(-\left((f-b6)/c6\right)^2\right)$$

a1 =	-4.508	b1 =	0.04255
c1 =	0.3194	a2 =	221
b2 =	-1.068	c2 =	0.8985
a3 =	-236.7	b3 =	-1.096
c3 =	0.8702	a4 =	2.477
b4 =	18.67	c4 =	28.49
a5 =	0.252	b5 =	2.963
c5 =	1.887	a6 =	0.08866
b6 =	5.63	c6 =	0.7901

R-square: 0.9759

Figure 4.8. Gaussian fit for the mean theoretical transfer function in Northwestern Türkiye based on NEHRP site class D with (a) strong motion (b) weak motion records

Gaussian function for the theoretical transfer function based on NEHRP site class D with strong motion is indicated with $AF_{strong-D}(f)$. R^2 value is found 0.99 with seven terms for this function. $AF_{weak-D}(f)$ symbolize the function based on NEHRP site class D with weak motion records. The R^2 value is found to be 0.97 with six terms for this function.

In summary, closed-form functions with high R^2 values are fitted to yield generic site amplification functions using representative sites in Northwestern Türkiye for NEHRP site classes A, B, C, and D. These fitted Gaussian functions can be used as amplification factors when there is no available local or site-specific data for various geotechnical and earthquake engineering studies in the future.

4.3 Comparison with Available Generic Amplification Factors for Other Regions

4.3.1 Boore & Joyner (1997) and Klimis et. al. (1999)

The generic amplification factors for Northwestern Türkiye with strong input motion records, the Hellenic (Klimis et al., 1999), and US data (Boore & Joyner, 1997) based on NEHRP C and D site classes are illustrated in Figure 4.9. For consistency with the previous studies, the comparisons are performed in the frequency domain.

While the amplification factors are obtained with the quarter wavelength method in the US and the Hellenic data, 1-D site response analyses are used for Northwestern Türkiye. When the general trend of amplification factors is observed, they increase up to the peak amplification points, then start to decrease. General observation for all of the studies is that NEHRP class C has smaller periods than class D with much smaller amplifications. Amplification functions are in good agreement in terms of both shape and the numerical values.

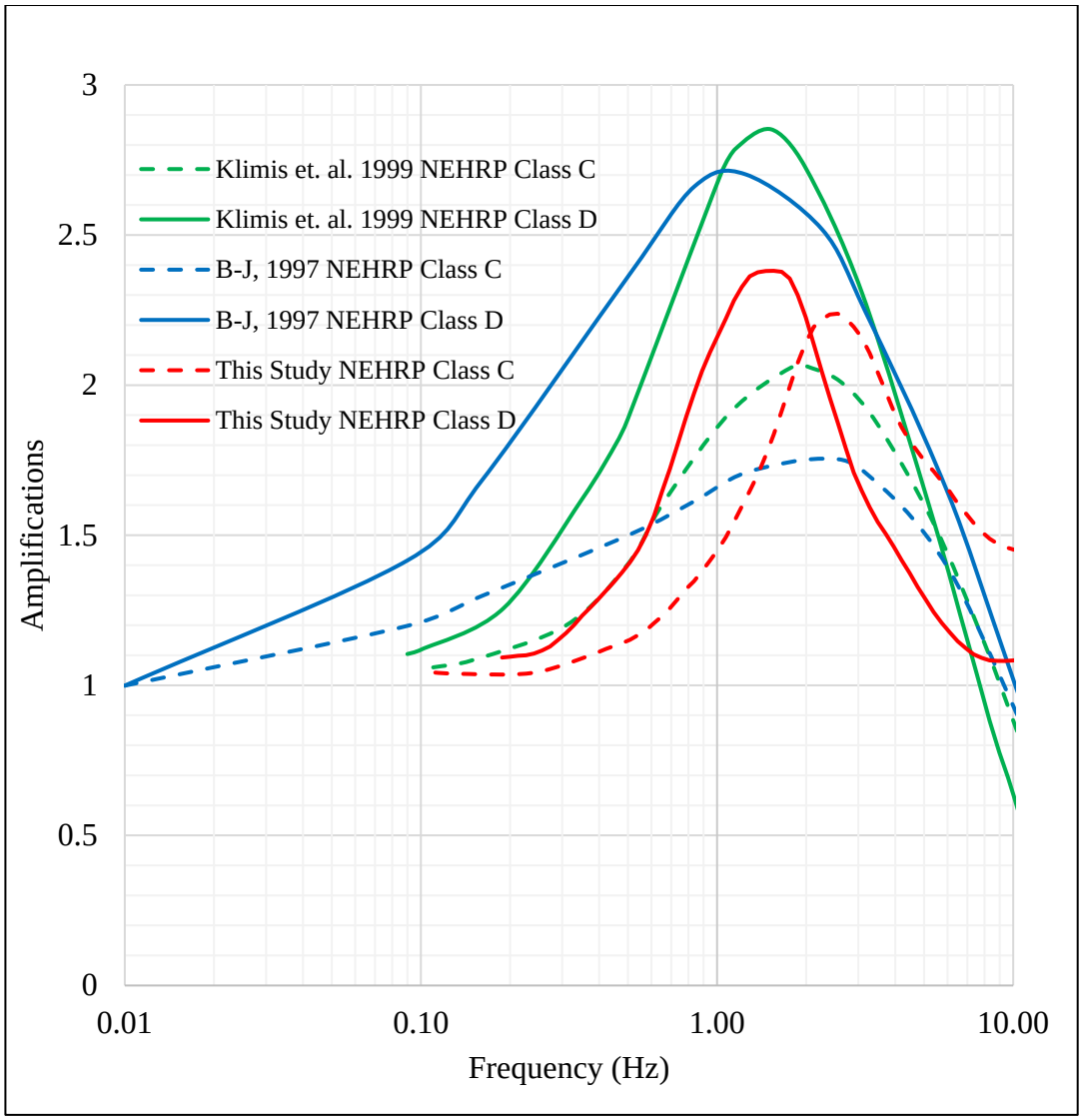

Figure 4.9. Comparison of available generic amplification factors for different regions

The Northwestern Türkiye amplification function presented for NEHRP site class C exhibits the smallest amplification values when compared with the other functions up to nearly 1.6 Hz, while showing the largest after 2 Hz. For site class C, amplification function (AF) from this study has the largest predominant frequency of 2.72 Hz compared to the Hellenic data with 1.78 Hz and the US with 2.26 Hz.

For NEHRP site class D, this study and the Hellenic data show very similar predominant frequencies of 1.55 Hz and 1.52 Hz, respectively. Data from Northwestern Türkiye show the smallest amplifications at all frequency ranges. This can be attributed to the difference in the range of V_s values. Also, the mean V_s value for the Northwestern Türkiye may be larger than those of Hellenic and US data.

As sites become softer, the difference in amplification factors between proposed models get more apparent. These differences are considered to be natural and can be attributed to the local characteristics of surface layers and geology.

CHAPTER 5

STOCHASTIC GROUND MOTION SIMULATION OF THE 1999 DÜZCE (M_W=7.1) EARTHQUAKE WITH ALTERNATIVE SITE AMPLIFICATION FACTORS

5.1 General

The amplification functions proposed in this thesis are used as input to the stochastic simulation model to compare the simulated and observed Fourier amplitude spectra (FAS) of acceleration records from the 12 November 1999 Düzce earthquake. The event (M_w=7.1) occurred on the Düzce fault. The earthquake, causing considerable casualties and losses, has affected an extensive area. The most affected four districts are Kocaeli, Sakarya, Bolu, and Yalova, which contain industrial facilities in Türkiye. The earthquake caused approximately 40 km surface fault rupture on the Düzce fault, with maximum right-lateral offsets of 4 m (Erdik, 2001). In this thesis, the 12 November 1999 Düzce earthquake, on which information is given in Table 5.1, is selected to perform stochastic ground motion simulation. The source mechanism of the earthquake showed a right-lateral strike-slip rupture Düzce fault, a splay of the North Anatolian fault (NAF) zone immediately to the east of the Kocaeli rupture. A total of 32 strong-motion stations within 200 km of the fault, operated by the General Directorate of Disaster Affairs, Kandilli Observatory and Earthquake Research Institute of Bogazici University, and Istanbul Technical University, have recorded the earthquake (Durukal, 2002). DZC, BOL, and IZT stations are selected since their input parameters for the simulations are well-known. The records at selected stations (Table 5.2) within 125 km epicentral distance are simulated in this study. Processed data for the acceleration time histories of the selected stations that recorded the 1999 Düzce earthquake are derived from the AFAD database (https://tadas.afad.gov.tr/).

In the stochastic finite fault simulations of the 1999 Düzce earthquake, a dynamic corner concept of Motazedian & Atkinson (2005) is used. The stochastic finite-fault method is preferred herein particularly since it can effectively model the intermediate to high frequencies (> 1 Hz) of the records, which are of engineering interest (Karimzadeh Naghshineh, 2016).

A stochastic finite-fault model based on a dynamic corner frequency was employed and validated for the 1999 Düzce event by Ugurhan & Askan, (2010); therefore, this study does not provide further theoretical details. Rather, the effect of amplification functions in simulations are assessed herein.

Table 5.1. Information on the 12 November 1999 Düzce Earthquake

Earthquake Name	**12 November 1999 Düzce Earthquake**
Date	12 November 1999 16:57 local time (GMT +3)
Location	Düzce (Bolu)
Latitude (°)	40.806
Longitude (°)	31.187
Focal Depth (km)	10.4
M_W	7.1

Table 5.2. Information on the strong motion stations used in the stochastic ground motion simulations of 12 November 1999 Düzce earthquake

Station Name	**Station Code**	**Longitude (°)**	**Latitude (°)**	**Site Class (NEHRP)**	**PGA-NS (cm/s^2)**	**PGA-EW (cm/s^2)**	**R_{jb} (km)**	**R_{epi} (km)**
Düzce	8101 (DZC)	31.1489	40.8436	D	400.08	512.95	0.00	5.27
Bolu	1401 (BOL)	31.6073	40.7457	D	724.03	806.98	11.31	36.12
Izmit	4101 (IZT)	29.9172	40.7665	B	31.57	42.26	67.86	107.3

5.2 Finite-Fault Model Parameters

In this study, ground motion simulations of the 1999 Düzce mainshock, recorded at several selected stations in Northwestern Türkiye, are performed by the finite fault simulation program EXSIM (Motazedian & Atkinson, 2005). During the simulations in this study, source and path parameters are kept constant. Source and path parameters are as employed in Ugurhan & Askan (2010) where site parameters are varied to see the changes in the resulting spectra as explained in the following sections.

5.2.1 Source Parameters

Fault geometry must be specified in the finite-fault method to accurately include the source effects. The epicenter of the earthquake and the focal depth are provided in Table 5.1. Ugurhan & Askan (2010) tested alternative fault models to minimize the error between real and simulated records, particularly for the low frequencies, and finally decided to follow the source model of Umutlu et al. (2004) (Table 5.3). The optimum stress drop value, which controls the spectral amplitudes, is estimated to be 100 bars.

Table 5.3. Source parameters of the 12 November 1999 Düzce earthquake used in the stochastic simulations

Parameter	**Value**
Fault plane dimensions	65 x 25 km
Strike angle	264°
Dip angle	64°
Number of subfaults along the strike and dip	13 x 5
Subfault size	5 km x 5 km

5.2.2 Path Parameters

Waves propagate through the crust to the top of the bedrock underneath the study site, known as the path effects. They are modeled as a function of three components: geometrical spreading, anelastic attenuation, and duration effects which are described briefly next.

i) Geometrical spreading:

The model of Ansal et al. (2009) is used as the following piecewise function:

$$\begin{aligned} &R^{-1}, && R \leq 30\ km \\ &R^{-0.4}, && 30 < R \leq 60\ km \\ &R^{-0.6}, && 60 < R \leq 90\ km \\ &R^{-0.8}, && 90 < R \leq 100\ km \\ &R^{-0.5}, && R > 100\ km \end{aligned} \tag{5.1}$$

where R is the fault distance.

ii) Anelastic attenuation:

The frequency-dependent Q model (quality factor) proposed by Boore (1984), which provides a close match between the observed and simulated FAS at higher frequencies, is used:

$$Q(f) = 88f^{0.9} \tag{5.2}$$

iii) Ground motion duration effects:

The duration model of Herrmann (1985) is used in defining distance-dependent duration:

$$T = T_0 + 0.05R \qquad (5.3)$$

where T_0 is the source duration, and R is the hypocentral distance.

5.2.3 Site Parameters

In this study, while source and path parameters are kept constant, different site parameters are utilized in the simulations. Site effects include a considerable amount of uncertainty due to the ambiguity of the parameters defining site models. Amplification factor and horizontal kappa factor (κ_h), the high-frequency spectral decay parameter, are among these site parameters.

As explained in previous chapters, there are different available methods for site amplification estimations, and among those, 1-D site response analysis is performed in this thesis. In stochastic ground motion simulations, the amplifications classified according to the NEHRP site classes proposed in this thesis and generic site amplifications in Boore & Joyner (1997) are used as alternative inputs.

For kappa estimations, the model by Askan et al. (2014) is followed:

Table 5.4. Regression variables in Northwestern-Türkiye Dataset (Askan et al., 2014)

Variable	Mean	Standard Deviation
κ_h	0.04986	0.01486

κ_h value depends on the site, thus in this thesis, in order to minimize the error between observed and simulated Fourier amplitude spectra at each station for different alternative amplification factors, the kappa values demonstrated in Table 5.5 and Table 5.6 are used. It is noted that all of these kappa values remain within $\pm 1\sigma$ of the mean kappa estimates of Askan et al. (2014).

Table 5.5. Kappa values used in the simulations with different amplification factors at station DZC

Amplifications	**Kappa Value**
Station DZC with strong motion records (This study)	0.05200
Station DZC with weak motion records (This study)	0.06472
NEHRP D with strong motion records (This study)	0.05000
NEHRP D with weak motion records (This study)	0.06500
B&J (1997) Generic D	0.05500

Table 5.6. Kappa values used in the simulations with different amplification factors at station BOL

Amplifications	**Kappa Value**
Station BOL with strong motion records (This study)	0.035
Station BOL with weak motion records (This study)	0.035
NEHRP D with strong motion records (This study)	0.035
NEHRP D with weak motion records (This study)	0.035
B&J (1997) Generic D	0.012

Table 5.7. Kappa values used in the simulations with different amplification factors at station IZT

Amplifications	**Kappa Value**
Station IZT with strong motion records (This study)	0.045
Station IZT with weak motion records (This study)	0.045
NEHRP B with strong motion records (This study)	0.045
NEHRP B with weak motion records (This study)	0.045
B&J (1997) Generic Rock Site	0.037

5.3 Comparison of Real and Simulated Ground Motion Data based on Fourier Amplitude Spectra

Fourier amplitude spectrum provides insight into the frequency content of a ground motion record. Fourier integral uses the simulated acceleration time histories and performs transformation from time domain to frequency domain to obtain Fourier amplitude spectrum as follows:

$$A(\omega) = \int_{-\infty}^{+\infty} a(t) \exp(i\omega t)\, dt \qquad (5.4)$$

where ω is angular frequency ($\omega = 2\pi f$), $a(t)$ is ground motion acceleration time series, $A(\omega)$ is the Fourier amplitude, t is the time.

In this section, observed and simulated Fourier amplitude spectra of acceleration records at stations DZC, BOL, and IZT from the 12 November 1999 Düzce earthquake obtained with alternative amplification factors are evaluated qualitatively and quantitatively. Throughout this thesis, FAS will indicate Fourier amplitude spectra for acceleration time histories.

5.3.1 Station DZC

For the stochastic ground motion simulations of the 1999 Düzce earthquake at station DZC, five alternative amplification factors are used as input: amplifications at station DZC obtained in this study with strong motion records as rock input motion, amplifications at station DZC obtained in this study with weak motion records as rock input motion, generic amplifications for NEHRP site class D developed in this study with strong motion records, generic amplifications for NEHRP site class D developed in this study with weak motion records, and generic amplifications for NEHRP site class D of Boore & Joyner (1997) Figure 5.1 represents simulations at station DZC with station-wise amplification factors obtained particularly for station DZC and Boore & Joyner (1997) against the corresponding observed motions while Figure 5.2 represents simulations at station DZC performed with generic amplifications for NEHRP site class D and Boore & Joyner (1997) against the corresponding observed motions.

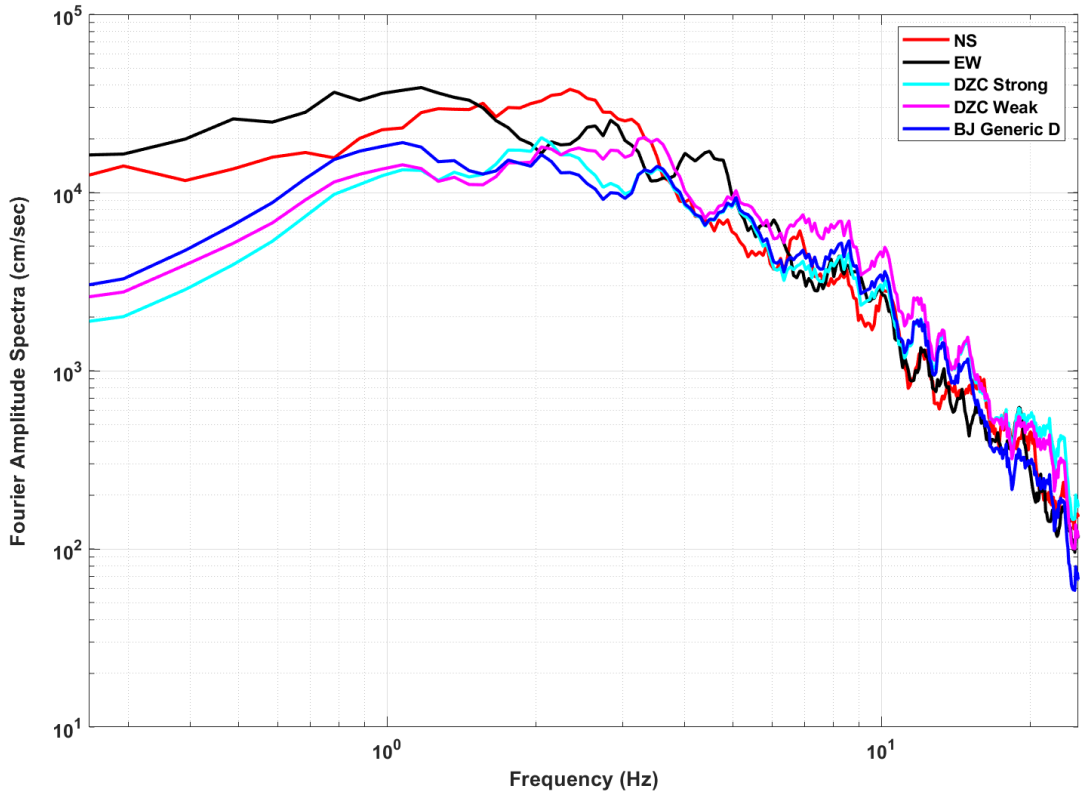

Figure 5.1. Comparison of the observed and simulated FAS of acceleration records from the 12 November 1999 Düzce earthquake performed with alternative amplification factors at station DZC (NS indicates the observed NS component of 1999 Düzce Earthquake, EW indicates the observed EW component of 1999 Düzce Earthquake, DZC Strong indicates the amplifications at station DZC obtained in this study with strong motion records, DZC Weak indicates the amplifications at station DZC obtained in this study with weak motion records, BJ Generic D indicates the generic amplifications for site class D in Boore & Joyner (1997))

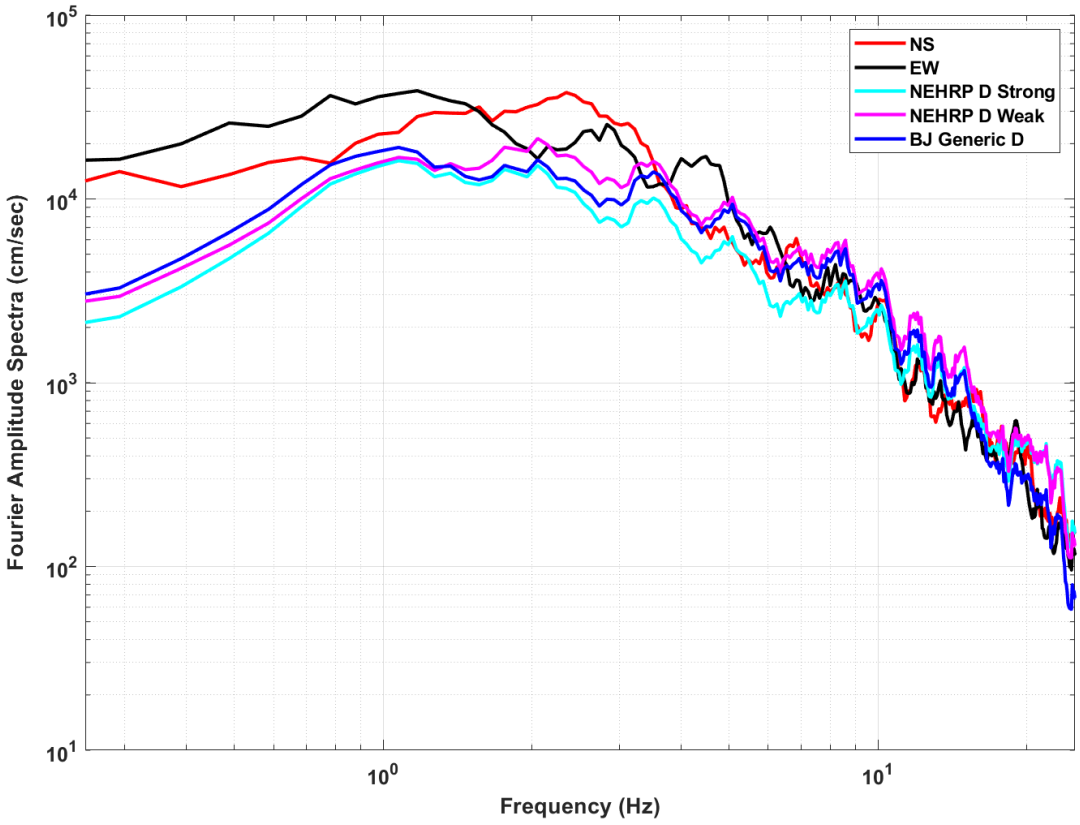

Figure 5.2. Comparison of the observed and simulated FAS of acceleration records from the 12 November 1999 Düzce earthquake performed with alternative amplification factors at station DZC (NS indicates the observed NS component of 1999 Düzce Earthquake, EW indicates the observed EW component of 1999 Düzce Earthquake, NEHRP D Strong indicates the amplifications for NEHRP D site classification obtained in this study with strong motion records, NEHRP D Weak indicates the amplifications for NEHRP D site classification obtained in this study with weak motion records, BJ Generic D indicates the generic site D amplifications in Boore & Joyner (1997))

The comparison of simulations against the observations at station DZC show that for frequencies less than 2 Hz, all of the simulated spectra are below the observed one for both NS and ES components. This discrepancy for the lower frequencies may arise from the near-source effects which could not be effectively simulated with the

stochastic finite fault approach at station DZC. This may be the reason of poor match between observed and simulated spectra for lower frequencies.

Among the alternatives in Figure 5.2, the simulated data with generic amplifications developed in this study for NEHRP site class D with strong motion records provide the closest match for the higher frequencies. However, it still underestimates the observed ones up to 5 Hz possibly due to insufficiently modelled source effects. Between 2 Hz and 6.5 Hz, the simulated motion with generic amplifications developed in this study for NEHRP site class D with weak motion records performs better than the one with strong motion records. The synthetic with generic site D amplifications in Boore & Joyner (1997) lies mostly somewhere between NEHRP site D amplifications obtained in this study with strong and weak motion records.

For the higher frequencies, all the synthetics match each other more closely than they do the observed ones. Among all of the alternatives, the simulated FAS with the amplifications at station DZC obtained with strong motion records provides the closest match with the observed data. This is mostly due to 1D site response analysis yielding more realistic soil behaviour with strong motion inputs for the 1999 Düzce event with Mw=7.1.

5.3.2 Station BOL

For the stochastic ground motion simulations of the 1999 Düzce earthquake at station BOL, five alternative amplification factors are used as input: amplifications at station BOL obtained in this study with strong motion records as rock input motion, amplifications at station BOL obtained in this study with weak motion records as rock input motion, generic amplifications for NEHRP site class D developed in this study with strong motion records, generic amplifications for NEHRP site class D developed in this study with weak motion records, and generic amplifications for NEHRP site class D of Boore & Joyner (1997). Figure 5.3 represents simulations at station BOL with station-wise amplification factors obtained particularly for station

BOL and Boore & Joyner (1997) against the corresponding observed motions while Figure 5.4 represents simulations at station BOL performed with generic amplifications for NEHRP site class D and Boore & Joyner (1997) against the corresponding observed motions.

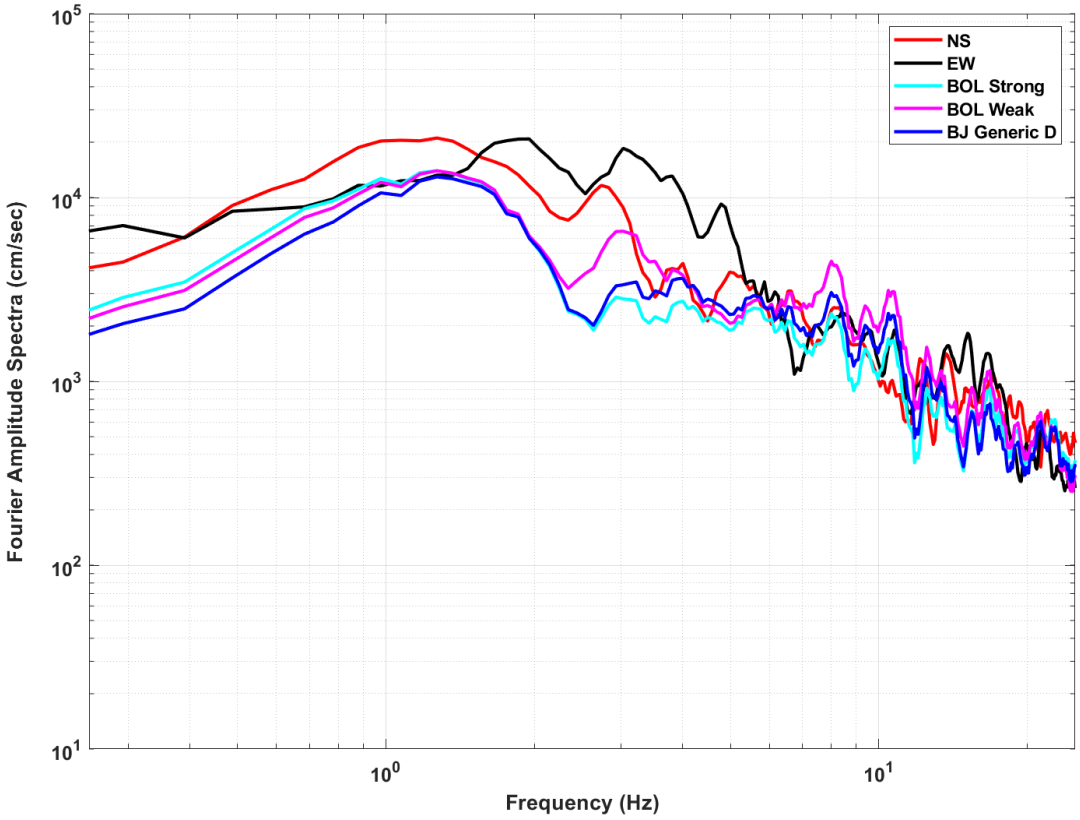

Figure 5.3. Comparison of the observed and simulated FAS of acceleration records from the 12 November 1999 Düzce earthquake performed with alternative amplification factors at station BOL (NS indicates the observed NS component of 1999 Düzce Earthquake, EW indicates the observed EW component of 1999 Düzce Earthquake, BOL Strong indicates the amplifications at station BOL obtained in this study with strong motion records, BOL Weak indicates the amplifications at station BOL obtained in this study with weak motion records, BJ Generic D indicates the generic site D amplifications in Boore & Joyner (1997))

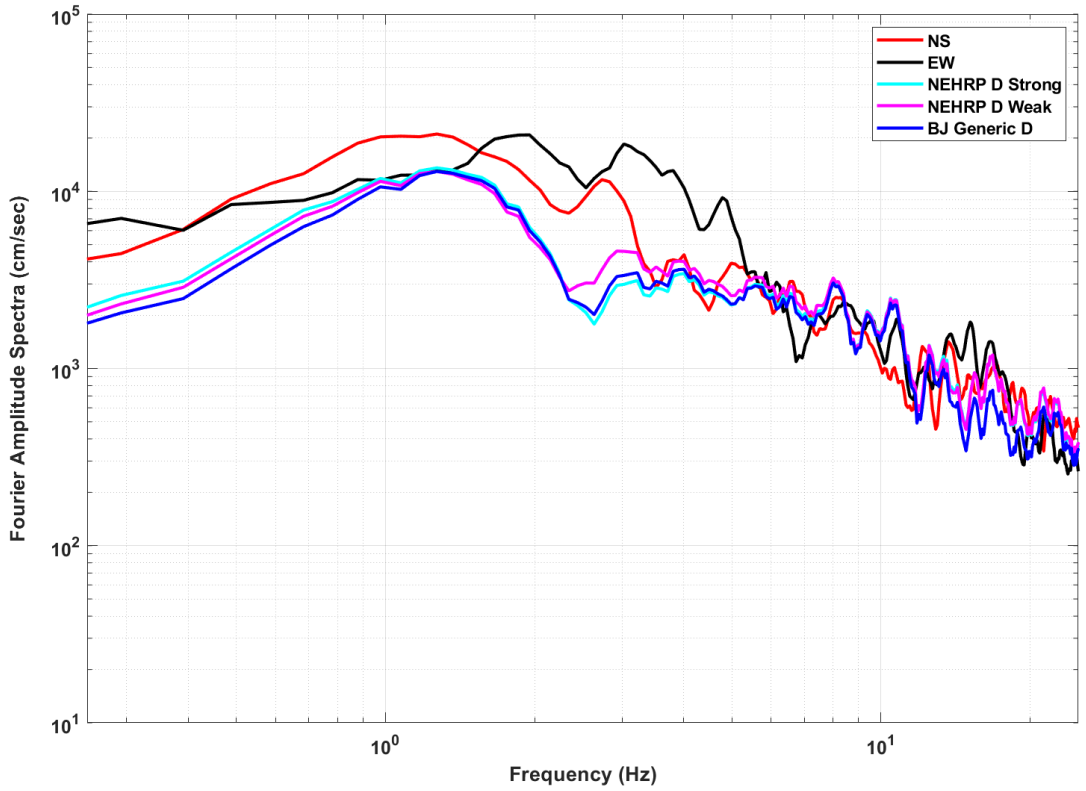

Figure 5.4. Comparison of the observed and simulated FAS of acceleration records from the 12 November 1999 Düzce earthquake performed with alternative amplification factors at station BOL (NS indicates the observed NS component of 1999 Düzce Earthquake, EW indicates the observed EW component of 1999 Düzce Earthquake, NEHRP D Strong indicates the amplifications for NEHRP D site classification obtained in this study with strong motion records, NEHRP D Weak indicates the amplifications for NEHRP D site classification obtained in this study with weak motion records, BJ Generic D indicates the generic site D amplifications in Boore & Joyner (1997))

The comparisons of simulations against the observations at station BOL show that all of the simulated motions underestimate the observed ones for frequencies between 0.1 and 3.2, except for the amplifications around 1.3 Hz where simulated data coincide with the observations. The overall discrepancy for the low frequencies

may arise from the near-source effects at station BOL, as in the case at station DZC. Also, a clear pulse in the fault parallel component is observed at station BOL which significantly affects the low frequencies or longer periods.

Among the alternatives in Figure 5.3, the simulated motions with amplifications at station BOL obtained with weak motion records provides the overall closest match. The simulated data with generic site D amplifications of Boore & Joyner (1997) remains mostly between the simulations with amplifications at station BOL developed with strong and weak motion records, especially for the frequencies larger than 2 Hz.

All of the simulated motions in Figure 5.4 perform very close to each other. The simulated motion with generic amplifications developed for NEHRP site class D with weak motion records provides a slightly better match with the observations than the one with strong motion records.

5.3.3 Station IZT

For the stochastic ground motion simulations of the 1999 Düzce earthquake at station IZT, five alternative amplification factors are used as input: amplifications at station IZT obtained in this study with strong motion records as rock input motion, amplifications at station IZT obtained in this study with weak motion records as rock input motion, generic amplifications for NEHRP site class B developed in this study with strong motion records, generic amplifications for NEHRP site class B developed in this study with weak motion records, and generic amplifications for rock sites of Boore & Joyner (1997). Figure 5.5 represents simulations at station IZT with station-wise amplification factors obtained particularly for station IZT and Boore & Joyner (1997) against the corresponding observed motions while Figure 5.6 represents simulations at station IZT performed with generic amplifications for NEHRP site class B delevoped in this study and Boore & Joyner (1997) against the corresponding observed motions.

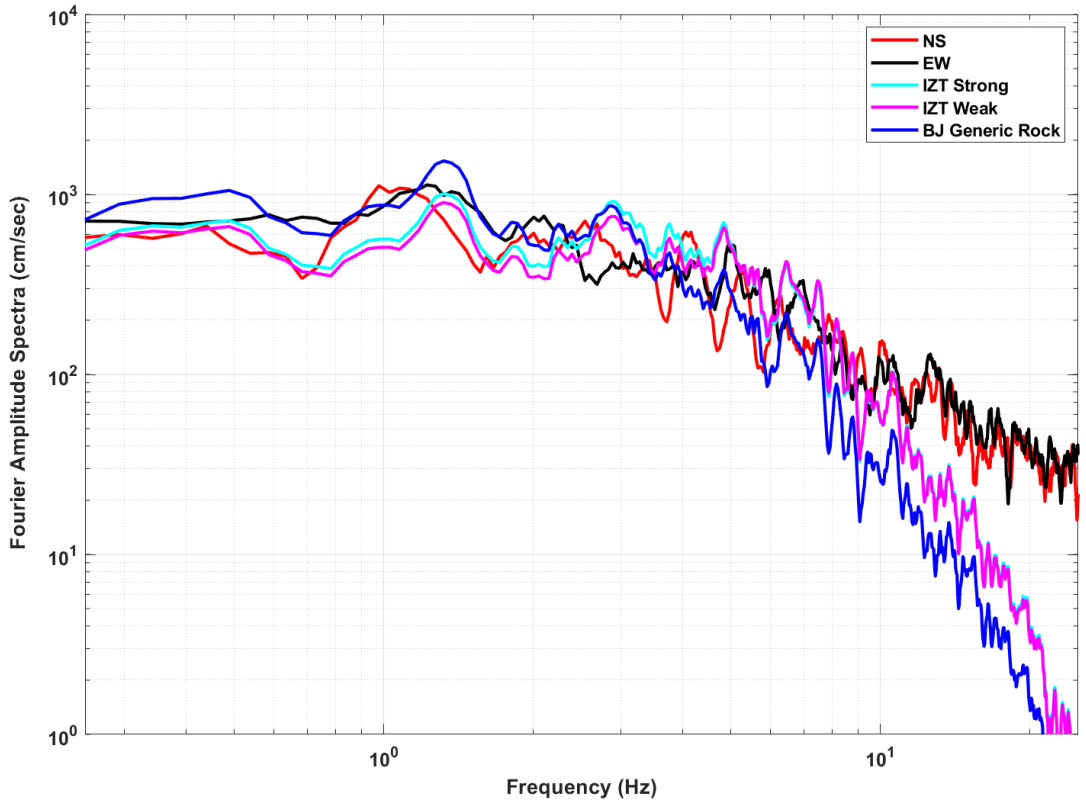

Figure 5.5. Comparison of the observed and simulated FAS of acceleration records from the 12 November 1999 Düzce earthquake performed with alternative amplification factors at station IZT (NS indicates the observed NS component of 1999 Düzce Earthquake, EW indicates the observed EW component of 1999 Düzce Earthquake, IZT Strong indicates the amplifications at station IZT obtained in this study with strong motion records, IZT Weak indicates the amplifications at station IZT obtained in this study with weak motion records, BJ Generic Rock indicates the generic rock site amplifications in Boore & Joyner (1997)).

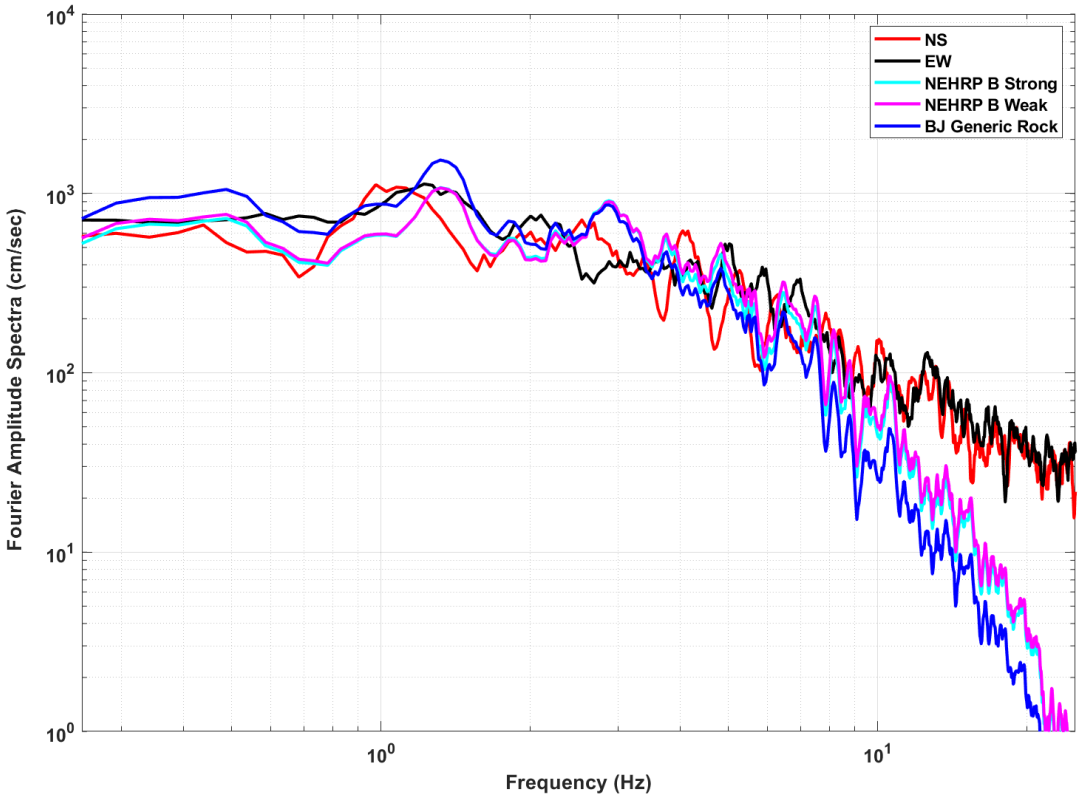

Figure 5.6. Comparison of the observed and simulated Fourier amplitude spectra of acceleration records from the 12 November 1999 Düzce earthquake performed with alternative amplification factors at station IZT (NS indicates the observed NS component of 1999 Düzce Earthquake, EW indicates the observed EW component of 1999 Düzce Earthquake, NEHRP B Strong indicates the amplifications for NEHRP B site classification obtained in this study with strong motion records, NEHRP B Weak indicates the amplifications for NEHRP B site classification obtained in this study with weak motion records, BJ Generic Rock indicates the generic rock site amplifications in Boore & Joyner (1997)).

The comparisons at station IZT show that the differences between the simulated and observed motions are the smallest when compared to misfits at other stations for the lower frequencies. This is attributed to the fact that station IZT is located at 100 km distance from the earthquake source. Thus, complex near field source effects is not

observed at the station when compared to the stations DZC and BOL. The simulated FAS with all of the amplification functions at station IZT provide a significant closer match for frequencies between 0.1 Hz and 8 Hz in comparison with the ones at stations DZC and BOL.

However, for the frequencies larger than 9 Hz, all the simulated spectra at station IZT perform poorly. It is noted that the kappa estimates in Askan et al. (2014) do not cover Izmit area. This could explain the discrepancy between simulated and observed amplitudes in the higher frequencies at station IZT. This observation points out the need for local kappa models for Izmit region as well.

5.3.4 Goodness of Fit Values

The comparisons are next quantified in terms of selected fundamental ground motion intensity parameters through Goodness-of-fit (GOF) criteria by Olsen & Mayhew (2010). Goodness-of-fit establishes the discrepancy between the observed and simulated ground motion parameters as follows:

$$GOF = 100 * erfc[NR], where\ NR = \frac{2|x-y|}{x+y} \tag{5.5}$$

Where x and y are two different competitive alternatives. GOF values are classified as proposed in Olsen & Mayhew (2010) (Table 5.8).

Table 5.8. GOF value classification by Olsen & Mayhew (2010)

GOF values (%) between		**Classification**
80	100	Excellent Fit
65	80	Very Good Fit
45	65	Fair Fit
35	45	Poor Fit
	Otherwise	Not Applicable (NA)

In this study, the GOF values are computed for selected ground motion parameters in the time and frequency domains for North-South and East-West components of 1999 Düzce earthquake separately. The variability in the misfits according to alternative site amplifications is evaluated.

GOF scores for PGA, PGV, Fourier amplitude spectra, and significant duration are evaluated. The scores are generally found to be consistent with the visual comparisons and physical reasons mentioned previously.

Table 5.9 and Table 5.10 represent the GOF values at station DZC for NS and EW components, respectively. GOF values for significant duration when compared to NS component of 1999 Düzce earthquake at station DZC result in excellent fit for all alternative amplification factors. GOF scores for simulated PGV values with alternative amplification functions reveal that simulated PGV values are not found close to the observed PGV value. Overall, the simulated FAS between 1 and 20 Hz with the station-wise amplifications at station DZC obtained with strong motion records provides the closest match with the observed data (Table 5.9).

Table 5.11 and Table 5.12 represent the GOF values at station BOL for NS and EW components, respectively. Similarly, GOF values for simulated significant durations when compared to the observed EW component of the event at station DZC result in excellent fit for all the alternative amplification factors. Table 5.10 shows that,

simulated FAS with alternative amplifications at station DZC when compared to EW component of the event does not give as good fits as NS component.

At station BOL, GOF values for PGV and significant duration result in poor fit for all alternative amplification functions except for the amplifications at station BOL obtained with strong motion records. Table 5.11 and Table 5.12 reveal that the best match between observed and simulated FAS for higher frequencies (between 1 Hz and 20 Hz) at station BOL is the simulated motion with generic amplifications developed for NEHRP site class D using weak motion records.

Table 5.13 and Table 5.14 represent the GOF values at station IZT for NS and EW components, respectively. Different from the simulated FAS at stations DZC and BOL, the FAS with all of the amplification functions at station IZT provide a significant closer match for lower frequencies (between 0.1 Hz and 1 Hz) resulting in very good fits. When the entire frequency range is considered, simulated FAS with the generic amplifications developed for NEHRP site class B with weak motion records provides the closest match at station IZT.

Table 5.9. GOF Values (%) for North-South (NS) Component of Observed 1999 Düzce Earthquake at Station DZC

GOF Values (%) for North-South (NS) Component of 1999 Düzce Earthquake at Station DZC								
Amplifications	**PGA**		**PGV**		**Fourier Amplitude Spectra (btw 1 Hz - 20 Hz)**		**Significant Duration (5% and 95% thresholds)**	
DZC strong	53.1	Fair Fit	16.3	NA	71.4	Very Good Fit	80.0	Excellent Fit
DZC weak	84.7	Excellent Fit	26.6	NA	58.1	Fair Fit	83.1	Excellent Fit
NEHRP D strong	43.6	Poor Fit	21.3	NA	69.8	Very Good Fit	83.5	Excellent Fit
NEHRP D weak	77.7	Very Good Fit	27.8	NA	63.0	Fair Fit	82.3	Excellent Fit
BJ Generic D	68.3	Very Good Fit	32.2	NA	64.9	Fair Fit	87.3	Excellent Fit

Table 5.10. GOF Values (%) for East-West (EW) Component of Observed 1999 Düzce Earthquake at Station DZC

GOF Values (%) for East-West (EW) Component of 1999 Düzce Earthquake at Station DZC								
Amplifications	**PGA**		**PGV**		**Fourier Amplitude Spectra (btw 1 Hz - 20 Hz)**		**Significant Duration (5% and 95% thresholds)**	
DZC strong	33.9	NA	11.8	NA	67.9	Very Good Fit	83.2	Excellent Fit
DZC weak	58.6	Fair Fit	19.3	NA	55.6	Fair Fit	86.3	Excellent Fit
NEHRP D strong	27.3	NA	15.4	NA	64.7	Fair Fit	86.7	Excellent Fit
NEHRP D weak	52.8	Fair Fit	20.2	NA	59.9	Fair Fit	85.5	Excellent Fit
BJ Generic D	45.3	Fair Fit	23.5	NA	67.2	Very Good Fit	90.6	Excellent Fit

Table 5.11. GOF Values (%) for North-South (NS) Component of Observed 1999 Düzce Earthquake at Station BOL

GOF Values (%) for North-South (NS) Component of 1999 Düzce Earthquake at Station BOL								
Amplifications	**PGA**		**PGV**		**Fourier Amplitude Spectra (btw 1 Hz - 20 Hz)**		**Significant Duration (5% and 95% thresholds)**	
BOL strong	11.5	NA	7.4	NA	60.6	Fair Fit	95.2	Excellent Fit
BOL weak	15.0	NA	44.4	Poor Fit	63.1	Fair Fit	15.2	NA
NEHRP D strong	15.1	NA	44.4	Poor Fit	66.7	Very Good Fit	15.2	NA
NEHRP D weak	15.0	NA	44.4	Poor Fit	67.8	Very Good Fit	15.2	NA
BJ Generic D	15.1	NA	44.3	Poor Fit	58.7	Fair Fit	15.2	NA

Table 5.12. GOF Values (%) for East-West (EW) Component of Observed 1999 Düzce Earthquake at Station BOL

GOF Values (%) for East-West (EW) Component of 1999 Düzce Earthquake at Station BOL								
Amplifications	**PGA**		**PGV**		**Fourier Amplitude Spectra (btw 1 Hz - 20 Hz)**		**Significant Duration (5% and 95% thresholds)**	
BOL strong	13.7	NA	9.7	NA	51.4	Fair Fit	89.2	Excellent Fit
BOL weak	17.8	NA	56.4	Fair Fit	53.4	Fair Fit	13.7	NA
NEHRP D strong	17.9	NA	56.4	Fair Fit	58.5	Fair Fit	13.7	NA
NEHRP D weak	17.8	NA	56.4	Fair Fit	58.6	Fair Fit	13.7	NA
BJ Generic D	17.9	NA	56.4	Fair Fit	52.9	Fair Fit	13.7	NA

Table 5.13. GOF Values (%) for North-South (NS) Component of Observed 1999 Düzce Earthquake at Station IZT

GOF Values (%) for North-South (NS) Component of 1999 Düzce Earthquake at Station IZT										
Amplifications	**PGA**		**PGV**		**Fourier Amplitude Spectra (btw 0.1 Hz - 1 Hz)**		**Fourier Amplitude Spectra (btw 1 Hz - 20 Hz)**		**Significant Duration (5% and 95% thresholds)**	
IZT strong	71.4	Very Good Fit	16.5	NA	72.2	Very Good Fit	37.6	Poor Fit	21.5	NA
IZT weak	66.2	Very Good Fit	15.7	NA	70.7	Very Good Fit	37.4	Poor Fit	21.5	NA
NEHRP B strong	66.3	Very Good Fit	16.5	NA	72.4	Very Good Fit	36.7	Poor Fit	21.5	NA
NEHRP B weak	72.7	Very Good Fit	20.1	NA	71.7	Very Good Fit	38.2	Poor Fit	21.6	NA
BJ Generic Rock	91.8	Excellent Fit	23.9	NA	68.1	Very Good Fit	28.5	NA	23.0	NA

Table 5.14. GOF Values (%) for East-West (EW) Component of Observed 1999 Düzce Earthquake at Station IZT

GOF Values (%) for East-West (EW) Component of 1999 Düzce Earthquake at Station IZT										
Amplifications	**PGA**		**PGV**		**Fourier Amplitude Spectra (btw 0.1 Hz - 1 Hz)**		**Fourier Amplitude Spectra (btw 1 Hz - 20 Hz)**		**Significant Duration (5% and 95% thresholds)**	
IZT strong	44.6	Poor Fit	8.1	NA	61.4	Fair Fit	39.1	Poor Fit	23.8	NA
IZT weak	40.8	Poor Fit	7.7	NA	54.5	Fair Fit	39.7	Poor Fit	23.9	NA
NEHRP B strong	40.8	Poor Fit	8.1	NA	62.8	Fair Fit	37.0	Poor Fit	23.8	NA
NEHRP B weak	45.6	Fair Fit	9.8	NA	65.0	Fair Fit	39.3	Poor Fit	24.0	NA
BJ Generic Rock	61.0	Fair Fit	11.6	NA	77.0	Very Good Fit	27.8	NA	25.5	NA

CHAPTER 6

SUMMARY AND CONCLUSIONS

6.1 Summary

Ground motions generated by earthquakes are influenced by source, path and local site properties. Among these three factors, local site conditions have a great effect on ground shaking and thus the structural damages observed during large earthquakes. Soil layers on top of hard rock can amplify the ground motion, which makes it essential to calculate the site amplification factors.

In this thesis, generic site amplification factors for Northwestern Türkiye, one of the most seismically active regions in the country and the world, are obtained by following 1-D site response analysis. A total of 76 shear wave velocity profiles are included in the analyses with varying resolved depths, layer thicknesses and soil properties. Strong and weak input ground motions with different characteristics are used separately to see the effect of the motions in the analyses. The equivalent linear analyses are performed using the DEEPSOIL software.

The amplification factors in the period domain are simply obtained by dividing the response spectrum of the motion computed at the top layer by the response spectrum of input motions. The selected sites in this thesis are classified according to the NEHRP classification system which uses Vs_{30} value as the main proxy. The mean amplification factors for each NEHRP site class are obtained by taking the average amplification at the stations of the same site class located in Northwestern Türkiye.

The resulting generic amplification factors are next fitted by a Gaussian function. The purpose is to define the best fit model for the amplification factors as a function of period using representative sites in Northwestern Türkiye for NEHRP site classes

A, B, C, and D. Comparisons of the results are made with available amplification factors in the literature for different regions.

Next, the proposed amplification factors are used as an input to the stochastic ground motion simulations of the 1999 Düzce Earthquake and the simulated data are compared to the corresponding real ground motions. Finally, the goodness-of-fit values are tabulated to demonstrate the variations between the simulated and recorded motions.

6.2 Conclusions

The main conclusions based on the analyses performed within this thesis are as follows:

- This study constitutes the first attempt to develop generic site amplification functions for Türkiye, focusing on the Northwestern regions.
- The amplification functions obtained from the 1-D site response analyses show significant differences with strong and weak input motions.
- Amplifications have higher values when analyzed with weak motion records compared to strong motion records at any site of interest. The differences between the peak amplification factors from the analyses with strong and weak input motions get larger as the soil site become softer. Numerically speaking, the analyses with strong motion inputs for site class C yield 29% lower peak amplification factors when compared to that with weak motion inputs. This difference is 52% for site class D.
- As a general trend, the fundamental peaks shift to longer periods when analyzed with strong motion records compared to those with weak motion records. The differences between the fundamental periods from the analyses with strong and weak input motions get larger as the soil site become softer. Numerically, the fundamental period for site class C with strong motion input is 28% larger when compared to the one with weak motion input. This

difference is 64% for site class D. These observations which are more obvious at softer soil sites could be attributed to nonlinearity.

- Amplification curves for different site classes are found to be similar in shape but different in amplitudes as anticipated. Regardless of the input motions, amplification factors have higher values as soil site gets softer, e.g., amplification function for NEHRP site class D have higher values compared to the one for NEHRP site class A.
- When the mean transfer functions are investigated for each NEHRP site classes, very clear and expected physical differences are observed: Stiffer sites will amplify short periods, while softer sites will amplify long periods.
- Lower fundamental frequency (longer period) values and lower amplification factors at soil sites are expected as a result of potential soil nonlinearity when strong motion records are used as input (e.g.: Sisman et al., 2018). The numerical results are found to be consistent with this trend.
- The standard deviations of amplification factors for site B are larger than those of site A. This is expected as the soil gets softer at any site of interest due to the more variable and complex behavior of softer soil layers.
- Gaussian functions that are fitted to yield generic site amplification factors using representative sites in Northwestern Türkiye for NEHRP site classes A, B, C, and D have high R^2 values, e.g., all larger than 0.8.
- The comparisons are made in the frequency domain for NEHRP C and D site classes to be consistent with earlier studies. Variable amplification factors yet similar shapes are observed in comparison with the other studies based on data from different regions in the world. As a general observation for all studies, NEHRP class C has smaller periods than class D with much smaller amplification factors. Amplification factors for Northwestern Türkiye for NEHRP site class C has the largest fundamental frequency compared to the Hellenic and the US data. Velocity models at sites located in Northwestern Türkiye yield the smallest amplification factors at all frequency ranges for NEHRP site class D. This difference can be attributed to the differences

among the earth structure (velocity profiles, damping factors and plasticity indices and etc.) at sites of interest. Thus, the differences between amplification functions are considered to be natural due to the local characteristics of surface layers and geology.

- Another explanation of smaller amplitudes obtained in this study compared to others in the literature could be due to the following: The other studies in the literature mostly employ either empirical methods or the quarter wavelength method. Yet, the equivalent linear method used in this thesis is known to potentially result in an overdamped and over softened response mostly for softer soils.
- The amplification functions derived in this thesis are used as input to the stochastic simulation model to compare the simulated and observed Fourier amplitude spectra at selected strong-motion stations which recorded the 1999 Düzce Earthquake.
- In the simulations of the 1999 Düzce earthquake, the amplification functions obtained from site response analyses with strong and weak motion records are used to observe the variations in the resulting simulated data. It is observed that at a very near field station (DZC) located on soft soils, amplification function from strong motions give closer matches with observed records while for stiffer sites distant from the source (IZT) AF from weak motions yield better results. This is mostly because weak motions show elastic soil behavior while strong motions represent the inelastic and indeed more realistic behavior during large events.
- To further validate the proposed amplification functions, simulations of other events are essential. Still, the proposed Gaussian functions can be used as amplification factors in the near future when there is no available local or site-specific data for all kinds of studies that requires generic site amplifications in geotechnical earthquake engineering.

6.3 Limitations of This Study and Future Recommendations

- In this study, only the Northwestern part of Türkiye is included. For future studies, 1-D site response analyses could be performed with a higher number of stations located at different regions in Türkiye.
- For 1-D site response analyses, in this thesis a set of 40 weak and strong input motions are employed in this thesis. A wider set of strong and weak ground motion records could be used in future studies. In particular, while selecting the input motions, a large number of bins including magnitude, shear wave velocity and R_{jb} range could be employed.
- In this thesis, theoretical amplification functions are developed. In future studies, empirical amplification factors could also be developed and compared to the theoretical ones. Indeed, whenever possible, the use of alternative methods for site amplification estimations would yield more realistic results.
- Due to its simplicity and fewer input variables, EQL method is preferred in this thesis. While EQL method is still a coarse approximation for the actual nonlinear behavior, nonlinear methods reflect the actual soil behavior. In an equivalent linear analysis, using an effective shear strain can result in an overdamped and over softened response. In the future, fully nonlinear 1D analyses could also be used.
- In this thesis, 1-D site response is considered for calculation of site amplifications. However, realistically, seismic response is indeed influenced by 3-D effects such as basin effects, bedrock slope, layer geometries, and topographical conditions. Therefore, in the future, wave propagations within 2-D or 3-D earth models could be used to derive generic site amplification factors.

REFERENCES

Anderson, J. G., Lee, Y., Zeng, Y., & Day, S. (1996). Control of strong motion by the upper 30 meters. *Bulletin of the Seismological Society of America*, *86*(6).

Ansal, A., Akinci, A., Cultrera, G., Erdik, M., Pessina, V., Tönük, G., & Ameri, G. (2009). Loss estimation in Istanbul based on deterministic earthquake scenarios of the Marmara Sea region (Turkey). *Soil Dynamics and Earthquake Engineering*, *29*(4). https://doi.org/10.1016/j.soildyn.2008.07.006

Askan, A., Sisman, F. N., & Pekcan, O. (2014). A regional near-surface high frequency spectral attenuation (kappa) model for Northwestern Turkey. *Soil Dynamics and Earthquake Engineering*, *65*. https://doi.org/10.1016/j.soildyn.2014.06.007

Baram, A., Yagoda-Biran, G., & Kamai, R. (2019). Evaluation of generic reference rock site conditions for Israel. In *Seismological Research Letters* (Vol. 90, Issue 4). https://doi.org/10.1785/0220180377

Boore, D. M. (1984). Use of seismoscope records to determine ML and peak velocities . *Bulletin of the Seismological Society of America*, *74*(1). https://doi.org/10.1785/bssa0740010315

Boore, D. M., & Joyner, W. B. (1997). Site amplifications for generic rock sites. *Bulletin of the Seismological Society of America*, *87*(2). https://doi.org/10.1785/bssa0870020327

Boore, D. M., Joyner, W. B., & Fumal, T. E. (1993). Estimation of response spectra and peak accelerations from western North American earthquakes: an interim report. In *USGS Open-File Report 93-509*.

Borcherdt, R. D. (1970). Effects of Local Geology on Ground Motion Near San Francisco Rbay. *Bulletin of the Seismological Society of America*, *60*(1).

Borcherdt, R. D. (1994). Estimates of Site-Dependent Response Spectra for Design (Methodology and Justification). *Earthquake Spectra*, *10*(4). https://doi.org/10.1193/1.1585791

Borcherdt, R. D. (2002). Empirical evidence for site coefficients in building code provisions. *Earthquake Spectra*, *18*(2). https://doi.org/10.1193/1.1486243

Boudghene Stambouli, A., Zendagui, D., Bard, P. Y., & Derras, B. (2017). Deriving amplification factors from simple site parameters using generalized regression neural networks: Implications for relevant site proxies. *Earth, Planets and Space*, *69*(1). https://doi.org/10.1186/s40623-017-0686-3

Building Seismic Safety Council (BSSC). (2003). *NEHRP RECOMMENDED PROVISIONS FOR SEISMIC REGULATIONS FOR NEW BUILDINGS AND OTHER STRUCTURES (FEMA 450) Part 1: Provisions*

Chen, C. H., Wang, W. H., & Teng, T. L. (2001). 3D velocity structure around the source area of the 1999 Chi-Chi, Taiwan, earthquake: Before ang after the mainshock. *Bulletin of the Seismological Society of America*, *91*(5). https://doi.org/10.1785/0120000737

Choi, Y., & Stewart, J. P. (2005). Nonlinear site amplification as function of 30 m shear wave velocity. *Earthquake Spectra*, *21*(1). https://doi.org/10.1193/1.1856535

Crouse, C. B., & McGuire, J. W. (1996). Site response studies for purpose of revising NEHRP seismic provisions. *Earthquake Spectra*, *12*(3). https://doi.org/10.1193/1.1585891

Danciu, L., Nandan, S., Reyes, C., Basili, R., Weatherill, G., Beauval, C., Rovida, A., Vilanova, S., Sesetyan, K., Bard, P.-Y., Cotton, F., Wiemer, S., & Giardini, D. (2021). *The 2020 update of the European Seismic Hazard Model: Model Overview. EFEHR Technical Report 001*.

Dobry, R., Ramos, R., & Power, M. S. (1997, May 29). Site factors and site categories in seismic codes: A perspective. *Pmceedings of the FHWA/NCEER Workhop on the National Representation on Seismic Gmund Motion for New and Ezisting Highway Facilities*.

Dobry, R., Ramos, R., & Power, M. S. (1999). *Site Factors and Site Categories in Seismic Codes*.

Dobry, R., & Vucetic, M. (1987). Dynamic properties and seismic response of soft clay deposits. *International Symposium on Geotechnical Engineering of Soft Soils, Ciudad de México, May*.

Durukal, E. (2002). Critical evaluation of strong motion in Kocaeli and Düzce (Turkey) earthquakes. In *Soil Dynamics and Earthquake Engineering* (Vol. 22, Issue 7). https://doi.org/10.1016/S0267-7261(02)00014-3

Erdik, M. (2001). *REPORT ON 1999 KOCAELI AND DÜZCE (TURKEY) EARTHQUAKES*. www.ipgp.jussieu.fr

Farrugia, J. J., Atkinson, G. M., & Molnar, S. (2018). Validation of 1D earthquake site characterization methods with observed earthquake site amplification in Alberta, Canada. *Bulletin of the Seismological Society of America*, *108*(1), 291–308. https://doi.org/10.1785/0120170148

Field, E. H. (2000). A modified ground-motion attenuation relationship for southern California that accounts for detailed site classification and a basin-depth effect. *Bulletin of the Seismological Society of America*, *90*(6 SUPPL.). https://doi.org/10.1785/0120000507

Finn, W. D. L. (1996). Ground motion amplification factors for use in building codes. *Proceedings of the International Workshop on Site Response Subjected to Stmng Earthquake Motions, Vol. 1*, 104–117.

Harmsen, S. C. (1997). Determination of site amplification in the Los Angeles urban area from inversion of strong-motion records. *Bulletin of the Seismological Society of America*, *87*(4).

Hashash, Y. M. A., Musgrove, M. I., Harmon, J. A., Okan, I., Xing, G., Numanoglu, O., Groholski, D. R., Phillips, C. A., & Park, D. (2020). *DEEPSOIL 7.0, User Manual*. Urbana, IL, Board of Trustees of University of Illinois at Urbana-Champaign.

Herrmann, R. B. (1985). An extension of random vibration theory estimates of strong ground motion to large distances. *Bulletin of the Seismological Society of America*, *75*(5). https://doi.org/10.1785/bssa0750051447

Huang, H. C., & Teng, T. L. (1999). An evaluation on H/V ratio vs. spectral ratio for site-response estimation using the 1994 Northridge earthquake sequences. *Pure and Applied Geophysics*, *156*(4). https://doi.org/10.1007/s000240050316

Huang, M. W., Wang, J. H., Hsieh, H. H., & Wen, K. L. (2009). High frequency site amplification evaluated from Borehole data in the Taipei Basin. *Journal of Seismology*, *13*(4), 601–611. https://doi.org/10.1007/s10950-009-9153-3

Huang, M. W., Wang, J. H., Hsieh, H. H., Wen, K. L., & Ma, K. F. (2005). Frequency-dependent sites amplifications evaluated from well-logging data in central Taiwan. *Geophysical Research Letters*, *32*(21), 1–4. https://doi.org/10.1029/2005GL023527

Huang, M. W., Wang, J. H., Ma, K. F., Wang, C. Y., Hung, J. H., & Wen, K. L. (2007). Frequency-dependent site amplifications with $f \geq 0.01$ Hz evaluated from velocity and density models in Central Taiwan. *Bulletin of the Seismological Society of America*, *97*(2). https://doi.org/10.1785/0120060139

Idriss, I. M., & Sun, J. I. (1972). *Shake91, A Computer Program for Conducting Equivalent Linear Seismic Response Analysis of Horizontally Layered Soil Deposits, Modified based on the original SHAKE program*.

Joyner, W. B., & Boore, D. M. (1981). Peak horizontal acceleration and velocity from strong-motion records including records from the 1979 imperial valley, California, earthquake. *Bulletin of the Seismological Society of America*, *71*(6). https://doi.org/10.1785/bssa0710062011

Joyner, W. B., & Boore, D. M. (2000). Recent developments in earthquake ground-motion estimation. *Proc. Sixth International Conference on Seismic Zonation*.

Joyner, W. B., & Fumal, T. E. (1985). PREDICTIVE MAPPING OF EARTHQUAKE GROUND MOTION. In *Geological Survey Professional Paper (United States)*.

Karimzadeh Naghshineh, S. (2016). *Use Of Simulated Strong Ground Motion Records In Earthquake Engineering Applications*. Middle East Technical University.

Kim, B., Hashash, Y. M. A., Stewart, J. P., Rathje, E. M., Harmon, J. A., Musgrove, M. I., Campbell, K. W., & Silva, W. J. (2016). Relative differences between nonlinear and equivalent-linear 1-D site response analyses. *Earthquake Spectra*, *32*(3), 1845–1865. https://doi.org/10.1193/051215EQS068M

Klimis, N. S., Margaris, B. N., & Koliopoulos, P. K. (1999). Site-dependent amplification functions and response spectra in Greece. *Journal of Earthquake Engineering*, *3*(2), 237–270. https://doi.org/10.1080/13632469909350346

Kokusho, T., Yoshida, Y., & Esashi, Y. (1982). DYNAMIC PROPERTIES OF SOFT CLAY FOR WIDE STRAIN RANGE. *Soils and Foundations*, *22*(4). https://doi.org/10.3208/sandf1972.22.4_1

Kramer, S. L. (1996). *Geotechnical Earthquake Engineering*. PRENTICE-HALL INTERNATIONAL SERIES IN CIVIL ENGINEERING AND ENGINEERING MECHANICS

Lee, C. T., Cheng, C. T., Liao, C. W., & Tsai, Y. ben. (2001). Site classification of Taiwan free-field strong-motion stations. *Bulletin of the Seismological Society of America*, *91*(5). https://doi.org/10.1785/0120000736

Lermo, J., & Chavez-Garcia, F. J. (1993). Site effect evaluation using spectral ratios with only one station. *Bulletin - Seismological Society of America*, *83*(5). https://doi.org/10.1785/bssa0830051574

Markham, C. S., Bray, J. D., & Macedo, J. (2015). Deconvolution of Surface Motions from the Canterbury Earthquake Sequence for use in Nonlinear Effective Stress Site Response Analyses. *6th International Conference on Earthquake Geotechnical Engineering*, *November*.

Mayne, P. W. (2001). Stress-strain-strength-flow parameters from enhanced in-situ tests. *International Conference on In-Situ Measurement of Soil Properties & Case Histories*.

Middle East Technical University Earthquake Engineering Research Center. (2006). *TÜBİTAK Research Project, No. 105G016 Compilation of Data Base for The National Strong-Motion Seismograph Network in Turkey Report on Seismic and Geotechnical Investigations*. https://ivmeservis.afad.gov.tr/files/station/1401/documents/1401_report_eng_pdf.pdf

Motazedian, D., & Atkinson, G. (2005). Ground-motion relations for Puerto Rico. *Special Paper of the Geological Society of America*. https://doi.org/10.1130/0-8137-2385-X.61

Nakamura, Y. (1989). Method for dynamic characteristics estimation of subsurface using microtremor on the ground surface. *Quarterly Report of RTRI (Railway Technical Research Institute) (Japan)*, *30*(1).

Olsen, K. B., & Mayhew, J. E. (2010). Goodness-of-fit criteria for broadband synthetic seismograms, with application to the 2008 Mw 5.4 Chino Hills,

California, Earthquake. *Seismological Research Letters*, *81*(5). https://doi.org/10.1785/gssrl.81.5.715

Rodriguez-Marek, A., D. Bray, J., & Abrahamson, N. (1999). Task 3: Characterization of Site Response General Site Categories. *PEER Report 1999/03 Pacific Earthquake Engineering Research Center* .

Sandikkaya, M. A., Yilmaz, M. T., Bakir, B. S., & Yilmaz, Ö. (2010). Site classification of Turkish national strong-motion stations. *Journal of Seismology*, *14*(3), 543–563. https://doi.org/10.1007/s10950-009-9182-y

Sandıkkaya, M. A., & Dinsever, L. D. (2018). A site amplification model for crustal earthquakes. *Geosciences (Switzerland)*, *8*(7). https://doi.org/10.3390/geosciences8070264

Satoh, T., Kawase, H., Iwata, T., Higashi, S., Sato, T., Irikura, K., & Huang, H. C. (2001). S-wave velocity structure of the Taichung Basin, Taiwan, estimated from array and single-station records of microtremors. *Bulletin of the Seismological Society of America*, *91*(5). https://doi.org/10.1785/0120000706

Schnabel, P. B., Lysmer, J., & Seed, H. B. (1972). SHAKE: a computer program for earthquake response analysis of horizontally layered sites. In *Earthquake Engineering Research Center*.

Sedaghati, F., Pezeshk, S., & Nazemi, N. (2018). Site amplification within the Mississippi embayment of the central United States: Investigation of possible differences among various phases of seismic waves and presence of basin waves. *Soil Dynamics and Earthquake Engineering*, *113*. https://doi.org/10.1016/j.soildyn.2018.04.017

Seed, H. B., & Idriss, I. M. (1970). *Soil Moduli and Damping Factors for Dynamic Response Analyses*. University of California at Berkeley: Earthquake Engineering Research Centre.

Sisman, F. N., Askan, A., & Asten, M. (2018). Evaluation of Site Response with Alternative Methods: A Case Study for Engineering Implications. *Pure and Applied Geophysics*. https://doi.org/10.1007/s00024-017-1685-9

Sokolov, V. Y., Loh, C. H., & Wen, K. L. (2004). Evaluation of generalized site response functions for typical soil classes (B, C, and D) in Taiwan. *Earthquake Spectra*, *20*(4), 1279–1316. https://doi.org/10.1193/1.1814121

Steidl, J. H. (2000). Site response in southern California for probabilistic seismic hazard analysis. *Bulletin of the Seismological Society of America*, *90*(6 SUPPL.). https://doi.org/10.1785/0120000504

Stewart, J. P., Liu, A. H., & Choi, Y. (2003). Amplification factors for spectral acceleration in tectonically active regions. *Bulletin of the Seismological Society of America*, *93*(1). https://doi.org/10.1785/0120020049

Sun, J. I., Golesorkhi, R., & Seed, H. B. (1988). Dynamic Moduli And Damping Ratios For Cohesive Soils. *Earthquake Engineering Research Center - Report No. Ucbteelc·881l 5 August 1988 (College Of Engineering University Of California At Berkeley)*.

Tran, N. L., Aaqib, M., Nguyen, B. P., Nguyen, D. D., Tran, V. L., & Nguyen, V. Q. (2021). Evaluation of Seismic Site Amplification Using 1D Site Response Analyses at Ba Dinh Square Area, Vietnam. *Advances in Civil Engineering*, *2021*. https://doi.org/10.1155/2021/3919281

Ugurhan, B., & Askan, A. (2010). Stochastic strong ground motion simulation of the 12 november 1999 Düzce (Turkey) earthquake using a dynamic Corner frequency approach. *Bulletin of the Seismological Society of America*, *100*(4), 1498–1512. https://doi.org/10.1785/0120090358

Umutlu, N., Koketsu, K., & Milkereit, C. (2004). The rupture process during the 1999 Düzce, Turkey, earthquake from joint inversion of teleseismic and strong-motion data. *Tectonophysics*, *391*(1-4 SPEC.ISS.). https://doi.org/10.1016/j.tecto.2004.07.019

Vucetic, M., & Dobry, R. (1991). Effect of soil plasticity on cyclic response. *Journal of Geotechnical Engineering*, *117*(1). https://doi.org/10.1061/(ASCE)0733-9410(1991)117:1(89)

Xu, R., & Wang, L. (2021). The horizontal-to-vertical spectral ratio and its applications. *Eurasip Journal on Advances in Signal Processing*, *2021*(1). https://doi.org/10.1186/s13634-021-00765-z

Yong, A., Askan, A., Cassidy, J., D'Amico, S., Parolai, S., Rilz, M., & Stephenson, W. (2022). Introduction to the Special Issue of the Consortium of Organizations for Strong Motion Observation Systems (COSMOS) International Guidelines for Applying Noninvasive Geophysical Techniques to Characterize Seismic Site Conditions. *Submitted to Journal of Seismology*

Yong, A., Thompson, E. M., & J. Wald, D. (n.d.). *Compilation of V S30 Data for the United States Data Series 978*.

Zen, K., Umehara, Y., & Hamada, K. (1978). *Laboratory tests and in-situ seismic survey on vibratory shear modulus of clayey soils with various plasticities*. 721–728.

APPENDICES

A. V_s Profiles at Selected Sites

V_s profiles at selected sites for each selected city in Northwestern Türkiye are tabulated in Tables A.1-A.17.

Table A.1. V_s profiles at selected sites (strong-motion stations) in Düzce (indicated with station codes)

8101		**8109**		**8110**	
Depth (m)	Vs (m/s)	Depth (m)	Vs (m/s)	Depth (m)	Vs (m/s)
0	154	0	154	0	297
1.6	154	1.28	154	1.06	297
1.6	176	1.28	157	1.06	311
3.7	176	2.88	157	2.39	311
3.7	182	2.88	148.0	2.39	209
6.2	182	4.87	148.0	4.05	209
6.2	262	4.87	135	4.05	176
9.4	262	7.37	135	6.12	176
9.4	276	7.37	133	6.12	362
13.4	276	10.49	133	8.72	362
13.4	305	10.49	165	8.72	472
18.4	305	14.38	165	11.96	472
18.4	407	14.38	201	11.96	493
24.6	407	19.26	201	16.01	493
24.6	449	19.26	233	16.01	496
32	449	25.35	233	21.07	496
		25.35	283	21.07	565
		32.97	283	27.41	565

Table A.1. (cont'd)

8101		**8109**		**8110**	
Depth (m)	Vs (m/s)	Depth (m)	Vs (m/s)	Depth (m)	Vs (m/s)
				27.41	1015
				34.26	1015

Table A.2. V_s profiles at selected sites (strong-motion stations) in Bolu (indicated with station codes)

1401		**1402**		**1403**		**1404**		**1405**	
Depth (m)	Vs (m/s)	Depth (m)	Vs (m/s)	Depth (m)	Vs (m/s)	Depth (m)	Vs (m/s)	Depth (m)	Vs (m/s)
0	163	0	414	0	426	0	258	0	216
1.9	163	2	414	2	426	1.7	258	1.3	216
1.9	181	2	368	2	369	1.7	247	1.3	117
4.2	181	4.5	368	4.4	369	3.8	247	2.9	117
4.2	277	4.5	345	4.4	351	3.8	256	2.9	200
7.1	277	7.6	345	7.5	351	6.4	256	4.8	200
7.1	298	7.6	567	7.5	273	6.4	197	4.8	302
10.8	298	11.6	567	11.4	273	9.7	197	7.3	302
10.8	261	11.6	581	11.4	515	9.7	348	7.3	325
15.3	261	16.5	581	16.2	515	13.8	348	10.4	325
15.3	323	16.5	359	16.2	627	13.8	432	10.4	404
21	323	22.6	359	22.2	627	18.9	432	14.3	404
21	438	22.6	517	22.2	741	18.9	502	14.3	544
28.1	438	30.2	517	29.7	741	25.3	502	19.2	544
28.1	495	30.2	711	29.7	877	25.3	591	19.2	628
32	495	32	711	32	877	32	591	25.2	628

Table A.2. (cont'd)

1401		**1402**		**1403**		**1404**		**1405**	
Depth (m)	Vs (m/s)	Depth (m)	Vs (m/s)	Depth (m)	Vs (m/s)	Depth (m)	Vs (m/s)	Depth (m)	Vs (m/s)
								25.2	687
								32	687

Table A.3. V_s profiles at selected sites (strong-motion stations) in Bolu (indicated with station codes)

1406		**1407**		**1409**		**1410**		**1411**	
Depth (m)	Vs (m/s)	Depth (m)	Vs (m/s)	Depth (m)	Vs (m/s)	Depth (m)	Vs (m/s)	Depth (m)	Vs (m/s)
0	244	0	178	0	259	0	274	0	184
1.5	244	2.41	178	2.74	259	2.93	274	1.61	184
1.5	165	2.41	172	2.74	228	2.93	222	1.61	185
3.5	165	5.41	172	6.16	228	6.6	222	3.61	185
3.5	247	5.41	194	6.16	295	6.6	249	3.61	173
5.9	247	9.17	194	10.45	295	11.18	249	6.12	173
5.9	222	9.17	282	10.45	403	11.18	363	6.12	171
8.9	222	13.87	282	15.8	403	16.91	363	9.26	171
8.9	345	13.87	342	15.8	448	16.91	447	9.26	206
12.7	345	19.75	342	22.49	448	24.06	447	13.18	206
12.7	450	19.75	392	22.49	520	24.06	529	13.18	250
17.4	450	27.09	392	30.85	520	33.01	529	18.08	250
17.4	537	27.09	429					18.08	285
23.3	537	36.27	429					24.21	285
23.3	637							24.21	312
30.7	637							31.87	312

Table A.3. (cont'd)

1406		**1407**		**1409**		**1410**		**1411**	
Depth (m)	Vs (m/s)	Depth (m)	Vs (m/s)	Depth (m)	Vs (m/s)	Depth (m)	Vs (m/s)	Depth (m)	Vs (m/s)
30.7	788								
32	788								

Table A.4. V_s profiles at selected sites (strong-motion stations) in Sakarya (indicated with station codes)

5401		**5402**		**5403**		**5404**		**5405**	
Depth (m)	Vs (m/s)	Depth (m)	Vs (m/s)	Depth (m)	Vs (m/s)	Depth (m)	Vs (m/s)	Depth (m)	Vs (m/s)
0	257	0	164	0	182	0	383	0	439
1.7	257	1.6	164	1.2	182	1.74	383	1.3	439
1.7	202	1.6	155	1.2	184	1.74	386	1.3	428
3.9	202	3.5	155	2.69	184	3.92	386	2.92	428
3.9	264	3.5	154	2.69	174	3.92	385	2.92	425
6.6	264	5.9	154	4.56	174	6.65	385	4.95	425
6.6	352	5.9	216	4.56	159	6.65	377	4.95	463
10.1	352	9	216	6.9	159	10.05	377	7.49	463
10.1	426	9	246	6.9	158	10.05	366	7.49	492
14.3	426	12.8	246	9.82	158	14.31	366	10.66	492
14.3	515	12.8	325	9.82	196	14.31	367	10.66	479
19.6	515	17.5	325	13.47	196	19.63	367	14.62	479
19.6	663	17.5	397	13.47	236	19.63	386	14.62	332
26.3	663	23.4	397	18.03	236	26.29	386	19.58	332
26.3	757	23.4	479	18.03	262	26.29	409	19.58	282
32	757	30.8	479	23.73	262	34.6	409	25.77	282

Table A.4. (cont'd)

5401		**5402**		**5403**		**5404**		**5405**	
Depth (m)	Vs (m/s)	Depth (m)	Vs (m/s)	Depth (m)	Vs (m/s)	Depth (m)	Vs (m/s)	Depth (m)	Vs (m/s)
		30.8	547	23.73	300			25.77	676
		32	547	30.86	300			33.51	676

Table A.5. V_s profiles at selected sites (strong-motion stations) in Istanbul (indicated with station codes)

3411		**3412**		**3416**		**3413**		**3417**	
Depth (m)	Vs (m/s)	Depth (m)	Vs (m/s)	Depth (m)	Vs (m/s)	Depth (m)	Vs (m/s)	Depth (m)	Vs (m/s)
0	311	0	197	0	432	0	458	0	1829
2.19	311	1.41	197	2.53	432	3.72	458	5.58	1829
2.19	314	1.41	242	2.53	433	3.72	453	5.58	1881
4.93	314	3.18	242	5.7	433	8.36	453	12.56	1881
4.93	306	3.18	215	5.7	430	8.36	417	12.56	1813
8.35	306	5.38	215	9.66	430	14.17	417	21.28	1813
8.35	293	5.38	138	9.66	424	14.17	417	21.28	1556
12.62	293	8.14	138	14.61	424	21.42	417	32.19	1556
12.62	303	8.14	186	14.61	418	21.42	515		
17.97	303	11.58	186	20.79	418	30.49	515		
17.97	342	11.58	279	20.79	411				
24.65	342	15.89	279	28.52	411				
24.65	379	15.89	305	28.52	401				
33.01	379	21.27	305	38.19	401				
		21.27	333						
		28	333						

Table A.5. (cont'd)

3411		**3412**		**3416**		**3413**		**3417**	
Depth (m)	Vs (m/s)	Depth (m)	Vs (m/s)	Depth (m)	Vs (m/s)	Depth (m)	Vs (m/s)	Depth (m)	Vs (m/s)
		28	414						
		36.41	414						

Table A.6. V_s profiles at selected sites (strong-motion stations) in Istanbul (indicated with station codes)

3403		**3402**		**3401**		**3404**		**3405**	
Depth (m)	Vs (m/s)	Depth (m)	Vs (m/s)	Depth (m)	Vs (m/s)	Depth (m)	Vs (m/s)	Depth (m)	Vs (m/s)
0	105	0	371	0	518	0	573	0	821.25
1.6	105	2.96	371	1.7	518	0.9	573	2.45	821.25
1.6	171	2.96	487	1.7	426	0.9	568	2.45	1755.94
3.6	171	6.67	487	3.7	426	2.2	568	5.5	1755.94
3.6	208	6.67	396	3.7	281	2.2	526	5.5	1809.25
6.1	208	11.3	396	6.3	281	3.7	526	9.33	1809.25
6.1	239	11.3	279	6.3	444	3.7	549	9.33	1702.6
9.2	239	17.09	279	9.5	444	5.6	549	14.4	1702.6
9.2	253	17.09	484	9.5	634	5.6	670	14.4	705.01
13.1	253	24.33	484	13.6	634	8	670	20.07	705.01
13.1	375	24.33	614	13.6	657	8	694	20.07	1411.07
18	375	33.37	614	18.6	657	11	694	27.54	1411.07
18	441			18.6	901	11	550	27.54	2214.07
24.1	441			24.9	901	14.8	550	36.87	2214.07
24.1	508			24.9	1047	14.8	757	36.87	2992.51
31.7	508			32	1047	19.4	757	48.53	2992.51

Table A.6. (cont'd)

3403		**3402**		**3401**		**3404**		**3405**	
Depth (m)	Vs (m/s)	Depth (m)	Vs (m/s)	Depth (m)	Vs (m/s)	Depth (m)	Vs (m/s)	Depth (m)	Vs (m/s)
31.7	576					19.4	977	48.53	2573.75
32	576					25.2	977	63.11	2573.75
						25.2	1359	63.11	5254.11
						31.6	1359	78.89	5254.11

Table A.7. V_s profiles at selected sites (strong-motion stations) in Istanbul (indicated with station codes)

3406		**3410**		**3418**	
Depth (m)	Vs (m/s)	Depth (m)	Vs (m/s)	Depth (m)	Vs (m/s)
0	402	0	572	0	1271
1.9	402	2.15	572	5.76	1271
1.9	401	2.15	585	5.76	1443
4.28	401	4.84	585	12.97	1443
4.28	353	4.84	556	12.97	1315
7.25	353	8.21	556	21.98	1315
7.25	322	8.21	471	21.98	891
10.96	322	12.41	471	33.23	891
10.96	398	12.41	462		
15.6	398	17.67	462		
15.6	527	17.67	680		
21.4	527	24.24	680		
21.4	563	24.24	855		
28.65	563	32.45	855		

Table A.7. (cont'd)

3406		**3410**		**3418**	
Depth (m)	Vs (m/s)	Depth (m)	Vs (m/s)	Depth (m)	Vs (m/s)
28.65	516				
37.72	516				

Table A.8. V_s profiles at selected sites (strong-motion stations) in Kocaeli (indicated with station codes)

4101		**4102**		**4104**		**4105**		**4106**	
Depth (m)	Vs (m/s)	Depth (m)	Vs (m/s)	Depth (m)	Vs (m/s)	Depth (m)	Vs (m/s)	Depth (m)	Vs (m/s)
0	652	0	895	0	611	0	229	0	624
1.3	652	1.6	895	1.3	611	0.8	229	2.1	624
1.3	581	1.6	788	1.3	588	0.8	221	2.1	643
3	581	3.6	788	2.9	588	1.9	221	4.7	643
3	378	3.6	645	2.9	481	1.8	222	4.7	455
5.1	378	6.2	645	5	481	3.2	222	7.9	455
5.1	444	6.2	952	5	346	3.2	243	7.9	446
7.6	444	9.4	952	7.6	346	4.9	243	12	446
7.6	756	9.4	1192	7.6	693	4.8	249	12	789
10.9	756	13.4	1192	10.8	693	7	249	17	789
10.9	931	13.4	1276	10.8	840	7	256	17	937
14.9	931	18.4	1276	14.8	840	9.4	256	23.3	937
14.9	1131	18.4	1141	14.8	1014	9.4	258	23.3	1097
20	1131	24.6	1141	19.9	1014	12.7	258	31.3	1097
20	1352	24.6	965	19.9	1217	12.7	265	31.3	1285
26.3	1352	32.4	965	26.2	1217	16.7	265	32	1285

Table A.8. (cont'd)

4101		**4102**		**4104**		**4105**		**4106**	
Depth (m)	Vs (m/s)	Depth (m)	Vs (m/s)	Depth (m)	Vs (m/s)	Depth (m)	Vs (m/s)	Depth (m)	Vs (m/s)
26.3	1590	32.4	801	26.2	1420	16.7	277		
32	1590	42.1	801	34	1420	21.7	277		
		42.1	1300	34	1865	21.7	448		
		52.6	1300	42.5	1865	27.1	448		

Table A.9. V_s profiles at selected sites (strong-motion stations) in Kocaeli (indicated with station codes)

4114		**4115**		**4116**		**4117**	
Depth (m)	Vs (m/s)	Depth (m)	Vs (m/s)	Depth (m)	Vs (m/s)	Depth (m)	Vs (m/s)
0	270	0	186	0	143	0	253
2.49	270	1.96	186	1.07	143	0.94	253
2.49	300	1.96	183	1.07	144	0.94	255
5.6	300	4.4	183	2.4	144	2.12	255
5.6	211	4.4	172	2.4	138	2.12	259
9.48	211	7.46	172	4.07	138	3.59	259
9.48	280	7.46	199	4.07	135	3.59	262
14.34	280	11.28	199	6.15	135	5.42	262
14.34	455	11.28	273	6.15	151	5.42	256
20.41	455	16.05	273	8.75	151	7.72	256
20.41	515	16.05	336	8.75	170	7.72	237
28	515	22.02	336	12.01	170	10.59	237
28	545	22.02	357	12.01	183	10.59	215
37.48	545	29.48	357	16.08	183	14.18	215

Table A.9. (cont'd)

4114		**4115**		**4116**		**4117**	
Depth (m)	Vs (m/s)	Depth (m)	Vs (m/s)	Depth (m)	Vs (m/s)	Depth (m)	Vs (m/s)
		29.48	361	16.08	197	14.18	231
		38.8	361	21.16	197	18.67	231
				21.16	216	18.67	312
				27.52	216	24.27	312
				27.52	315	24.27	560
				34.4	315	30.34	560

Table A.10. V_s profiles at selected sites (strong-motion stations) in Kocaeli (indicated with station codes)

4118		**4119**		**4120**		**4121**	
Depth (m)	Vs (m/s)	Depth (m)	Vs (m/s)	Depth (m)	Vs (m/s)	Depth (m)	Vs (m/s)
0	173	0	872	0	164	0	285
1.09	173	1.77	872	1.8	164	1.29	285
1.09	174	1.77	976	1.8	147	1.29	289
2.46	174	3.99	976	4.06	147	2.9	289
2.46	172	3.99	1057	4.06	147	2.9	285
4.17	172	6.76	1057	6.88	147	4.91	285
4.17	171	6.76	1048	6.88	165	4.91	270
6.31	171	10.22	1048	10.4	165	7.42	270
6.31	175	10.22	846	10.4	212	7.42	256
8.98	175	14.54	846	14.8	212	10.56	256
8.98	173	14.54	594	14.8	259	10.56	270
12.31	173	19.95	594	20.3	259	14.49	270

Table A.10. (cont'd)

4118		**4119**		**4120**		**4121**	
Depth (m)	Vs (m/s)	Depth (m)	Vs (m/s)	Depth (m)	Vs (m/s)	Depth (m)	Vs (m/s)
12.31	171	19.95	934	20.3	296	14.49	304
16.48	171	26.71	934	27.18	296	19.4	304
16.48	184	26.71	1451	27.18	349	19.4	337
21.7	184	35.17	1451	35.78	349	25.54	337
21.7	222					25.54	395
28.22	222					33.21	395
28.22	364						
35.27	364						

Table A.11. V_s profiles at selected sites (strong-motion stations) in Kocaeli (indicated with station codes)

4123		**4124**		**4126**		**4127**	
Depth (m)	Vs (m/s)	Depth (m)	Vs (m/s)	Depth (m)	Vs (m/s)	Depth (m)	Vs (m/s)
0	215	0	717	0	159	0	202
2.41	215	1.29	717	1.29	159	1.39	202
2.41	230	1.29	928	1.29	160	1.39	203
5.43	230	2.9	928	2.89	160	3.13	203
5.43	223	2.9	1021	2.89	153	3.13	200
9.2	223	4.91	1021	4.9	153	5.3	200
9.2	226	4.91	861	4.9	148	5.3	194
13.92	226	7.43	861	7.41	148	8.01	194
13.92	307	7.43	539	7.41	159	8.01	195
16.7	307	10.58	539	10.55	159	11.4	195

Table A.11. (cont'd)

4123		**4124**		**4126**		**4127**	
Depth (m)	Vs (m/s)	Depth (m)	Vs (m/s)	Depth (m)	Vs (m/s)	Depth (m)	Vs (m/s)
16.7	307	10.58	786	10.55	183	11.4	203
19.81	307	14.51	786	14.48	183	15.64	203
19.81	375	14.51	963	14.48	200	15.64	218
23	375	19.42	963	19.38	200	20.94	218
23	375	19.42	1073	19.38	218	20.94	236
27.18	375	25.57	1073	25.51	218	27.57	236
27.18	427	25.57	1473	25.51	261	27.57	277
30	427	33.25	1473	33.18	261	35.85	277
30	427						
33.5	427						
33.5	427						
36.39	427						

Table A.12. V_s profiles at selected sites (strong-motion stations) in Kocaeli (indicated with station codes)

4128		**4129**		**4130**		**4131**	
Depth (m)	Vs (m/s)	Depth (m)	Vs (m/s)	Depth (m)	Vs (m/s)	Depth (m)	Vs (m/s)
0	229	0	147	0	462	0	401
1.72	229	1.04	147	1.98	462	1.53	401
1.72	231	1.04	147	1.98	495	1.53	396
3.88	231	2.34	147	4.46	495	3.44	396
3.88	224	2.34	138	4.46	480	3.44	363
6.57	224	3.96	138	7.56	480	5.83	363

Table A.12. (cont'd)

4128		**4129**		**4130**		**4131**	
Depth (m)	Vs (m/s)	Depth (m)	Vs (m/s)	Depth (m)	Vs (m/s)	Depth (m)	Vs (m/s)
6.57	216	3.96	131	7.56	406	5.83	356
9.94	216	5.99	131	11.43	406	8.82	356
9.94	231	5.99	155	11.43	399	8.82	415
14.15	231	8.53	155	16.27	399	12.56	415
14.15	264	8.53	188	16.27	512	12.56	474
19.41	264	11.7	188	22.32	512	17.23	474
19.41	304	11.7	210	22.32	601	17.23	492
25.99	304	15.66	210	29.88	601	23.07	492
25.99	336	15.66	230	29.88	654	23.07	533
34.21	336	20.61	230	39.34	654	30.36	533
		20.61	267				
		26.8	267				
		26.8	429				
		33.5	429				

Table A.13. V_s profiles at selected sites (strong-motion stations) in Bursa (indicated with station codes)

1633		**1621**		**1631**		**1612**		**1609**	
Depth (m)	Vs (m/s)	Depth (m)	Vs (m/s)	Depth (m)	Vs (m/s)	Depth (m)	Vs (m/s)	Depth (m)	Vs (m/s)
0	375	0	405	0	346	0	144	0	186
2.05	375	3.02	405	1.27	346	1.1	144	1.8	186
2.05	386	3.02	407	1.27	372	1.1	220	1.8	195
4.61	386	6.8	407	2.87	372	2.5	220	4.1	195

Table A.13. (cont'd)

1633		**1621**		**1631**		**1612**		**1609**	
Depth (m)	Vs (m/s)	Depth (m)	Vs (m/s)	Depth (m)	Vs (m/s)	Depth (m)	Vs (m/s)	Depth (m)	Vs (m/s)
4.61	383	6.8	395	2.87	356	2.5	202	4.1	193
7.82	383	11.52	395	4.86	356	4.2	202	7	193
7.82	334	11.52	376	4.86	296	4.2	113	7	179
11.82	334	17.42	376	7.34	296	6.4	113	10.5	179
11.82	299	17.42	382	7.34	261	6.4	194	10.5	253
16.83	299	24.8	382	10.45	261	9.1	194	15	253
16.83	384	24.8	431	10.45	375	9.1	156	15	253
23.09	384	34.02	431	14.34	375	12.5	156	20.6	253
23.09	480			14.34	477	12.5	163	20.6	297
30.91	480			19.2	477	16.8	163	27.6	297
				19.2	537	16.8	248	27.6	327
				25.27	537	22.1	248	36.3	327
				25.27	641	22.1	276	36.3	350
				32.86	641	28.7	276	47.2	350
						28.7	384	47.2	524
						32	384	59	524

Table A.14. V_s profiles at selected sites (strong-motion stations) in Bursa (indicated with station codes)

1602		**1606**		**1615**		**1608**		**1607**	
Depth (m)	Vs (m/s)	Depth (m)	Vs (m/s)	Depth (m)	Vs (m/s)	Depth (m)	Vs (m/s)	Depth (m)	Vs (m/s)
0	242	0	201	0	343	0	306	0	118
1.24	242	1	201	1.4	343	1.7	306	1	118

Table A.14. (cont'd)

1602		**1606**		**1615**		**1608**		**1607**	
Depth (m)	Vs (m/s)	Depth (m)	Vs (m/s)	Depth (m)	Vs (m/s)	Depth (m)	Vs (m/s)	Depth (m)	Vs (m/s)
1.24	244	1	197	1.4	338	1.7	308	1	114
2.8	244	2.3	197	3.2	338	3.8	308	1.8	114
2.8	239	2.3	204	3.2	345	3.8	322	1.8	110
4.74	239	4	204	5.3	345	6.4	322	2.8	110
4.74	228	4	138	5.3	350	6.4	298	2.8	114
7.17	228	6	138	8.1	350	9.8	298	4	114
7.17	230	6	239	8.1	345	9.8	306	4	138
10.2	230	8.5	239	11.5	345	13.9	306	5.4	138
10.2	251	8.5	300	11.5	336	13.9	374	5.4	163
14	251	11.7	300	15.8	336	19	374	7.3	163
14	278	11.7	374	15.8	340	19	451	7.3	180
18.74	278	15.6	374	21.1	340	25.5	451	9.6	180
18.74	307	15.6	454	21.1	357	25.5	521	9.6	189
24.67	307	20.5	454	27.8	357	33.6	521	12.5	189
24.67	350	20.5	530	27.8	397	33.6	574	12.5	288
32.08	350	26.7	530	36.1	397	43.6	574	15.6	288
		26.7	759	36.1	641	43.6	840		
		33.4	759	45.1	641	54.6	840		

Table A.15. V_s profiles at selected sites (strong-motion stations) in Bursa (indicated with station codes)

1603		**1605**		**1616**		**1617**		**1610**	
Depth (m)	Vs (m/s)	Depth (m)	Vs (m/s)	Depth (m)	Vs (m/s)	Depth (m)	Vs (m/s)	Depth (m)	Vs (m/s)
0	320	0	485	0	330	0	1723	0	158
1.9	320	2.3	485	1.5	330	2.1	1723	1.3	158
1.9	294	2.3	524	1.5	221	2.1	1753	1.3	113
4.3	294	5.2	524	3.3	221	4.7	1753	2.9	113
4.3	385	5.2	492	3.3	437	4.7	1756	2.9	178
7.3	385	8.9	492	5.7	437	8	1756	4.9	178
7.3	435	8.9	365	5.7	395	8	1681	4.9	174
11.1	435	13.4	365	8.6	395	12	1681	7.5	174
11.1	497	13.4	406	8.6	650	12	1518	7.5	205
15.8	497	19	406	12.2	650	17.1	1518	10.6	205
15.8	521	19	635	12.2	688	17.1	1406	10.6	291
21.7	521	26.1	635	16.7	688	23.4	1406	14.6	291
21.7	570	26.1	719	16.7	780	23.4	1663	14.6	338
29.1	570	35	719	22.4	780	31.4	1663	19.5	338
29.1	720	35	792	22.4	1005	31.4	2260	19.5	391
38.3	720	46	792	29.4	1005	41.3	2260	25.6	391
38.3	845	46	763	29.4	1140	41.3	2597	25.6	383
49.8	845	59.9	763	38.3	1140	53.8	2597	32	383
49.8	1200	59.9	1135	38.3	1765	53.8	3708		
62.3	1200	74.8	1135	47.8	1765	67.2	3708		

Table A.16. V_s profiles at selected sites (strong-motion stations) in Bursa (indicated with station codes)

1611		**1613**		**1614**		**1618**	
Depth (m)	Vs (m/s)	Depth (m)	Vs (m/s)	Depth (m)	Vs (m/s)	Depth (m)	Vs (m/s)
0	204	0	313	0	160	0	286
2.1	204	1.5	313	1.3	160	1.42	286
2.1	189	1.5	161	1.3	149	1.42	298
4.8	189	3.5	161	3	149	3.19	298
4.8	243	3.5	256	3	168	3.19	302
8.1	243	5.9	256	5.1	168	5.41	302
8.1	223	5.9	406	5.1	194	5.41	272
12.3	223	8.9	406	7.7	194	8.18	272
12.3	192	8.9	408	7.7	233	8.18	223
17.5	192	12.8	408	10.9	233	11.64	223
17.5	333	12.8	470	10.9	257	11.64	251
23.9	333	17.5	470	15	257	15.97	251
23.9	377	17.5	572	15	337	15.97	358
32	377	23.5	572	20.1	337	21.39	358
		23.5	731	20.1	408	21.39	436
		30.8	731	26.4	408	28.15	436
		30.8	851	26.4	468	28.15	503
		40.1	851	32	468	36.61	503
		40.1	1371				
		50.1	1371				

Table A.17. V_s profiles at selected sites (strong-motion stations) in Yalova (indicated with station codes)

7707		**7711**		**7706**		**7712**		**7709**	
Depth (m)	Vs (m/s)	Depth (m)	Vs (m/s)	Depth (m)	Vs (m/s)	Depth (m)	Vs (m/s)	Depth (m)	Vs (m/s)
0	300	0	191	0	200	0	242	0	281
1.49	300	1.34	191	1.27	200	1.04	242	1.21	281
1.49	304	1.34	193	1.27	232	1.04	245	1.21	297
3.36	304	3	193	2.86	232	2.33	245	2.73	297
3.36	294	3	192	2.86	170	2.33	240	2.73	259
5.68	294	5.09	192	4.84	170	3.95	240	4.63	259
5.68	277	5.09	188	4.84	138	3.95	227	4.63	218
8.6	277	7.7	188	7.32	138	5.97	227	7	218
8.6	265	7.7	178	7.32	272	5.97	212	7	289
12.24	265	10.96	178	10.42	272	8.5	212	9.96	289
12.24	289	10.96	178	10.42	354	8.5	218	9.96	450
16.79	289	15.04	178	14.3	354	11.67	218	13.67	450
16.79	334	15.04	190	14.3	349	11.67	260	13.67	466
22.47	334	20.13	190	19.14	349	15.62	260	18.3	466
22.47	373	20.13	220	19.14	336	15.62	299	18.3	447
29.58	373	26.5	220	25.19	336	20.56	299	24.09	447
29.58	415	26.5	265	25.19	433	20.56	345	24.09	621
38.47	415	34.46	265	32.76	433	26.74	345	31.33	621
						26.74	556		
						33.42	556		

B. Sample Computation of Amplification Factors in DEEPSOIL

In Figure B.1, site response analyses at DZC (8101) station are performed with the strong motion record of Düzce earthquake's EW component as the input motion (Figure B.1) and average of the 40 strong motion records yield the amplification factors for that station, right hand side of the corresponding figure.

When the general trend of amplification factors is observed, they increase up to the peak point, then start to decrease, and finally continue with nearly constant values.

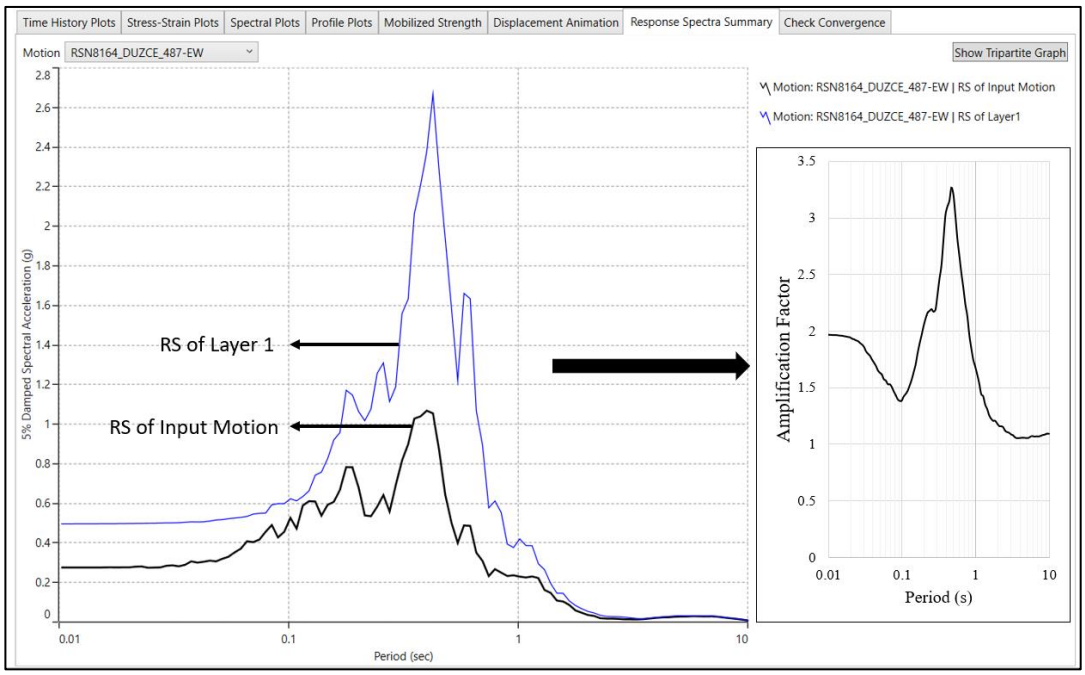

Figure B.1. DEEPSOIL output showing the response spectra summary for station DZC (8101) with a selected strong motion record (The amplification factor in the period domain is obtained by dividing the response spectrum of the motion computed at the top layer (blue curve) by the response spectrum of input motions (black curve)).